Imaging of tumor specific antigens and microenvironment

The work presented in this thesis was mainly performed at the Nuclear Medicine Unit, Department of Medical-Surgical Sciences and of Translational Medicine, Faculty of Medicine and Psychology, “Sapienza” University of Rome, Italy, in collaboration with the department of Nuclear Medicine and Molecular Imaging, University Medical Centre Groningen, University of Groningen, The Netherlands, the National "Frederic Joliot Curie" Research Institute for Radiobiology and Radiohygiene, Budapest, Hungary and the Molecular Oncogenesis Laboratory, Experimental Oncology Department, Regina Elena National Cancer Institute, Rome, Italy.

The Printing of this thesis was financially supported by:
University Medical Centre Groningen
Trophogen Inc.

Cover design: Barbara Marcantonio
ISBN: 978-90-367-8175-6

university of groningen

Imaging of tumor specific antigens and microenvironment

PhD thesis

to obtain the degree of PhD at the
University of Groningen
on the authority of the
Rector Magnificus Prof. E. Sterken
and in accordance with
the decision by the College of Deans.

This thesis will be defended in public on

Wednesday 28 October 2015 at 12.45 hours

by

Filippo Galli

born on 22 March 1985
in Terni, Italië

Supervisors
Prof. A. Signore
Prof. R.A.J.O. Dierckx

Co-supervisor
Dr. G. Piaggio

Assessment Committee
Prof. T.P. Links
Prof. C. van de Wiele
Prof. P. Marchetti

Paranymphs:
Giulia Federici
Luz Kelly Anzola Fuentes

Contents

A Luigina

Chapter 1

Introduction

Parts of this chapter have been published in:

Galli F, Histed S, Aras O.
NK cell imaging by in vitro and in vivo labelling approaches.
Q J Nucl Med Mol Imaging. 2014 Sep;58(3):276-83.

Galli F, Iodice V, Lauri L, Signore A.
New approaches to image thyroid cancer cells and microenvironment
Q J Nucl Med Mol Imaging. 2015 Jun;59(2):184-96

Lauri C, Di Traglia S, Galli F, Pizzichini P, Signore A.
Current status of PET imaging of thyroid tumors with second generation radiopharmaceuticals
Q J Nucl Med Mol Imaging. 2015 Mar;59(1):105-15

TUMOR MICROENVIRONMENT

The events that drive tumor progression and metastatization initiate within the cancer cell itself, that accumulates mutation and de-differentiate until reaching a very unstable stage [1]. But these events alone are not sufficient to maintain sustained metastasis development and growth. Cell-matrix interaction and support from the host is required in order to promote angiogenesis and inhibit immune response that would kill cancer cells. The sum of these events is the result of the interaction between tumor and the surrounding microenvironment [2]. Indeed, the microenvironment is formed by both cellular and non-cellular elements with growth promoting or inhibiting effects and all of them offer a huge pool of targets for diagnostic or therapeutic applications. Non-cellular microenvironmental components involved in cancer progression and metastasis are matrix remodelling, cytokines, growth factors and mechanisms triggered by hypoxia, whether cellular components include immune cells, fibroblasts and other stromal cells [3, 4].

CELLULAR COMPONENTS

Stromal cells

Endothelial cells play a key role in the establishment of tumor microenvironment, since angiogenesis is a vital physiological process involving the growth and re-modelling of new blood vessels from pre-existing ones [5]. Excessive and pathologic angiogenesis, termed neoangiogenesis, have been implicated in many

diseases, but is crucial in cancer metastatization and progression [6, 7)]. Neoangiogenesis is essential for tumor development beyond a diameter of 2 to 3 mm as well as for local and distant metastases through both blood and lymphatic vessel. This process is mediated by proangiogenic factors and provides tumors not only with nutrients for growth, but also increases the opportunity for cancer cells to enter the circulation and metastasize. The most potent angiogenic molecule is the vascular endothelial growth factor A (VEGF-A), a member of the subfamily of heparin-binding glycoproteins with potent angiogenic, lymphangiogenic, mitogenic, vascular and lymphatic permeability-enhancing activities initially thought specific for endothelial cells. However, also other activities of VEGF-A directly on neoplastic cells, where expression of at least one form of its receptor is present, have been reported 8]. The effects of VEGF isoforms are mediated through two homologous tyrosine kinase receptors located in the cell membrane specifically of endothelial cells: the kinase domain receptor (KDR) and FMS-like tyrosine kinase (FLT-1) also termed VEGF2 receptor (VEGFR2) and VEGF1 receptor (VEGFR1 respectively [9, 10]. The elevated expression of VEGFR2 receptors in tumor and/or tumor-related endothelial cells have been confirmed in numerous studies and it is related to tumor cells secreting VEGF. By contrast, non-stimulated and quiescent endothelial cells express low levels of VEGFRs. Hypoxia is also able to enhance angiogenesis as a response to the production of hypoxia inducible factor 1α (HIF-1α) that is a regulator of VEGF and its expression correlates with increasing tumor grade invasion and metastasis [11, 12].

Anti-VEGF treatment, in combination with chemotherapy improved progression-free survival in many types of metastatic cancer. Moreover, many tyrosine kinase inhibitors (TKI) interfere with VEGFRs signalling, reducing new blood vessels formation. VEGF is also produced by fibroblasts, mesenchymal cells of the connective tissue with a high degree of heterogeneity. Upon tumor growth factor-beta (TGF-ß) stimulation, they transform in myofibroblasts that can secrete extracellular matrix (ECM) components and produce α-smooth actin [13]. In the tumor microenvironment they are referred as cancer associated fibroblasts (CAFs) with a promoting tumor growth role through paracrine effects on epithelial cancer cells. CAFs may have stimulatory or inhibitory effects on T lymphocytes through the production of different molecules. Among these α2ß1integrin, an adhesion molecule also present in the ECM, showed to increase T cell proliferation and interferon-γ (IFN-γ) production. On the other hand TGF-ß1 and hepatocyte growth factor (HGF) showed an inhibitory effect on T lymphocytes proliferation. However, many other factors do not have a clear enhancing or suppressive effect, since they are in a complex equilibrium with fine modulating outcomes. Fibroblasts are also able to increase T cell trafficking producing chemokines like monocyte chemotactic protein-1 (MCP-1), but, in turn, they are regulated by them.

Dendritic cells (DCs)

In general, DCs infiltrates the tumor represents an early-triggered response, inducing apoptosis in cancer cell and producing several chemokines (CCR1, CCR5

or CCR6), thus recruiting additional DCs that migrate from lymph nodes. Mature DCs can also migrate back to lymph node to present antigens to T cells and inducing Th_1 recruitment [14]. Imbalance between chemokines like CCR7 and their ligands (CCL19 and CCL21) may lead either to tolerant or anti-tumor DCs, with opposed consequences. The same chemokines may also recruit other cell types like natural killer (NK) cells, inducing also IFN-γ production. NKs have a great anti-tumor activity either by direct cancer cell killing or by production of soluble factors that, like a circle, enhance DCs infiltration and chemokine secretion, amplifying the immune response [15].

T regulatory cells (T_{reg})

T_{reg} is a CD4(+)CD25(+)FoxP3(+) T cell subtype recruited in tumors by CCL1 and CCL22 ligands. Also $CD8^+$ T cells are able to attract T_{reg} by CCR4 ligand production [16]. However they may have a suppressive effect on immune cells from the host, favouring tumor progression. In particular they are able to directly kill NK cells that are one of the same cell type responsible for their recruitment. Different cancer cell types are able to produce CCL1 and other chemokines that can recruit T_{reg}, enhancing a defensive mechanism to promote their growth. Therefore, targeting such ligands with specific drug may allow stopping T_{reg} recruitment in tumors and enhancing the host immune response.

Tumor associated macrophages (TAMs)

TAMs may have both pro- and anti-tumor effects after migrating into the tumor and maturating in either M1 or M2 phenotype. M1 are able to mediate tumor suppressing effects producing type I cytokine and presenting tumor-related antigens, whereas M2 are able to produce type II cytokine promoting tumor growth and metastatization [17, 18]. The latter is present in higher percentages in solid tumors, since the cancer cell itself is able to drive TAMs polarization to M2 phenotype. M2 are also able to produce T_{reg} attracting chemokines and it has been reported that their high presence is associated with poor prognosis. Since TAMs migration is induced by chemoattractans like GPCRs, in many cancers including thyroid cancer such ligands may represent a candidate target for therapies with novel immunotherapeutic drugs [19, 20].

Myeloid-derived suppressor cells (MDSCs)

MDSCs are immature myeloid cells with either monocytic or granulocytic morphology and infiltrate tumors via the chemokine GPCRs CCR2, CXCR2, or CXCR4. They promote both tumor growth and metastatization producing suppressing anti-tumoral effectors. They are able to inhibit T cell functions via iNOS and arginase and to sustain T_{reg} activity proucing GPCRs ligands [21]. In the literature is reported that this population is increased in cancer and that their characterization is a hard task, because of its variable phenotype. Indeed, they can even differentiate into a TAMs phenptype.

NK cells

NK cells are an important lymphocyte subset with distinctive morphology, function and molecular markers. They can be described as $CD3^{-}CD56^{+}$ lymphocytes furtherly divided in $CD56^{dim}CD16^{+}$ and $CD56^{bright}CD16^{-}$ subsets with cytotoxic and regulatory functions respectively [22]. They are involved in immune surveillance and are able to infiltrate tumors and directly kill cancer cells. $CD56^{dim}$ NK cells are the most potent cytotoxic subtype and are able to both directly kill cancer cells and produce regulatory factors that indirectly limit tumor growth and enhance the host immune response. However, cancer cells may escape T-cell response but are directly recognized by NK cells through a "missing self" mechanism [23]. NK cells can kill cancer cells inducing caspase-dependent or caspase-independent apoptosis, by releasing granules that contain perforin and granzymes or by expressing FasL. They are also able to produce tumour necrosis factor alpha (TNFα) and interferon γ (IFNγ), with several antitumor functions, including tumor angiogenesis restriction and adaptive immunity stimulation [24]. These are only a few of the many mechanisms to induce cancer cells death and, in addition, killed cells can provide a pool of antigens to present to DCs, inducing their maturation and CTL responses [25]. Given the natural anti-tumor activity of NK cells, many immunotherapies aimed at increasing their infiltration into tumors are being studied [26].

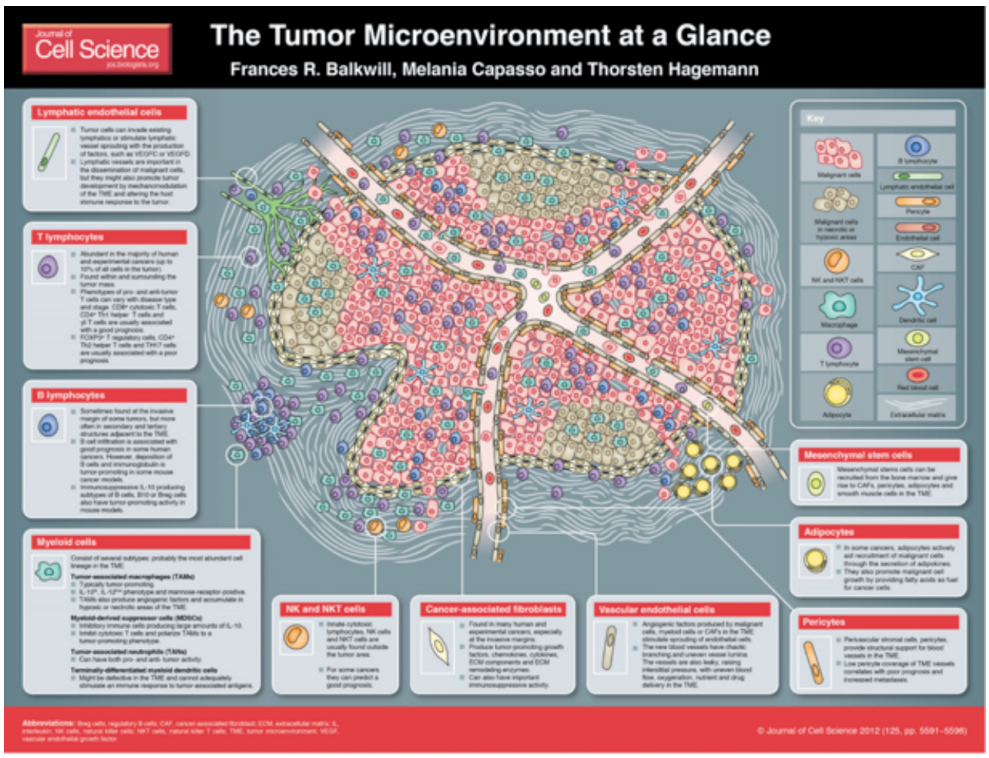

Fig. 1. Schematic representation of components involved in tumor microenvironment. Reproduced with permission from Balkwill et al. Journal of Cell Science 125, 5591–5596.

NON-CELLULAR COMPONENTS

VEGF

The VEGF family currently comprises seven members with a common VEGF homology domain. VEGF-A, the most potent angiogenic member, is a 34- to 42-kDa, dimeric, disulfide-bound glycoprotein. In normal tissues, the highest levels of VEGF-A mRNA are found in adult lung, kidney, heart, and adrenal gland. Lower, but still readily detectable, quantities of VEGF-A transcript levels occur in liver,

spleen, and gastric mucosa. VEGF-A exists in at least seven homodimeric isoforms. The monomers consist of 121, 145, 148, 165, 183, 189, or 206 amino acids. The primary VEGF-A transcript derives from a single VEGF-A gene, coding for eight exons [27]. The amino acids encoded by exons 1 to 5 and 8 are conserved in all isoforms except VEGF-A_{148}, whereas variable alternative splicing occurs in exons 6 and 7, which encode two distinct heparin-binding domains. The presence or absence of these domains influences solubility and receptor binding. The heparin-binding domain encoded by exon 6 determines binding to the extracellular matrix, and therefore isoforms containing this domain (VEGF-A_{145}, VEGF-A_{189}, and VEGF-A_{206}) are bound tightly to cell surface heparin-containing proteoglycans in the extracellular matrix, whereas those lacking the domain are diffusible. VEGF-A_{165}, which contains only one heparin-binding region encoded by exon 7, is moderately diffusible, and VEGF-A_{121}, which lacks the domains encoded by both exons 6 and 7, is highly diffusible [28]. As already discussed, VEGF is able to promote the growth and migration of vascular endothelial cells derived from arteries, veins, and even lymphatics. It is also responsible for the chaotic growth of vessel network that characterizes tumors and prevents drugs from diffusing correctly. Therefore, many anti-VEGF therapies, that prevent the binding of the ligand to its receptors, are under investigation.

TNFα

TNFα is a major inflammatory cytokine with a controversial history. It was

identified for its ability to induce rapid haemorrhagic necrosis of experimental cancers, but, by paradox, after more intense studies it showed a tumor-promoting effect [29]. TNFα is a TAM-derived pro-inflammatory cytokine and it is an important effector molecule in $CD8^+$ T cell and NK cells killing of immunogenic tumour cells. However, at low doses it is also able to sustain tumor growth because of its ability to induce proangiogenic functions, to promote the expression of matrix metalloproteinases (MMP) and endothelial adhesion molecules, and to cause DNA damage via reactive oxygen, the overall effect of which is promotion of tumor-related processes. Moreover, in some cancer types, it is able to induce its production constitutively to sustain tumor growth even more. Nowadays, there is a stronger evidence that cancer-related inflammation may help proliferation and survival of malignant cells, therefore, when produced by malignant or host cells in the tumour microenvironment, TNFα is a major mediator of such inflammation. Not only malignant cells are able to produce TNFα in the tumour microenvironment, but as already mentioned, also myeloid cells and macrophages.

Integrins

Integrins are adhesion molecules expressed in almost any cellular component of tumor microenvironment. They are formed by α and β subunits with different binding specificities and signalling pathways and contribute to regulate cell survival, migration and adhesion [30]. Being responsible of cell-to-cell adhesion they have a critical role in the interaction between cancer cells and the surrounding

matrix. Indeed, malignant cells are able to express their ligand and anchor to the extracellular matrix. The presence of pro-metastatic integrins has also been documented to favor tumor formation and progression and a strong interaction between them and VEGF/VEGFR have been documented [31]. Indeed αvβ3- and α5β1-integrins increase new vessel formation, whereas other subtypes can bind fibronectin. These interactions and the formation of extracellular matrix recruit macrophages and fibroblast that as mentioned above, contribute to the production of tumor promoting factors.

Other growth factors

These are only some of the many soluble factors involved in tumor microenvironment. Others that should be mentioned are plancetal growth factor (PIGF), which is a member of the VEGF family and is able to bind VEGFRs with similar pro-angiogenic activities. PlGF is present in low levels in normal tissue, contributing to the angiogenic switch in pregnancy, wound healing and ischemic conditions. It may be expressed by tumors inducing angiogenesis, lymphangiogenesis, and tumor cell motility. Insulin-like growth factors (IGF-1 and IGF-2) are proteins with high sequence similarities with insulin. It is important in regulating physiological processes, but can produced in tumor microenvironment promoting cell proliferation, especially in metastatic cancer. Indeed, IGF inhibiton can reduce tumor growth and metastatization. Finally, also epidermal growth factor (EGF) and its receptors are expressed by cancer, inducing survival and

proliferation [1].

TARGETING TUMOR MICROENVIRONMENT

The concept of tumor microenvironment gained more and more importance during the recent years due to the possibility to develop a wide range of therapeutic approaches based on targeted anticancer drugs. They consist in molecules able to reduce or block the growth and spread of cancer by interfering with specific molecular targets expressed by cancer cells or the microenvironment [32]. Nowadays, they are the cornerstone of personalized medicine and are currently the focus of much anticancer drugh development. Many targeted cancer therapies have been approved by the Food and Drug Administration (FDA) to treat specific types of cancer. Others are being studied in clinical trials, and many more are in preclinical testing. However, for these therapies to be effective, it is required that their target is present in the lesions and/or overexpressed. Unfortunately, different tumour cells can show distinct morphological and phenotypic profiles, and this phenomenon is know as intra- or inter-tumor heterogeneity [33]. In such cases, in the same patient, the same targeted drug may be effective only in a fraction of tumor lesions, leading to waste of money, time and with potential, and unpleasant, side-effects. This is because the drug will select only resistant cancer cell clones and the physician will have to adjust the therapy accordingly, with no real benefits. Sometimes, it may even occur that cancer cells gradually lose their peculiar

markers during their dedifferentiation process, causing specific targeted drugs to be uneffective.

Although a partial heterogeneity may characterize also the microenvironment, in general, its common features suggest that it is possible to target its cellular or non-cellular components with applications across different tumor types and could also complement other treatment options. Therefore, its lack of innate plasticity, may allow companies to develop new targeted drugs that could be used in a very broad range of tumor types. Clinical trials with antibodies, ex-vivo cultured immune cells and other immunotherapy approaches, for instance, are being conducted in several types of advanced cancer [34]. Angiogenesis and multi-targeted tyrosine kinase inhibitors (TKIs) that block the VEGF signaling pathway, have been already approved for clinical use [35]. The tumor stroma might also be a target in order to increase the access of drugs to the tumor. Finally, since cancer-related inflammation is being intensively studied, we are about to translate knowledge into clinical trials with the use of agents already available for inflammatory diseases [36].

IMAGING OF TUMOR MICROENVIRONMENT

In a pre-clinical setting, to assess treatment effect of targeted drugs and to characterize the markers expressed in tumor lesions, postmortem histological techniques are mainly used. However, they are not repeatable over time and obviously non applicable at all in humans. Therefore, imaging, and in particular

nuclear medicine, may play an important role. Indeed, the many markers expressed by cancer cells or present in tumor microenvironment can be targeted also for diagnostic purposes using radiolabelled probes. Indeed, it would be possible to develop a whole set of radiopharmaceuticals against each target. This will allow a more accurate diagnosis and an in vivo characterization of each tumor lesion. Moreover, it would be possibile to non-invasively monitor, at both preclinical and clinical stages, the efficacy of new anti-cancer drugs and to select the best therapy, or combination of therapies, for each patient. Similarly to targeted therapies, diagnostic radiopharmaceuticals bind specific targets expressed by cancer cells. However, some cancers undergo a dedifferentiation process losing their initial phenotype. For example, thyroid cancer, in 10% of affected patients, progresses into metastatic disease with loss of some typical biological characteristics of differentiated thyroid cancer. These poorly differentiated (PDTC) or undifferentiated (UDTC) thyroid cancers are life-threatening pathologies with poor clinical outcome and no efficient therapies to date [37]. This is because cancer cells during de-differentiation lose the NIS symporter, not being able to uptake radioiodine anymore, [38] and become more aggressive. In these cases, it is important to find new specific targets expressed either by cancer cells or microenvironment. Indeed, VEGF and VEGFR, somatostatin and other markers have been correlated with the degree of cell differentiation, revealing that PDTC and UDTC are highly heterogeneous pathologies that need to be well characterized in vivo to plan the most appropriate therapy [39, 40]. Therefore, in this cancer and

in many others, the approach has to be widened focusing not only on cancer cells, but also on the microenvironment that surrounds them. To this purpose many attempts have been made to develop suitable radiopharmaceuticals to image angiogenetic processes, immune cells and soluble factors, adhesion molecules and other component of the microenvironment and some of the most relevant have been reported in the present thesis.

Imaging VEGF and VEGFRs

Being one of the major responsible of neoangiogenesis that drives tumor growth, VEGF has focused the attention of the scientific world. The most studied splice variants are $VEGF_{121}$, freely soluble, and $VEGF_{165}$, $VEGF_{189}$, $VEGF_{206}$ that are mainly located in the extra cellular matrix [41]. This results in a particularly high concentration in the tumor microenvironment. Moreover, it is well known that VEGFR are overexpressed on the tumor vasculature, therefore, many antioangiogenic therapies are under investigation and it would be very important to develop a suitable radiopharmaceutical to image angiogenesis and monitor the efficacy of novel drugs [42]. In the literature there are many reports on the use of radiolabelled $VEGF_{165}$ or $VEGF_{121}$ radiolabelled with either ^{99m}Tc or ^{123}I in vitro and in vivo in various tumor cell lines [43-48]. Among them, Blankenberg et al. developed a C-tagged VEGF radiolabelled with ^{99m}Tc to monitor the efficacy of cyclophosphamide against a mammary carcinoma [49]. Their results suggest that such radiopharmaceutical is able to visualize the vasculature surrounding the tumor

and to monitor the efficacy of the administered drug. The advantage of using the VEGF itself is its natural high binding affinity for its receptors. However, many authors reported a very high uptake by major organs, especially liver and kidneys, resulting in low uptake by the tumors [50]. Some, hypothesized that ^{99m}Tc labelling with HYNIC was one of the main reasons of such high uptake by kidneys and other groups tried to radiolabel $VEGF_{121}$ with positron emitting isotopes (^{64}Cu, ^{68}Ga) for PET imaging [51, 52]. They obtained promising results and rapid and specific uptake by tumor xenografts in mice, but the kidneys remained the dose-limiting organ because of its high expression of VEGFR-1. Some groups presented promising results also in thyroid cancer, unfortunately confirming a high background by major organs [53]. Another approach to image angiogenesis is based on the use of the radiolabelled mAb bevacizumab [54]. Bevacizumab is a recombinant humanized monoclonal antibody that binds VEGF, approved by the FDA for treatment of metastatic cancers, glioblastoma and non-small cell lung cancer. The binding of antibody to soluble and/or bound to extracellular matrix VEGF, prevents its binding to tyrosine-kinase receptor, inhibiting the angiogenesis. It has been radiolabelled with both SPECT and PET radionuclides with promising results in colorectal and ovarian cancer [55-60].

Imaging tumor infiltrating NK cells

Since NK cells are known to infiltrate tumors, attempts have been made to radiolabel cells and follow their trafficking into tumors. This approach may be

useful to both image lesion and monitor the efficacy of novel immunotherapies based on the use of the very same NK cells. In the literature there are mainly reports of ^{111}In-oxine radiolabelled NK cells used in patients with metastatic renal carcinoma. The authors reported the uptake of labelled cells by lesions, confirmed by ^{18}[F]-FDG-PET. However, they also reported a high circulating activity by released ^{111}In [61]. Similar results were obtained in patients affected by melanoma or colorectal cancer [62, 63]. NK cells have been also labelled with both ^{11}C and ^{18}F and used in pre-clinical studies in mice. Melder et al. incubated murine NK cells with ^{11}C-methyl iodide and performed whole body PET imaging in a fibrosarcoma model, demonstrating an increased signal of activated NK cells in the tumor when compared with non-activated lymphocyte controls [64]. Similarly, Meier et al radiolabelled the cells with [^{18}F]-FDG and injected them into HER2/neu positive mouse xenografts with increased radioactivity in tumors after 60 minutes confirmed by ex vivo autoradiography [65]. In addition to other techniques, like optical and magnetic resonance imaging, a novel approach has been proposed and reported in the chapter 4 of the present thesis. It is based on the use of a radiolabelled mAb against the CD56 antigen expressed by NK cells. The radiopharmaceutical is able to bind to its ligand in vivo, withouth the need of in vitro manipulations of withdrawn cells. The radiopharmaceutical was able to image NK cells infiltrating undifferentiated thyroid cancer tumors in mice with a high T/B ratio [66]. Therefore, it is a promising tool to monitor NK cell trafficking into tumors.

Radiolabelled integrins

Integrin a_vb_3 has been confirmed in various malignant tumors with high density, and it is essential for cell migration and invasion and plays an important role in tumor angiogenesis. Ligands bearing RGD (Arg-Gly-Asp) peptide have a high affinity and specificity for integrin a_vb_3, especially cyclic RGD dimers with PEG4 linkers [67]. Unlike ^{18}F-FDG PET/CT as a diagnosis-only modality, integrin a_vb_3 imaging by radiolabelled RGD peptide provides a specific method for visualizing tumor angiogenesis and a therapeutic target for antiangiogenetic and anti-integrin drugs. The RGD molecules ^{99m}Tc-NC100692, ^{18}F-P-PRGD2, ^{18}F-AH111585, and ^{18}F-galacto-RGD have already been used in the molecular imaging of cancer cell lines, animal models, or clinical cancer patients (including in murine osteosarcoma, human colon and renal adenocarcinoma, rat pancreatic tumors, ovarian carcinoma, human breast carcinoma, human glioblastoma, and human melanoma) to image tumor angiogenesis and metastasis with PET or SPECT [68-71]. The integrin a_vb_3 expression level on tumor cell membranes correlates well with the RGD radiotracer tumor uptake on scintigraphy imaging. Therefore, Zhao et al studied the possibility to study patients affected by iodine refractory DTC using ^{99m}Tc-PEG(4)-E[PEG(4)-c(RGDfK)](2) ((99m)Tc-3PRGD2) scintigraphy [72]. They obtained promising results being able to visualize all the studied lesions, concluding that the technique was promising to diagnose RAI-refractory metastases and for antiangiogenic therapy decision-making. The study was

followed-up by Weiwei et al, that performed ^{18}F-FDG and ^{18}F-AIF-NOTA-PRGD2 PET/CT in 20 DTC patients [73]. Even though both glucose metabolism and integrin expression were thought to be associated with tumor aggressiveness, no significant correlation was found between the two radiopharmaceuticals. In addition, the mean SUV from ^{18}F-AIF-NOTA-PRGD2 PET/CT scans in both malignant and benign lesions was significantly lower than ^{18}F-FDG. Therefore they concluded that even if the diagnostic value of ^{18}F-AIF-NOTA-PRGD2 was lower than FDG, it can still allow to select or monitor patients to be treated with antiangiogenic drugs. At the moment, a proof of concept trial is being performed in up to 30 patients with various kinds of cancer, including differentiated thyroid cancer.

Radiolabelled EGF

EGF is a single chain polypeptide of 53 amino acids. It acts on different cell types both in vitro and in vivo [74] and promotes proliferation, survival, and differentiation through transmembrane receptor EGF-R. EGF-R is a member of ErbB family of receptors, exposed on the extracellular side of the membrane and activated by binding of its ligands: EGF binding on monomeric form of EGF-R, causes the dimerization of EGF-R and the activation of intracellular protein-tyrosine kinase activity [75]. The signaling cascade conduces to DNA synthesis and consequent cellular proliferation. Mutations that lead to EGF-R overexpression or its upregulation have been associated with a number of cancers

and in particular with lung cancer. The epidermal growth factor receptor (EGFR) is overexpressed on the surface of several cancer cells. Viehweger et al studied a peptide-based imaging probe targeting the EGFR and performed preclinical in vitro studies to on FaDu and A431 cell lines [76]. However, despite a dissociation constant of 10 nM, the probe showed to be biased or partial allosteric agonist of the EGFR and to be a non-competitive antagonist.

Imaging IGF receptors

Many types of cancers may overexpress the insulin-like growth factor-1 receptor (IGF1R) that was reported to be associated with resistance to IGF-1R targeted therapy. In particular, several studies reported that IGF-1R is expressed in thyroid cancer and plays an important role in proliferation and metastatization [77]. Mitran et al performed a study on the development of a novel ^{99m}Tc-labelled-affibody targeting the IGF1R for the selection of patients that could respond to therapy. They tested two distinct compound containing In vitro the radiopharmaceutical was able to bind to IGF1R^{+} cell lines of prostate and breast cancer [78]. They also performed in vivo studies on nude mice bearing tumor xenografts of the same cell lines reporting high T/B ratios, but also high liver or kidneys uptake. Therefore, more studies are ongoing to reduce signal from major organs due to natural biodistribution of those radiopharmaceuticals.

Targeting cancer-related inflammation

Cancer-related inflammation has been defined the seventh hallmark of cancer and, recent data suggest that it is responsible of the genetic instability that lead to tumor heterogeneity. Therefore, in addition to immune cells, targeting chemokines and other signaling molecules in the tumor microenvironment is a promising approach. Among the available targets, TNFα, IL-1, IL-6 and CXCL8 have proved to be implicated in cancer growth and metastatization, but the list is very long [36] Given the availability of radiopharmaceuticals already used in inflammatory disease, their use in imaging cancer-related inflammation could be explored. This would allow to apply already available targeted therapies from inflammatory disorder into cancer.

Imaging PIGF

RO5323441 is a humanized monoclonal antibody against PlGF-1 and PlGF-2. It has been used in a phase I clinical trial as PIGF inhibitor in tumor microenvironment. Patients showed stable disease at different dose levels, but, ano maximal tolerated dose was defined, limiting phase II studies. This is a good example where a non-invasive tool to evaluate PIGF expression in lesions is needed. Therefore, the same antibody has been radiolabelled with ^{111}In or ^{89}Zr, and tested in mice to image PIGF in tumor microenvironment. Results showed that radiolabelled RO5323441 tumor uptake was time-, dose-, and PlGF-dependent,

supporting the feasibility of implementing the use ^{89}Zr-RO5323441 with PET scanning for clinical studies [79].

OUTLINE OF THIS THESIS

Targeted drugs are promising therapeutic tools against tumors. However, overexpression of their target is required and sometimes tumor intra- and inter-tumor heterogeneity may limit drug development and the therapy decision-making. In this scenario, imaging techniques may be of great help. In particular, nuclear medicine is in continuos evolution and every year more radiopharmaceutical have been developed to image several pathological and physiological processes. Given the wide range of targets present in the tumor microenvironment, the development of specific radiopharmaceutical may provide researchers or clinicians fundamental tools for tumor imaging, in vivo characterization of cancer lesions and evaluation of the efficacy of therapeutic drugs for therapy decision making. In the present thesis we report four different approaches to target and image tumor specific antigens and microenvironment.

In chapter 2 the thyrotropin receptor (TSHR) has been chosen as a suitable target for imaging of non-iodine uptaking thyroid cancer metastases. To this purpose, a promising radiopharmaceutical was developed radiolabelling the superagonist rhtSH analogue TR1401. It was tested in vitro and in vivo proving a high affinity for its receptor and the capacity to image NIS-negative tumors.

In chapter 3 a radiolabelled anti-TNFα mAb was used to evaluate the presence of the cytokine in granulomatous lesions and investigate the possibility to use this radiopharmaceutical to select candidate patients for infliximab therapy. Being granulomas benign tumors, this is a practical example of possible approaches to image factors involved in microenvironment.

In chapter 4 a similar approach is reported, but this time, the target was an antigen expressed by NK cells to image their trafficking into tumors. The radiopharmaceutical of choice was a radiolabelled anti-CD56 mAb that has proved to successfully image tumor infiltrating NK cells in nude mice with an ARO xenograft in the right thigh. This strategy will allow to non-invasively evaluate at both pre-clinical and clinical stages the efficacy of new immunotherapies that aim at increasing NK infiltration into tumors. could allow to follow the efficacy of new immunotherapies, monitoring.

Chapter 6 describes a similar approache, but the target is the VEGFR expressed by both endothelial and tumor cells. Since angiogenesis is a key process that leads to tumor growth and metastatization many antiangiogenic therapies try to block the VEGF/VEGFR pathways either by sequestering the ligand or blocking the signal transduction. The use of a radiolabelled $VEGF_{165}$ analogue to image angiogenesis in tumors from different cell lines was investigated. The radopharmaceutical

proved to be a promising tool for non-invasive evaluation of the presence of VEGFRs, but the high production of endogenous ligand by both endothelial and tumor cells may hamper the possibility to image the receptors.

At the end of the thesis conclusion and future perspectives are described in chapter 6 emphasizing the need of an accurate personalized medicine. Elucidating the role and discovering new targets involved in tumor microenvironment may help in a better understanding of tumor growth and metastatization. Moreover, it would be possible to develop new radiopharmaceuticals targeting tumor specific and microenviromental targets to 1) non-invasively characterize lesions in vivo, 2) evaluate therapy efficacy, 3) select the best therapy in each patient and 4) develop new targeted drugs.

REFERENCES

1. Goubran HA, Kotb RR, Stakiw J, Emara ME, Burnouf T. Regulation of tumor growth and metastasis: the role of tumor microenvironment. Cancer Growth Metastasis 2017;7:9-18.
2. Nelson CM, Bissell MJ. Of extracellular matrix, scaffolds, and signaling: tissue architecture regulates development, homeostasis, and cancer. Ann Rev Cell Dev Biol. 2006;22:287–309.
3. Erler JT, Bennewith KL, Cox TR, Lang G, Bird D, Koong A et al. Hypoxia-induced lysyl oxidase is a critical mediator of bone marrow cell recruitment to form the pre-metastatic niche. Cancer cell 2009;15:35-44.
4. Zeng J, Xie K, Wu H, Zhang B, Huang C. Identification and functional study of cytokines and chemokines involved in tumorigenesis. Comb Chem High Throughput Screen 2012;15:276-85 .
5. McDonald DM, Baluk P. Significance of blood vessel leakiness in cancer. Cancer Res 2002;62:5381–5385.
6. Hashizume H, Baluk P, Morikawa S, McLean JW, Thurston G, Roberge S et al. Openings between defective endothelial cells explain tumor vessel leakiness. Am J Pathol 2000;156:1363–1380.
7. Moschetta M, Mishima Y, Sahin I, Mainer S, Glavey S, Vacca A et al. Role of endothelial progenitor cells in cancer progression. Biochim Biophysi Acta 2014;1846:26-39.

8. Folkman J. Role of angiogenesis in tumor growth and metastasis. Semin Oncol 2002;29(6 Suppl 16):15-8.

9. Maertens L, Erpicum C, Detry B, Blacher S, Lenoir B, Carnet O et al. Bone marrow-derived mesenchymal stem cells drive lymphangiogenesis. PloS One 2014;9:e106976.

10. Goel HL, Mercurio AM. VEGF targets the tumor cell. Nat Rev Cancer 2013;13:871-82.

11. Olsson AK, Dimberg A, Kreuger J, Claesson-Welsh L. VEGF receptor signalling – in control of vascular function. Nat Rev Mol Cell Biol 2006;7:359-71.

12. Maru Y, Yamaguchi S, Shibuya M. Flt-1, a receptor for vascular endothelial growth factor, has transforming and morphogenic potentials. Oncogene 1998;16:2585-95.

13. Gray J, Evans N, Taylor B, Rizzo J, Walker M. State of the evidence: the connection between breast cancer and the environment. Int J Occup Environ Health 2009;15:43–78.

14. Wyckoff J, Wang W, Lin EY, Wang Y, Pixley F, Stanley ER et al. A paracrine loop between tumor cells and macrophages is required for tumor cell migration in mammary tumors. Cancer Res 2004;64:7022–7029.

15. Wathelet N, Moser M. Role of dendritic cells in the regulation of antitumor immunity. Oncoimmunol 2013;2:e23973.

16. Campbell DJ. Control of Regulatory T Cell Migration, Function, and Homeostasis. J Immunol. 2015;195:2507-13

17. Baay M, Brouwer A, Pauwels P, Peeters M, Lardon F. Tumor cells and tumor-associated macrophages: secreted proteins as potential targets for therapy. Clini Dev Immunol 2011;2011:565187.

18. Komohara Y, Ohnishi K, Kuratsu J, Takeya M. Possible involvement of the M2 anti-inflammatory macrophage phenotype in growth of human gliomas. J Pathol 2008;216: 15–24.

19. Ryder M, Ghossein RA, Ricarte-Filho JC, Knauf JA, Fagin JA. Increased density of tumor-associated macrophages is associated with decreased survival in advanced thyroid cancer. Endocr Relat Cancer 2008;15:1069-74.

20. Bingle L, Brown NJ, Lewis CE. The role of tumour-associated macrophages in tumour progression: implications for new anticancer therapies. J Pathol 2002;196:254–265.

21. Caronni N, Savino B, Bonecchi R. Myeloid cells in cancer-related inflammation. Immunobiology 2014;pii: S0171-2985:00192-2.

22. Baume DM, Robertson MJ, Levine H, Manley TJ, Schow PW, Ritz J. Differential responses to interleukin 2 define functionally distinct subsets of human natural killer cells. Eur J Immunol 1992;22:1-6.

23. Kärre K, Ljunggren HG, Piontek G, Kiessling R. Selective rejection of H-2-deficient lymphoma variants suggests alternative immune defence strategy. Nature 1986;319:675-8.

24. Dighe AS, Richards E, Old LJ, Schreiber RD. Enhanced in vivo growth and resistance to rejection of tumor cells expressing dominant negative IFN gamma receptors. Immunity 1994;1:447-56.
25. Schott M. Immunesurveillance by dendritic cells: potential implication for immunotherapy of endocrine cancers. Endocr Relat Cancer 2006;13:779-95.
26. Cheng M, Chen Y, Xiao W, Sun R, Tian Z. NK cell-based immunotherapy for malignant diseases. Cell Mol Immunol 2013;10: 230–252.
27. Tischer E, Mitchell R, Hartman T, Silva M, Gospodarowicz D, Fiddes JC et al. The human gene for vascular endothelial growth factor. Multiple protein forms are encoded through alternative exon splicing. J Biol Chem 1991;266:11947-54.
28. Hoeben A, Landuyt B, Highley MS, Wildiers H, Van Oosterom AT, De Bruijn EA. Vascular endothelial growth factor and angiogenesis. Pharmacol Rev 2004;56:549-80.
29. Balkwill F. Tumour necrosis factor and cancer. Nature Reviews. Cancer. 2009;9:361-71.
30. Hood JD, Cheresh DA. Role of integrins in cell invasion and migration. Nat Rev Cancer 2002;2:91–100.
31. Soldi R, Mitola S, Strasly M, et al. Role of avb3 integrin in the activation of vascular endothelial growth factor receptor-2. EMBO J 1999;18:882–892.
32. Pérez-Herrero E, Fernández-Medarde A. Advanced targeted therapies in cancer: Drug nanocarriers, the future of chemotherapy. Eur J Pharm

Biopharm. 2015 Jun;93:52-79.

33. Sun XX, Yu Q. Intra-tumor heterogeneity of cancer cells and its implications for cancer treatment. Acta Pharmacol Sin. 2015 Sep 21
34. Mellman I, Coukos G, Dranoff G. Cancer immunotherapy comes of age. Nature. 2011;480(7378):480-9.
35. Carmeliet P, Jain RK. Molecular mechanisms and clinical applications of angiogenesis. Nature. 2011;473(7347):298-307.
36. Candido J, Hagemann T. Cancer-related inflammation. J Clin Immunol 2013;33 Suppl 1:S79-84. Epub 2012 Dec 9.
37. Patel KN, Shaha AR. Poorly differentiated and anaplastic thyroid cancer. Cancer Control 2006;13:119-28.
38. Spitzweq C, Bible KC, Hofbauer LC, Morris JC. Advanced radioiodine-refractory differentiated thyroid cancer: the sodium iodide symporter and other emerging therapeutic targets. Lancet Diabetes Endocrinol 2014;2:839-42.
39. De Jong M, Breeman WA, Kwekkeboom DJ, Valkema R, Krenning EP. Tumor imaging and therapy using radiolabeled somatostatin analogues. Acc Chem Res 2009;42:873-80.
40. Krajewska J, Jarzab B. Novel therapies for thyroid cancer. Expert Opin Pharmacother 2014;15;2641-52.
41. Neufeld G, Cohen T, Gengrinovitch S, Poltorak Z. Vascular endothelial growth factor (VEGF) and its receptors. FASEB J 1999;13:9–22.

42. Perri F, Pezzullo L, Chiofalo MG, Lastoria S, Di Gennaro F, Scarpati G et al. Targeted therapy: A new hope for thyroid carcinomas. Crit Rev Oncol Hematol 2014 Nov 1. pii: S1040-8428(14)00172.

43. Dijkgraaf I, Boerman OC. Molecular imaging of angiogenesis with SPECT. Eur J Nucl Med Mol Imaging. 2010;37 Suppl 1:S104-13.

44. Li S, Peck-Radosavljevic M, Kienast O, Preitfellner J, Hamilton G, Kurtaran A, et al. Imaging gastrointestinal tumours using vascular endothelial growth factor-165 (VEGF165) receptor scintigraphy. Ann Oncol 2003;14:1274–7.

45. Yoshimoto M, Kinuya S, Kawashima A, Nishii R, Yokoyama K, Kawai K. Radioiodinated VEGF to image tumor angiogenesis in a LS180 tumor xenograft model. Nucl Med Biol 2006;33:963–9.

46. Chan C, Sandhu J, Guha A, Scollard DA, Wang J, Chen P, et al. A human transferrin-vascular endothelial growth factor (hnTf- VEGF) fusion protein containing an integrated binding site for (111)In for imaging tumor angiogenesis. J Nucl Med 2005;46: 1745–52.

47. Blankenberg FG, Backer MV, Levashova Z, Patel V, Backer JM. In vivo tumor angiogenesis imaging with site-specific labeled (99m)Tc-HYNIC-VEGF. Eur J Nucl Med Mol Imaging 2006;33:841–8.

48. Li S, Peck-Radosavljevic M, Kienast O, Preitfellner J, Havlik E, Schima W et al. Iodine-123-vascular endothelial growth factor-165 (123I-VEGF165). Biodistribution, safety and radiation dosimetry in patients with pancreatic carcinoma. Q J Nucl Med Mol Imaging 2004;48:198-206.

49. Blankenberg FG, Mandl S, Cao YA, O'Connell-Rodwell C, Contag C, Mari C, et al. Tumor imaging using a standardized radiolabeled adapter protein docked to vascular endothelial growth factor. J Nucl Med 2004;45:1373–80.

50. Lu E, Wagner WR, Schellenberger U, Abraham JA, Klibanov AL, Woulfe SR, et al. Targeted in vivo labeling of receptors for vascular endothelial growth factor: approach to identification of ischemic tissue. Circulation 2003;108:97–103.

51. Haubner R, Beer AJ, Wang H, Chen X. Positron emission tomography tracers for imaging angiogenesis. Eur J Nucl Med Mol Imaging 2010 Aug;37 Suppl 1:S86-103.

52. Cai W, Chen K, Mohamedali KA, Cao Q, Gambhir SS, Rosenblum MG, et al. PET of vascular endothelial growth factor receptor expression. J Nucl Med 2006;47:2048–56

53. Galli F, Manni I, Piaggio G, Dierckx RAJO, Signore A. Radiolabelling of VEGF analogues to image tumor angiogenesis. Q J Nucl Med Mol Imaging 2014;58:suppl. 1.

54. Nagengast WB, de Vries EG, Hospers GA, et al. In vivo VEGF imaging with radiolabeled bevacizumab in a human ovarian tumor xenograft. I Nucl Med 2007;48:1313-9.

55. Nagengast WB, Hooge MN, van Straten EM, et al. VEGF-SPECT with ^{111}In-bevacizumab in stage III/IV melanoma patients. Eur J Gancer 2011;47:1595-602.

56. Hosseinimehr SJ, Orlova A, Tolmachev V. Preparation and in vitro evaluation of ^{111}In-CHX-A"-DTPA-labeled anti-VEGF monoclonal antibody bevacizumab. Hum Antibodies 2010;19:107.

57. Paudyal B, Paudyal P, Oriuchi N, et al. Positron emission tomography imaging and biodistribution of vascular endothelial growth factor with 64Cu-labeled bevacizumab in colorectal cancer xenografts. Cancer Sci 2011;102:117.

58. Ashrafi SA, Hosseinimehr SJ, Varmira K, Abedi SM. Radioimmunotherapy with ^{131}I-bevacizumab as a specific molecule for cells with overexpression of the vascular endothelial growth factor. Cancer Biother Radiopharm 2012;27:420-5.

59. Gaykema SB, Schröder CP, Vitfell-Rasmussen J, Chua S, Oude Munnink TH, Brouwers AH et al.. 89Zr-trastuzumab and 89Zr-bevacizumab PET to evaluate the effect of the HSP90 inhibitor NVP-AUY922 in metastatic breast cancer patients. Clin Cancer Res. 2014;20:3945-54.

60. Van Asselt SJ, Oosting SF, Brouwers AH, Bongaerts AH, de Jong JR, Lub-de Hooge MN et al. Everolimus Reduces 89Zr-Bevacizumab Tumor Uptake in Patients with Neuroendocrine Tumors. J Nucl Med. 2014;55:1087-1092.

61. Meller B, Frohn C, Brand JM, Lauer I, Schelper LF, von Hof K et al. Monitoring of a new approach of immunotherapy with allogenic ^{111}In-labelled NK cells in patients with renal cell carcinoma. Eur J Nucl Med Mol Imaging 2004; 31;403-407.

62. Matera L, Galetto A, Bello M, Baiocco C, Chiappino I, Castellano G et al. In vivo migration of labeled autologous natural killer cells to liver metastases in patients with colon carcinoma. J Transl Med 2006;4;49.

63. Schäfer E, Dummer R, Eilles C, Börner W, Martin R, Rendl J, Burg G. Imaging pattern of radiolabelled lymphokine-activated killer cells in patients with metastatic malignant melanoma. Eur J Nucl Med 1991;18:106-10.

64. Melder RJ, Brownell AL, Shoup TM, Brownell GL, Jain RK. Imaging of activated natural killer cells in mice by positron emission tomography: preferential uptake in tumors. Cancer Res 1993;53;5867-5871.

65. Meier R, Piert M, Piontek G, Rudelius M, Oostendorp RA, Senekowitsch-Schmidtke R et al. Tracking of [18F]FDG-labeled natural killer cells to HER2/neu-positive tumors. Nucl Med Bio 2008; 35;579-588.

66. Galli F, Histed S, Aras O. NK cell imaging by in vitro and in vivo labelling approaches. Q J Nucl Med Mol Imaging 2014;58:276-83.

67. Beer AJ, Kessler H, Wester HJ, Schwaiger M. PET imaging of integrin avb3 expression. Theranostics 2011;1:48–57.

68. Battle MR, Goggi JL, Allen L, Barnett J, Morrison MS. Monitoring tumor response to antiangiogenic sunitinib therapy with 18F-fluciclatide, an 18F-labeled avb3-integrin and avb5-integrin imaging agent. J Nucl Med 2011;52:424–430.

69. Kenny LM, Coombes RC, Oulie I, Contractor KB, Miler M, et al. Phase I trial of the positron-emitting Arg-Gly-Asp (RGD) peptide radioligand 18F-

AH111585 in breast cancer patients. J Nucl Med 2008;49:879–886.

70. Zhu Z, Miao W, Li Q, Dai H, Ma Q, et al. 99mTc-3PRGD2 for integrin receptor imaging of lung cancer: a multicenter study. J Nucl Med 2012;53: 716–722.

71. Winick J. A proof-of-concept study to assess the ability of [18F] AH-111585 PET imaging to detect tumours and angiogenesis. ClinicalTrials.gov 2007. US National Institutes of Health; Nov 28, 2007.

72. Zhao D, Jin X, Li F, Liang J, Lin Y. Integrin avb3 imaging of radioactive iodine–refractory thyroid cancer using 99mTc-3PRGD2. J Nucl Med 2012;53:1872–1877.

73. Cheng W, Wu Z, Liang S, Fu H, Wu S, Tang Y et al. Comparison of 18F-AIF-NOTA-PRGD2 and 18F-FDG uptake in lymph node metastasis of differentiated thyroid cancer. PLoS One 2014;9:e100521.

74. Fisher DA, Lakshmanan J. Metabolism and effects of epidermal growth factor and related growth factors in mammals. Endocr Rev 1990;11:418–442.

75. Yarden Y, Schlessinger J. Epidermal growth factor induces rapid, reversible aggregation of the purified epidermal growth factor receptor. Biochemistry 1987;26:1443–1451.

76. Viehweger K, Barbaro L, Garcia KP, Joshi T, Geipel G, Steinbach J et al. EGF receptor-targeting peptide conjugate incorporating a near-IR fluorescent dye and a novel 1,4,7-triazacyclononane-based (64)Cu(II) chelator assembled via click chemistry. Bioconjug Chem 2014;25:1011-22.

77. da Cunha Santos G, Shepherd FA, Tsao MS. EGFR mutations and lung cancer. Annu Rev Pathol 2011;6:49-69.

78. Mitran B, Altai M, Hofstrom C, Honarvar H, Sandstrom M, Orlova A et al. Evaluation of 99mTc-Z-IGF1R:4551-GGGC affibody molecule, a new prove for imaging insulin-like growth factor receptor expression. Amino acids 2014;27.

79. Oude Munnink TH, Tamas KR, Lub-de Hooge MN, Vedelaar SR, Timmer-Bosscha H, Walenkamp AM et al. Placental growth factor (PlGF)-specific uptake in tumor microenvironment of 89Zr-labeled PlGF antibody RO5323441. J Nucl Med. 2013;54:929-35.

Chapter 2

---

^{99m}Tc-labeled-rhTSH analogue (TR1401) for imaging poorly differentiated metastatic thyroid cancer

Filippo Galli,[1,2] Isabella Manni,[3] Giulia Piaggio,[3] Lajos Balogh,[4] Bruce D. Weintraub,[5] Mariusz W. Szkudlinski,[5] Valerie Fremont[5], Rudi A.J.O. Dierckx[2], and Alberto Signore[1,2]

[1]Nuclear Medicine Unit, Department of Medical-Surgical Sciences and of Translational Medicine, Faculty of Medicine and Psychology, ''Sapienza'' University of Rome, Rome, Italy.
[2]Department of Nuclear Medicine and Molecular Imaging, University Medical Centre Groningen, University of Groningen, Groningen, The Netherlands.
[3]Molecular Oncogenesis Laboratory, Experimental Oncology Department, Regina Elena National Cancer Institute, Rome, Italy.
[4]National ''Frederic Joliot Curie'' Research Institute for Radiobiology and Radiohygiene, Budapest, Hungary.
[5]Trophogen, Inc., Rockville, Maryland.

Thyroid. 2014;24:1297-308

ABSTRACT

Background: Differentiated thyroid carcinomas originating from thyroid follicular cells are frequent tumors of the thyroid with relatively good prognosis due to improved surgical techniques and follow-up procedures. Poorly differentiated thyroid cancers, which lose iodine uptake ability, in most cases still express thyrotropin (TSH) receptors (TSHR). Therefore, the aim of this study was to radiolabel a superagonist recombinant human TSH (rhTSH) analogue for imaging poorly differentiated thyroid cancer.

Methods: The TSHR superagonist, TR1401, was labeled with ^{99m}Tc using an indirect method via succinimidyl-6-hydrazinonicotinate hydrochloride conjugation. In vitro quality controls included SDS-PAGE, cysteine challenge, and cell-binding assay on TSHR positive cell lines (JP09 and ML-1). In vivo studies included tumor targeting experiments in athymic nude CD-1 mice xenografted with several different TSHR positive cells (JP09, K1, and ML-1) and TSHR negative cells (JP02) as control.

Results: The superagonist rhTSH analogue TR1401 was labeled with high labeling efficiency (>95%) and high specific activity (9250 MBq/mg). The labeled molecule retained its biologic activity and structural integrity. In tumor targeting experiments, a focal uptake of radiolabeled TR1401 was observed in TSHR positive cells but not in TSHR negative cells. The same observation was made in a dog with spontaneous intraglandular thyroid cancer.

Conclusions: We were able to radiolabel the rhTSH superagonist analogue TR1401 with ^{99m}Tc efficiently with retention of in vitro and in vivo binding capacity to TSHR. The relative role of such novel radiopharmaceutical versus ^{131}I scanning of thyroid cancer will require future histopathologic and clinical studies, but it may open new perspectives for presurgical staging of thyroid cancer, and diagnosis of radioiodine negative local relapses and/or distant metastases.

INTRODUCTION

Papillary and follicular thyroid carcinomas are usually well-differentiated tumors that retain in part the biologic characteristics of normal thyroid follicular cells. Under thyrotropin (TSH) stimulation, metastases take up radioiodine through the sodium/iodide symporter (NIS), synthesize, and release thyroglobulin (Tg) [1]. Thyroid cancer cells retain the capacity of synthesizing thyroid peroxidase (TPO) and, in particular, the TSH receptor (TSHR) that is expressed on the basolateral membrane [2, 3], which is essential for stimulation through TSH for ^{131}I scanning and therapy, measurement of stimulated Tg levels, and, in some cases, (^{18}F)-Fluoro-deoxy-glucose (FDG) positron emission tomography (PET) imaging. The incidence of differentiated thyroid cancers originating from thyroid follicular cells has increased significantly since 1983 [4], not only because of the improvement of detection techniques, but also because of an increase in risk factors. Approximately 10–15% of differentiated thyroid cancers lose NIS expression and the capacity to iodine uptake, but they still retain the ability to express the TSHR and Tg [5]. The loss of NIS is often caused by a de-differentiation or, because of the genetic instability of cancer cells, NIS-deficient clones may survive after radioiodine therapy and cause distant metastases that are not radioiodine avid. These cancers may or may not produce Tg, and are classified as poorly differentiated or undifferentiated thyroid cancers and require different diagnostic and therapeutic approaches compared to typical differentiated thyroid cancers. The diagnosis of

local recurrences or distant metastases in differentiated thyroid cancers is routinely performed after total thyroidectomy, under conditions of hypothyroidism, or after stimulation induced by wild-type recombinant human TSH (rhTSH; Thyrogen®) to obtain an increase of TSH levels and stimulate NIS expression and Tg production [6]. This is followed by the administration of a diagnostic dose of 74–370MBq of ^{131}I and a whole body scan (WBS) to detect thyroid remnants, local residual or recurrent disease, and/or distant metastases. Demonstration of residual disease on ^{131}I-WBS is the basis on which to perform therapy with high doses of ^{131}I. This approach has been used in the last decades with few modifications, and significantly prolongs the survival of patients with well-differentiated thyroid cancer [7, 8]. Interestingly, a minority of patients with a negative diagnostic ^{131}I-WBS (dWBS) can still show iodine uptake by metastases, as confirmed by positivity on post-therapy ^{131}I-WBS (tWBS) or positivity on diagnostic ^{124}I-PET scans [9–11]. In patients with poorly differentiated thyroid cancer with low or no iodine uptake (either ^{124}I or ^{131}I) but with high Tg values, a PET scan with [^{18}F]-FDG can be performed for staging [12, 13]. This often allows the detection of residual disease and enables surgery to be planned in selected cases. In most cases of poorly differentiated thyroid cancer, however, there is no satisfactory therapy to date, despite recent at- tempts using tyrosine kinase inhibitors [14]. PET scanning with [^{18}F]-FDG has also shown a higher diagnostic accuracy when performed in hypothyroidism or after rhTSH administration, indicating that poorly differentiated thyroid cancers still express TSHR despite loss of NIS [15]. The expression of

other receptors has been correlated with the degree of cell differentiation, such as, for example, the somatostatin and VEGF receptors (VEGFR) [16–19]. Therefore, it appears that a wide range of differentiation can occur in thyroid cancer cells from well-differentiated ones, expressing NIS, TSHR, making Tg, and expressing low levels of glucose transporters (GLUTs), to non-differentiated cancer cells with complete loss of NIS and low production of Tg but high expression of glucose transporters, TSHR, and VEGFR [5, 20]. Given this wide range of de-differentiation characteristics, it is relevant to develop new diagnostic tools for the in vivo characterization of thyroid-derived lesions, with the aim of performing better staging and follow-up evaluations in order to select the most appropriate therapy. In the present study, we describe the radiolabeling with ^{99m}Technetium (^{99m}Tc) of a new superagonist rhTSH analogue to produce a new radiopharmaceutical for single photon emission computed tomography (SPECT) imaging of differentiated and poorly differentiated thyroid cancer. We selected the analogue TR1401 [21, 22] whose sequence mainly differs from hTSH by four additional positively charged amino acids located in close spatial proximity at the α-L1 loop, of which three are located at identical positions in bovine TSH (bTSH). Such positive charges are involved in receptor binding, increasing the affinity of TR1401 (and bTSH) for the TSHR, as revealed by increased cAMP signalling. Specific negatively charged amino acids in the hinge region of the TSHR have been implicated as mediators of the superagonistic activity of TR1401 as compared to the wild-type rhTSH [21].

MATERIALS AND METHODS

Labeling of superagonist rhTSH analogue TR1401 with ^{99m}Tc

The human rhTSH analogue TR1401 was produced at Trophogen, Inc., by site-directed mutagenesis techniques in stably transfected Chinese Hamster Ovary (CHO) cells, and purified by a combination of dye, ion exchange, and gel filtration high-performance liquid chromatography (HPLC). The TR1401 molecule contains four lysine substitutions (Q13K + E14K + P16K + Q20K) in the α subunit of the glycoprotein in comparison to the wild-type molecule [21–23]. Indirect labeling of the highly purified TR1401 molecule was performed by conjugation with the bifunctional chelator succinimidyl-6-hydrazinonicotinate hydrochloride (HYNIC), which is able to bind both proteins and ^{99m}Tc. The analogue was modified by conjugation with SHNH (SoluLink) in dimethylformamide (DMF; Sigma-Aldrich Chemical) and purified from free SHNH by G-25 Sephadex PD10 column (GE Healthcare) using nitrogen-purged phosphate buffer saline (pH 7.4) as an eluant. In order to identify the best labeling conditions, 40 μg TR1401 (in 100 μL phosphate-buffered saline (PBS)) was labeled with 370 MBq of freshly eluted $^{99m}TcO_4^-$ (100 μL) in the presence of 200 μL tricine (Sigma-Aldrich; from 0.9 mg/mL to 200 mg/mL PBS) and 5 μL $SnCl_2$ (Sigma-Aldrich; from 2 mg/mL to 20 mg/mL 0.1 M HCl). The reaction volume was always 405 μL. Labeling efficiency (LE) and colloid percentages were measured after 10, 30, and 60 min. After labeling, an

additional purification by size exclusion chromatography was performed using a PD10 column (GE Healthcare). Free pertechnetate, tricine, and $SnCl_2$ were eluted with the flow-through. The number of HYNIC groups bound per molecule of TR1401 was determined by molar substitution ratio (MSR) assay. Briefly, 2 µL of conjugated TR1401 was added to 18 µL of a 0.5 mM solution of 2-sulfobenzaldehyde in 0.1 M 2-(N-morpholino)-ethanesulfonic acid (MES) buffer, pH 5.0, and incubated at room temperature for 2 h. PBS alone was used as blank, and duplicates were prepared. After 2 h, the absorbance at 345 nm (A_{345}) of each reaction was measured with a spectrophotometer, and the number of HYNIC groups per molecule was calculated as indicated in the SoluLink data sheet.

In vitro quality controls

Quality controls were performed using both instant thin- layer chromatography-silica gel (ITLC-SG) strip (Pall Life Sciences) and thin-layer chromatography silica gel (TLC-SG) plates (J.T. Baker). Results were analysed by a radio-scanner (Bioscan, Inc.) to calculate the LE of ^{99m}Tc-HYNIC-TR1401. The mobile phase for LE determination was a 0.9% NaCl solution, whereas for colloid determination it was a NH_3: H_2O:EtOH (1:5:3) solution. Quality controls were performed before and after an additional purification step with a PD10 column. Stability assays were performed adding 100 µL of ^{99m}Tc-HYNIC-TR1401 to 900 µL of fresh human blood serum or to 900 µL of 0.9% NaCl solution. The vials were incubated for up to 24 h at 37°C in a water bath. The radiochemical purity was measured at 1, 3, 6,

and 24 h by ITLC analysis. In addition, a cysteine challenge assay was performed, incubating the labeled TR1401 at 37°C for 60 min with different cysteine concentration, ranging from 1000:1 (cysteine:TR1401) to 0.1:1 molar ratio. For each time point, radiochemical purity was evaluated by ITLC as described above. All known chemical forms of ^{99m}Tc-cysteine have R_f values between 0.5 and 1, when normal saline was used as mobile phase. Integrity of the labeled TR1401 molecule was also checked by SDS- PAGE electrophoresis carried out according to Laemmli's method [24] on a 15% polyacrylamide gel under non-reducing conditions. Proteins were visualized by staining the gels with Coomassie Brilliant Blue (Pierce). Radioactivity associated with each band was determined scanning the gel with a radio scanner.

Cell lines and FACS analysis

Chinese hamster ovary (CHO) JP09 and JP02 cell lines [25, 26] were cultured in complete Ham's F12 medium (Eurobio Laboratories) with 10% fetal calf serum (FCS; Gibco), 100 IU/mL penicillin, 100 µg/mL streptomycin, and 2 mM l-glutamine at 37°C in a 5% CO_2 atmosphere. JP09 cells were transfected with the cDNA encoding the human TSHR and were reported to express up to 100,000 receptors per cell [25,26]. JP02 transfected with an empty vector were used for negative controls [25,26]. Human ML-1 cells [27], deriving from differentiated thyroid cancer, were cultured in complete Dulbecco's modified Eagle's medium (DMEM) containing 100 µM sodium pyruvate, 2 mM l-glutamine, 1 mg/mL

glucose, and 3.7 g/L $NaHCO_3$, supplemented with 10% FCS, 100 IU/mL penicillin, and 100 µg/mL streptomycin. These cells express approximately 10,000 receptors per cell (data provided by B.W.). K1 cells, expressing 10,000–100,000 receptors/cell [28] were grown in 1:1 mixture of DMEM high glucose (Gibco) and Kaighn's F12 (Gibco), both supplemented with 10% FCS, 100 IU/mL penicillin, 100 µg/mL streptomycin, and 2 mM l-glutamine. TSHR expression was analysed in JP09, JP02, ML-1, and K1 cell lines by immunofluorescence staining and cytofluorimetric analysis. Experiments were repeated twice. Briefly, one million cells were seeded in Eppendorf vials and incubated for 15 min with 10% inactivated murine serum in PBS at 4°C. At the end of the incubation, 10 µL of a PE-conjugated anti-TSHR antibody (Santa-Cruz) was added. Vials were incubated at 4°C for 30 min before the cells were analysed by cytofluorimeter.

In vitro binding studies

Measurements of cell uptake and retention of labeled TR1401 was performed in vitro using a semi-automatic system: LigandTracer™ (Ridgeview Instruments AB) [29]. Briefly, 10^6 mL^{-1} cells were seeded in a tilted Petri dish and incubated in a humidified incubator at 37°C and 5% CO^2 for 24 h. The dish was then placed in the LigandTracer and allowed to rotate continuously for 15 min to allow weakly attached cells to detach. After one gentle wash, 2 mL of 30 nM radiolabeled TR1401 was added to the cell culture medium, and the dish rotated for 1 h. The device was then stopped, and the liquid was removed and replaced with culture

medium without labeled TR1401 for calculating the release of radioactivity from the cells. Additionally, the medium was counted over time to evaluate the duration of the signal from internalized ^{99m}Tc-HYNIC-TR1401. A binding/release curve was obtained, and data were analysed with GraphPad Prism (GraphPad Software, Inc.) for calculating k_{on}, k_{off}, and K_d values. For binding assay with JP09 cells that do not stably adhere to Petri dishes [30], a standard saturation binding assay was performed, as described elsewhere [31]. Briefly, $3 \cdot x10^6$ cells were placed in triplicate in Eppendorf vials and incubated with decreasing concentrations of labeled TR1401 for 1 h at 4°C to calculate the total binding curve. The same experiment was performed adding a 100-fold molar excess of unlabeled TR1401 to each vial, to calculate nonspecific binding. At the end of the incubation time, the cells were washed twice with 0.5 mL of PBS. Cell pellets and the supernatants were counted separately in a single-well gamma counter (Gammatom). Nonlinear regression analysis was performed using GraphPad Prism.

In vivo high-resolution imaging

A high-resolution portable mini-gamma camera (HRC), IP-Guardian (Li-tech S.r.l.) was used as previously described [32,33]. It is composed of a crystal-collimator structure coupled to a Hamamatsu H8500 Position Sensitive Photo Multiplier Tube (PSPMT), a charge readout electronics, and a data-acquisition system. The system allows real-time acquisitions to be performed with a refresh time of 0.5 s. The HRC energy resolution is about 20% at 140 keV (^{99m}Tc), the

sensitivity is 210 cps/MBq, and the uniformity is ± 5%, while it provides 2.2mm intrinsic resolution suitable for imaging experiments in vivo in small animals. For in vivo biodistribution studies, 5.5 MBq (100 μL) of labeled TR1401 was injected in the tail vein of 12 nude CD-1 mice, and static planar posterior images were acquired using the HRC at 1, 3, 6, and 24 h, under light ether anesthesia. At the end of each imaging point, three mice were sacrificed, and major organs were collected and counted in a single-well gamma counter. Time–activity curves in organs were created for both in vitro and ex vivo data. For in vivo cell-targeting studies, we studied 12 nude CD-1 mice divided into four groups (three mice per group). Each group was injected subcutaneously with a different cell line. Cells—$8 \cdot 10^6$ JP09, K1, ML-1, or JP02—were mixed with BD Matrigel (BD Biosciences; 1:1) and injected subcutaneously into the right thigh; the same volume of BD Matrigel alone was injected into the left thigh as control. Approximately 1 h after cell injection, 5.5 MBq of labeled TR1401 were administered intravenously (i.v.), and static planar posterior HRC images were acquired at 1, 3, 6, and 24 h under light ether anesthesia. In another set of experiments, three groups of three nude CD-1 mice were injected in the right thigh with $2 \cdot 10^6$ JP09, ML-1, or K1 cells. In the first group, $2 \cdot 10^6$ TSHR negative JP02 cells were also injected in the left thigh. After consistent tumor growth (approximately 0.6–1 cm^3 in 20 days), mice were injected i.v. with 5.5 MBq of labeled TR1401, and static HRC images were acquired at 1, 3, 6, and 24 h under light ether anesthesia. All images were acquired positioning the HRC over the back of the mouse, in contact with it, for 60 s per

image.

Case study in a Dachshund dog with spontaneous thyroid cancer

A seven-year-old castrated Dachshund with a visible, palpable cervical mass (about 3 cm in diameter) was selected for the study. Blood tests and fine-needle aspiration biopsy were performed to assess the thyroidal origin of the lesion, suspected to be a papillary thyroid carcinoma. A whole body SPECT/CT was performed 3 h after injection of 222 MBq of ^{99m}Tc-HYNIC-TR1401 under deep anesthesia. The dog underwent surgery, the lesion was removed, and immunohistochemistry was performed using a rabbit anti-dog TSHR mAb (LifeSpan Biosciences).

RESULTS

Labeling of TR1401 with ^{99m}Tc and quality controls

The highest labeling efficiency was obtained when the analogue was conjugated with a HYNIC:TR1401 ratio higher than 8:1. Determination of the molar substitution ratio of HYNIC-conjugated TR1401 demonstrated that an average of 1.9, 4.7, and 6.6 molecules of SHNH were bound per molecule of analogue, using a 4:1, 8:1, and a 12:1 HYNIC:TR1401 ratio respectively. The 8:1 ratio was selected for further experiments to avoid overconjugation of the hormone and possible structural modification (Fig. 1). Optimization of the labeling procedure of

the HYNIC-TR1401 conjugate (40 μg) with ^{99m}Tc showed that the use of 200 μL of tricine (1.1 mM) and 5 μL of $SnCl_2$ (50 nM), $SnCl_2$:tricine ratio of 1:800, gave the highest LE (94 – 2%) and the lowest amount of colloids (<5%) after just 10 min of incubation (Fig. 1A). Specific activity of resulting ^{99m}Tc-TR1401 was 7400 MBq/mg. Radio- labeled TR1401 was stable up to 24 h both in human serum and in a 0.9% NaCl solution at 37°C (Fig. 1B), as well as in solutions containing increasing cysteine concentrations (Fig. 1C). A slight decrease in the radiochemical purity was observed only at high cysteine concentrations (>1000:1). SDS- PAGE analysis of radiolabeled, conjugated, and unconjugated analogue showed no significant differences and the absence of significant degradation or aggregation resulting from conjugation and/or labeling (Fig. 1D).

Cell lines and FACS analysis

JP09, JP02, ML-1, and K1 showed excellent growth in vitro, although a progressive decrease of TSHR expression was noticed by JP09 cells in following passages. ML-1 cells had a very slow growing rate when injected in mice. Mean fluorescence intensity (range of MFI) was higher for K-1 cells (14.64–23.34), followed by ML-1 (6.93–7.99) and JP09 (5.59–8.93). JP02 cells showed a MFI < 3, as expected, due to the absence of TSHR expression.

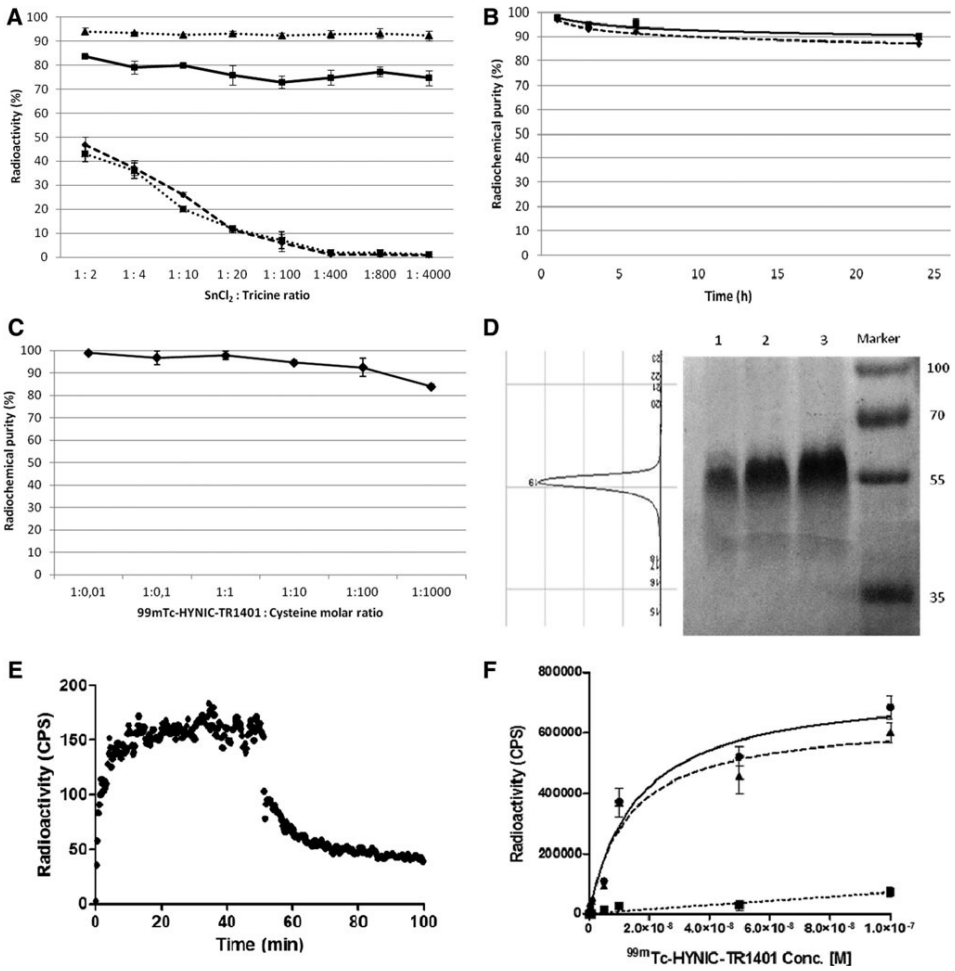

Fig. 1. In vitro quality controls of ^{99m}Tc-HYNIC-TR1401. (A) Optimization of the TR1401 labeling protocol performed varying both $SnCl_2$ and tricine. Labeling efficiency (LE) of TR1401:HYNIC, 1:4 (continuous line) and 1:8 (dotted line) ratios did not vary significantly, whereas the amount of colloids of both 1:4 (dashed line) and 1:8 (semi-hashed-dotted line) ratios decreased with an increase of the $SnCl_2$:tricine ratio. (B) Stability of radiolabeled ^{99m}Tc-HYNIC-TR1401 in saline (dashed line) and in plasma (straight line) over time assessed by instant thin-layer chromatography (ITLC). (C) Cysteine challenge assay of radiolabeled TR1401 assessed after 1 h of incubation by ITLC at increasing analogue:cysteine ratios. The labeled analogue shows excellent stability up to 10-fold molar excess of cysteine. (D) SDS-PAGE electrophoresis of unconjugated (1), conjugated (2), and radiolabeled (3) TR1401, performed in non-reducing conditions. On the left, a scan of the gel, for radioactivity detection, is shown. Native, conjugated, and labeled analogue bands co-migrate, and the radio- activity is associated with the only visible band of TR1401. (E) Binding, retention, and dissociation assay (decay-corrected) of radiolabeled TR1401 to/from ML-1 cells. The assay was performed using the LigandTracer™ instrument and provided a K_d of 2.51 nM. (F) Binding assay of radiolabeled TR1401 on JP09 cells showing the total binding (straight line), specific binding (dashed line) and the nonspecific binding (dotted line). By nonlinear regression analysis, the calculated K_d is 8.79 nM.

In vitro binding studies

ML-1 cells showed very fast radiopharmaceutical uptake, by LigandTracer, reaching a plateau within 20 min and a slow dissociation from the TSHR with time. The calculated K_d was 2.51 nM (Fig. 1E), and a retention experiment allowed us to determine that a third of the bound radioactivity was internalized, decreasing over time, with a half-life of 13.6 – 2 h. The binding assay performed with JP09 cells showed a K_d of 8.79 nM (Fig. 1F) by nonlinear regression analysis.

In vivo high-resolution imaging

Visual analysis of images related to the biodistribution of ^{99m}Tc-HYNIC-TR1401 in mice showed a rapid and persistent uptake by the kidneys and a moderate uptake by the liver with almost no signal from other organs and blood pool, as shown in Figure 2. Single organ counting revealed that thyroid uptake, even if low in absolute amounts compared to other major organs, is very high per gram of tissue and in- creases over time up to 6 h, with a decrease at 24 h (Fig. 3). Figure 4 shows the images acquired in mice injected with different cell lines in the right thigh. In animals injected with TSHR-positive cells, there is a focal uptake of the radio-pharmaceutical where cells were injected. Regions of interest (ROIs) were drawn over the right and left thigh, and tumor/ background (T/B) ratios were calculated at each time point (Fig. 5). All cell lines showed the highest T/B ratio at 3 h, and a slight decrease was observed at 6 h up to 24 h. Tumor xenografts in mice injected with JP09 and K1 cells were detectable after 20 days, and radiolabeled TR1401

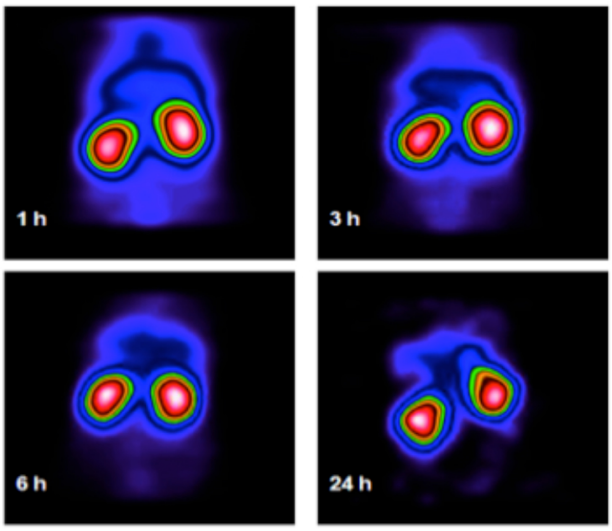

Fig. 2. Planar posterior whole body images, at different time points, of nude CD1 mice after the injection of 370 Bq of TR1401. Images were acquired with a portable high-resolution mini-gamma camera and show the rapid and persistent kidney activity.

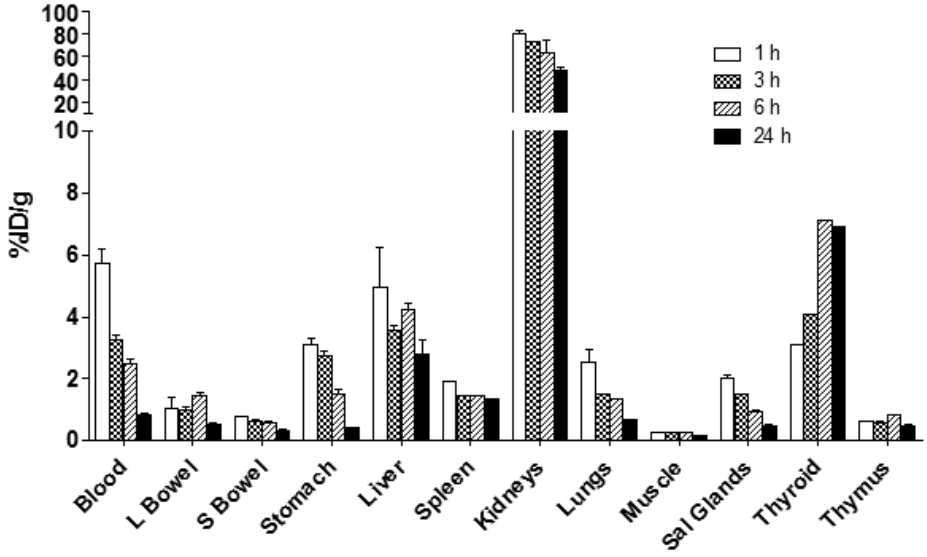

Fig. 3. Single organ counts at 1 h (white bar), 3 h (squared bar), 6 h (dashed bar), and 24 h (black bar). Data are shown as % ID/g over time. Each point is the average of three mice. An evident uptake was found in the thyroid, kidneys, and liver.

was able to visualize the lesion with a high T/B ratio (6.8 and 2.9 respectively) as early as at 3 h after injection. No uptake was observed in tumors derived from TSHR negative cells (Fig. 6). ML-1 tumors were smaller and less vascularized than other tumors at autopsy. Images with ^{99m}Tc-HYNIC-TR1401 showed the tumors best at 3 h after injection with a calculated T/B of 1.7.

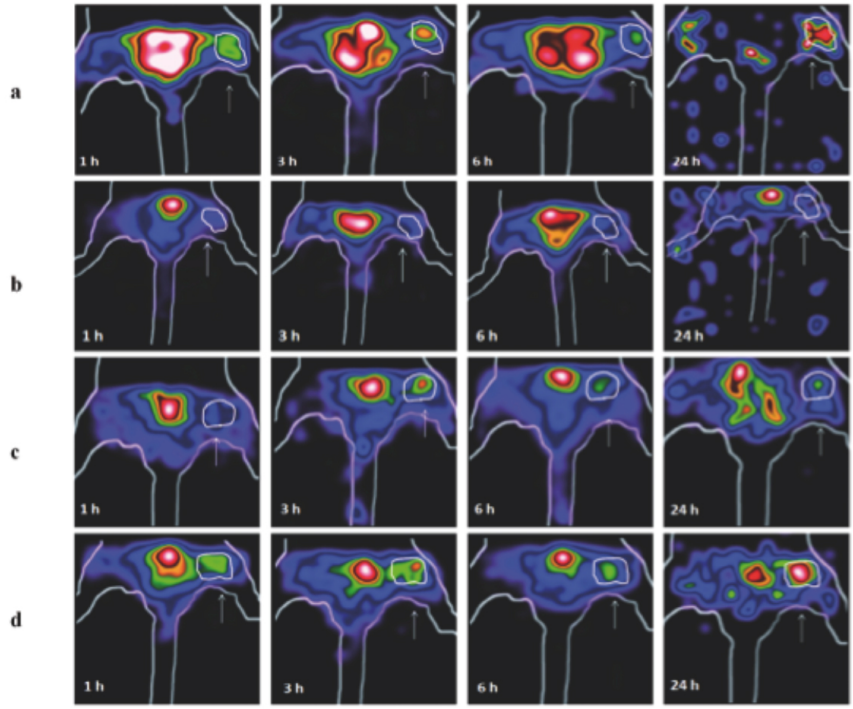

Fig. 4. Planar posterior high-resolution camera (HRC) images of the legs of mice injected in the right thigh with TSHR- positive JP09 (A), JP02 TSHR-negative (B), ML-1 TSHR-positive (C), and K1 TSHR-positive (D) cells. Images were obtained 1, 3, 6, and 24h after intravenous (i.v.) injection of ^{99m}Tc-HYNIC-TR1401. The left thigh was injected with Matrigel only. Very high kidney uptake resulted in high counts in the bladder. The arrows indicate the right thigh and the site of cell injection. Images are not easily comparable due to different activity in the bladder, and therefore semi-quantitative analysis of the tumor/background (T/B) ratio is more reliable, as shown in Figure 5.

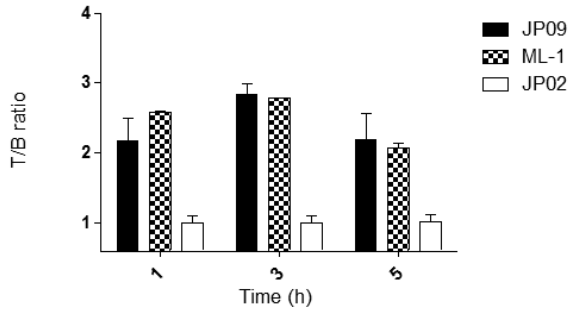

Fig. 5. T/B ratios calculated on planar posterior images obtained at 1, 3, 6, and 24h after i.v. injection of ^{99m}Tc- HYNIC-TR1401, by drawing a region of interest (ROI) over the injected cells and over the contralateral leg. JP09 (black bar), ML-1 (squared bar), K1 (dotted bar), and JP02 cells (white bar). The best T/B ratios were obtained at 3 h for all cell lines, confirming results of visual analysis of images and demonstrating the rapid uptake of this radiopharma- ceutical with very fast plasma clearance.

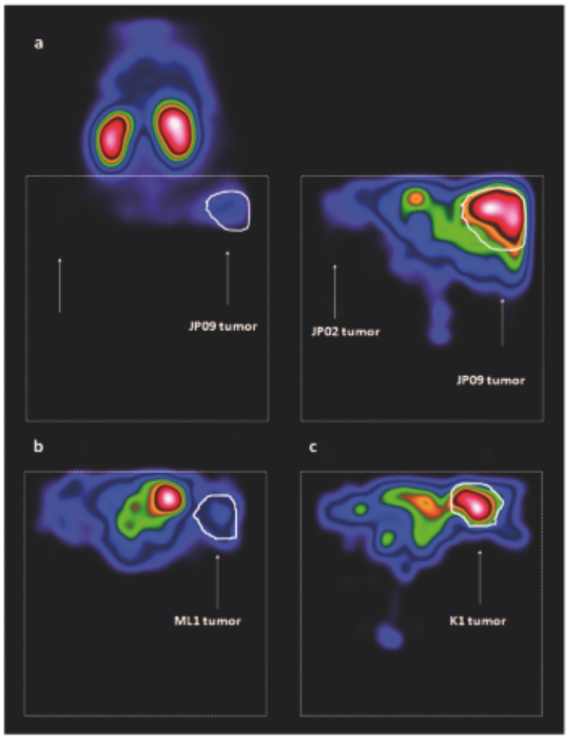

Fig. 6. Planar posterior HRC images of nude mice bearing a JP09 tumor in the right thigh and a JP02 tumor in the left thigh (A) or a ML-1 tumor (B) or a K1 tumor (C). To avoid the high kidney activity, images were also ac- quired of the lower part of the mouse as shown in the figure. There is tracer up- take in JP09 and K1 tumors, less uptake in the ML-1 tumor, and no uptake in the JP02 tumor (arrows).

Case study in a Dachshund dog with spontaneous thyroid cancer

The Dachshund dog was clinically symptom free, and routine hematologic and biochemical parameters were all within the reference ranges, including thyroxine and TSH levels. SPECT/CT images showed high uptake in the left thyroid lobe corresponding to the thyroid nodule with no significant uptake in the contralateral lobe (Fig. 7). No focal uptake was found in regional lymph nodes nor in other tissues, but it was found in the liver and kidneys as a consequence of ^{99m}Tc-TR1401 metabolism. Despite the initial diagnosis, histologic examinations revealed that the excised lesion was a poorly differentiated thyroid cancer with high TSHR expression (Fig. 8).

a. 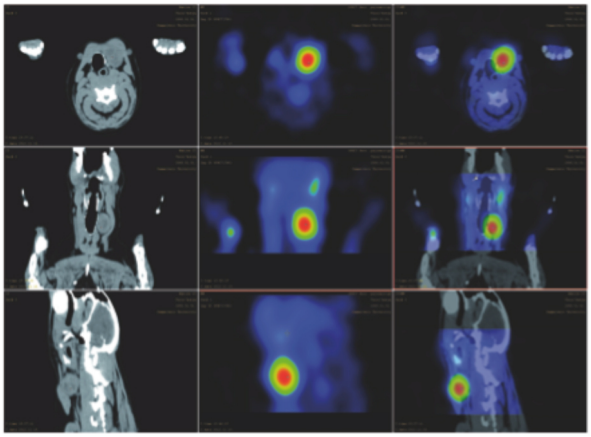 b. 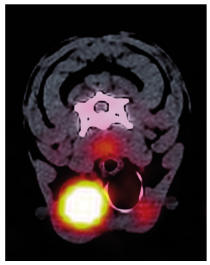

Fig. 7. (A) Single photon emission computed tomography (SPECT)/CT scan of a dog bearing a spontaneous thyroid tumor. CT scans (left column), SPECT scans (middle column), and fusion images (right column) are shown. Transaxial, coronal, and sagittal sections are shown the different rows. (B) High uptake of ^{99m}Tc-HYNIC- TR1401 is clearly seen in the thyroid nodule (papillary cancer) in the left thyroid lobe, whereas negligible activity is detectable in the normal right thyroid lobe.

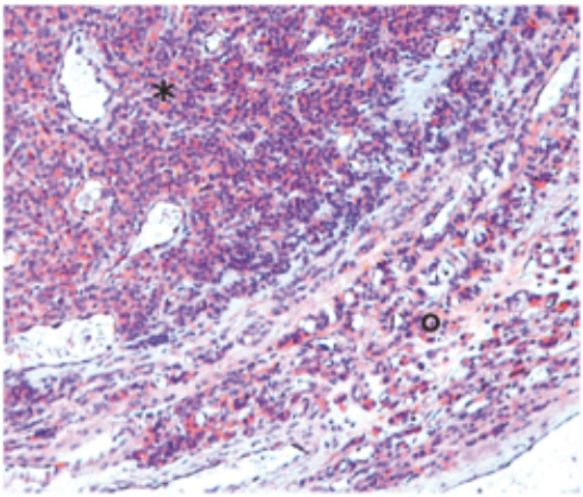

Fig. 8. Histologic section of the excised lesion showing a poorly differentiated thyroid carcinoma (*) and the surrounding normal thyroid tissue (o). The section is stained with he- matoxylin and eosin and with an anti-TSHR antibody specific for canine TSHR. The malignant tissue shows much higher density of TSHR expression compared to the normal tissue.

DISCUSSION

Although ^{99m}Tc-methoxyisobutylisonitrile (MIBI) scintigraphy [34], [^{18}F]-FDG PET (13), radiolabeled somatostatin analogues [35], Doppler-US [36], contrast-enhanced magnetic resonance imaging [37], and others [38] have shown to be useful for the in vivo characterization of thyroid and extra-thyroid lesions, more accurate imaging techniques are needed. We previously published an alternative approach for imaging differentiated thyroid cancers based on the use of a radiolabeled anti-Galectin-3 mAb [39]. Despite the excellent results in preclinical studies, we had difficulties in translating this methodology to humans due to the murine nature of the antibody and the long plasma half-life of the labeled antibody that reduces T/B ratios and the possibility of detecting small lesions. A humanized

antibody fragment radiolabeled with a positron-emitting isotope would have been more successful in humans. In the following years, we investigated, like others, the use of radiolabeled peptides and receptor agonist analogues. Along this line, Sager et al. [40] investigated the role of scintigraphy with radiolabeled somatostatin analogues that showed a sensitivity ranging between 25% and 75% de- pending on patient selection criteria. They compared ^{18}[F]- FDG and ^{99m}Tc-MIBI with ^{99m}Tc-HYNIC-TOC, preferring it to ^{111}In-octreotide due to its lower cost, higher resolution, and lower radiation dose to the patient. They found that the sensitivity of somatostatin receptor scintigraphy was higher than MIBI, but lower than ^{18}[F]-FDG-PET. Similarly, Rodrigues et al. [41] proposed the use of ^{99m}Tc-depreotide that showed, in many cases, a higher sensitivity than ^{18}[F]-FDG-PET, but also nonspecific uptake in cells that play a role in granulomatous diseases, such as activated lymphocytes, leading to false-positive results. Finally, Zhao et al. [42] proposed the use of the Arginine- Glycine-Aspartic acid (RGD) molecule 3PRGD2 labeled with ^{99m}Tc that has a high affinity and specificity for integrin a_vb_3, present in various malignant tumors. In 10 patients with negative ^{131}I-WBS and high Tg, ^{99m}Tc-3PRGD2 scintigraphy was able to visualize thyroid cancer metastases with a high T/B ratio that also correlated with growth rate. More- over, the low background in the lungs facilitated the detection of metastases in the chest. As an alternative to the above-mentioned imaging approaches, we have investigated the use of radiolabeled human TSH [43]. Since the TSHR is overexpressed in some de- differentiated thyroid cancer, the relevance of this imaging approach depends

on the potential of using this radiopharmaceutical not only for follow-up but also for preoperative staging of differentiated thyroid cancer. A further advantage of this technique could be the possibility of avoiding the induction of hypothyroidism either by thyroxine withdrawal or rhTSH administration. We therefore radiolabeled rhTSH with ^{123}I and obtained interesting preclinical results. However, images obtained with ^{123}I-rhTSH were of relatively poor quality for three possible reasons: (a) the low specific activity of the radio- pharmaceutical as a consequence of the low labeling efficiency of rhTSH with ^{123}I; (b) the low affinity binding of rhTSH to the TSHR; (c) the possible saturation of the TSHR by endogenous TSH. We therefore attempted to label rhTSH with ^{99m}Tc with high specific activity and performed preliminary studies in animals and patients with metastatic thyroid cancer (unpublished data). However, tumor lesions were poorly distinguishable from background, and we explained these results by the low binding affinity of rhTSH to the TSHR. This highlighted the need of searching for a new TSH analogue (TSH receptor agonist) with higher receptor binding affinity than rhTSH [44, 45]. The relatively low affinity of rhTSH, which is much lower than bovine or rodent TSH, is the result of an evolutionary change from an acute thermo- genic hormone to one whose primary role in humans is to promote a gradual and chronic increase of NIS during periods of fasting or low iodine diet, as an adaptation to nomadic life [22, 45]. Recently, a novel second-generation superagonist rhTSH analogue named TR1401 has been produced and purified to homogeneity (>99%). It has very high in vitro receptor binding affinity and in vivo bioactivity

(Trophogen, Inc., unpublished data). This new analogue has higher bio- potency and maximal efficacy compared to standard wild- type hormone and first generation rhTSH analogues, and previous studies demonstrated its capacity to increase radio- iodine and ^{18}[F]-FDG uptake in FRTL-5 cells [22, 46, 47]. Since the heterodimeric TSH molecule has crucial disulfide bonds, involved in the formation of a cysteine-knot in each subunit, we focused on the labeling of TR1401 with ^{99m}Tc using an indirect method based on SHNH conjugation, obtaining a reliable and reproducible protocol that allowed us to radiolabel the analogue without affecting its biologic activity. SHNH is bound to lysine residues and then chelates the reduced technetium, thus avoiding opening the S–S bonds to insert Technetium, as this is done with the so-called direct methods [48]. Using the indirect method, tricine is used as a coligand, and its quantity, as well as that of $SnCl_2$, must be carefully selected in order to reduce ^{99m}Tc-colloid formation and increase LE. We found that a $SnCl_2$:tricine ratio of 1:800 gave a 94% LE with negligible amounts of colloids (SA of 7400 MBq/mg). Labeled TR1401 was stable in both saline and human serum for up to 24 h and the binding on TSHR- positive cells was specific because in saturation binding as- says performed on JP09 cells, an excess of unlabeled TR1401 was able to saturate the receptors and prevent further binding of labeled molecules. With ML-1 cells, a K_d of 2.51 nM was calculated. This high affinity of TR1401 and the high specific activity of ^{99m}Tc-TR1401 allowed us to inject relatively low doses of the radiopharmaceutical into the animals and obtain excellent tumor localization by gamma camera imaging.

This could also be achieved in humans, thus reducing the radiation dose and any biologic effect on TSHR positive tumors. In mice, the radiolabeled analogue showed early targeting to tumors and the thyroid, as well as fast renal metabolism with very low blood pool activity at late time points. The thyroid showed, ex vivo, the highest % ID/g, even if it could not be clearly visualized with the mini-gamma camera because of its small size, which was below its resolution. JP09 tumors were visualized in vivo with a high T/B ratio (6.8) at 3 h, whereas K1 and ML-1 tumors showed a lesser uptake (2.9 and 1.7 respectively, both at 3 h). It should be mentioned that T/B values did not quantitatively correlate with the TSHR density calculated by FACS analysis. Our interpretation of these results is based on the consideration that cells in xenografts behave very differently from cultures, and the vascularization of xenografts may also vary and affect the uptake of radiopharmaceutical. Thus, ML-1 tumors were slow growing, small, and poorly vascularised. K1 tumors grew well but differ from ML-1 and JP09 because of their origin. The case study in a Dachshund dog with a spontaneous poorly differentiated thyroid cancer, although not fully conclusive, is of interest because it highlights the potential of this new radiopharmaceutical for detection of intrathyroidal lesions. SPECT/CT images performed 3 h after i.v. injection confirmed that TR1401 rapidly binds in vivo to tumor cells, with a very low blood pool activity and pre- dominant kidney accumulation observed previously for highly sialylated rhTSH preparations [47]. The clear visualization of the tumor within the thyroid gland in euthyroid conditions suggests the possibility of using

this radiopharmaceutical for preoperative TSHR-based staging in addition to patient follow-up and for imaging de-differentiated thyroid cancer metastases. Indeed, we can assume that the lower the level of endogenous TSH, the better the condition for using radiolabeled TR1401 because of a decreased likelihood of competition at the TSHR. However, radiolabeled TR1401 affinity for the human TSHR is much higher than that of wild- type hTSH, and suppression of endogenous TSH will most likely not be necessary in patients. Because of this favorable biodistribution, high binding affinity, and retention in the cytoplasm, radiolabeled-TR1401 could also be suitable for therapeutic purposes, if radiolabeled with a beta-emitting isotope such as ^{177}Lu, providing the ability to perform a renal protection by amino acid infusion, as for other radiolabeled peptides [49]. Moreover, novel long-acting superagonist rhTSH analogues are under development and may replace the high renal uptake of TR1401. From a therapeutic point of view, ^{99m}Tc-TR1401 could be useful to predict which radioiodine-negative thyroid cancers might respond to therapies with ^{177}Lu-labeled TSH analogues, which are currently under development in our laboratory and at Trophogen. The relative role of ^{99m}Tc-TR1401 versus ^{131}I scanning of thyroid cancer will require future histopathologic and clinical studies in patients receiving both scanning modalities, since the in vivo functional status of the TSHR versus NIS has not yet been clarified. Therefore, it would be important to understand which patients may benefit from such novel radiopharmaceuticals, and whether ^{99m}Tc-TR1401 scintigraphy could become complementary to radioiodine scanning

in the management of differentiated thyroid cancer patients. As a minimum, ^{99m}Tc-TR1401 scanning will provide a major new unmet clinical need to image thyroid cancers that have lost the expression or membrane insertion of NIS while retaining expression of functional TSHRs. These thyroid cancers are typically associated with finding a positive serum Tg and a negative iodine scan, thus posing a major diagnostic and therapeutic challenge. The fact that most of these patients respond with an increase in serum Tg to endogenous or rhTSH proves that they retain an appreciable numbers of TSHRs that allow cancer imaging with the new high affinity TSH analogue. In addition, even in cancers with a functional NIS and TSHR overexpression, ^{99m} Tc-TR141 may have advantages for imaging of intrathyroidal cancers, or local nodes in presurgical staging and distant metastases, allowing physicians to perform the scintigraphy before thyroidectomy without interference of the thyroid. This would allow the surgeon to remove local non-iodine uptaking nodes at the moment of the thyroidectomy. Our study, as a proof of concept, opens new diagnostic and therapeutic strategies.

CONCLUSIONS

The highly pure rhTSH superagonist TR1401 was efficiently labeled with ^{99m}Tc with high specific activity and used for imaging TSHR-positive cell lines in vitro and TSHR-positive thyroid tumor xenografts in mice. A spontaneous poorly differentiated thyroid cancer within the thyroid was also imaged in a dog. In the

light of these results, we will investigate the possibility of using this radiopharmaceutical for imaging intrathyroidal differentiated thyroid cancer and, particularly, radioiodine-negative metastases. Due to fast in vivo binding of ^{99m}Tc-HYNIC-TR1401, a possible use of short half-life positron emitting isotopes can also be considered (such as ^{18}F or ^{68}Ga) for PET/CT imaging. More studies are necessary to evaluate the possibility of labeling TR1401 with a beta-emitting isotope for therapeutic purposes.

REFERENCES

1. Elisei R, Pinchera A, Romei C, Gryczynska M, Pohl V, Maenhaut C, Fugazzola L, Pacini F. Expression of thyroytopin receptor (TSH-R), thyroglobulin, thyroperoxidase and calcitonin messenger ribonucleic acid in thyroid carcinomas: evidence of TSH-R gene transcript in medullary histotype. J Clin Endocr Metab 1994;78:867-871.
2. Clark OH, Castner BJ. Thyrotropin "receptors" in normal and neoplastic human thyroid tissue. Surgery 1979; 85:624-632.
3. Szkudlinski MW, Fremont V, Ronin C, Weintraub BD. Thyroid-stimulating hormone and thyroid-stimulating hormone receptor structure-function relationships. Physiol Rev 2001;82:473-502.
4. Morris LG, Myssiorek D. Improved detection does not fully explain the rising incidence of well-differentiated thyroid cancer: a population-based analysis. The Am J Surg 2010;200:454-461.
5. Lazar V, Bidart JM, Caillou B, Mahé C, Lacroix L, Filetti S, Schlumberger M. Expression of the Na+/I- symporter gene in human thyroid tumors: a comparison study with other thyroid-specific genes. J Clin Endocr Metab 1999,84:3228-3234.
6. Maffioli L, Florimonte L, Fugazzola L, Banti E, Bagnasco M, Dottorini ME, Perotti G, Rubello D, Seregni E, Bombardieri E, Testori O. The widened use

of exogenous stimulation with recombinant human TSH to treat metastatic thyroid carcinoma in Italy Q J Nucl Med Mol Im 2012;56:476-84.

7. Schlumberger MJ, Torlantano M. Papillary and follicular thyroid carcinoma. Bailliere Clin Endoc 2000;14:601-613.

8. Ladenson PW, Braverman LE, Mazzaferri EL, Brucker-Davis F, Cooper DS, Garber JR, Wondisford FE, Davies TF, DeGroot LJ, Daniels GH, Ross DS, Weintraub BD. Comparison of administration of recombinant human thyrotropin with withdrawal of thyroid hormone for radioactive iodine scanning in patients with thyroid carcinoma. The New Eng J Med 1997;337:888-896.

9. Capoccetti F, Criscuoli B, Rossi G, Ferretti F, Manni C, Brianzoni E. The effectiveness of 124I PET/CT in patients with differentiated thyroid cancer. Q J Nucl Med Mol Im 2009;53:536-545.

10. Phan HT, Jager PL, Paans AM, Plukker JT, Sturkenboom MG, Sluiter WJ, Wolffenbuttel BH, Dierckx RA, Links TP. The diagnostic value of 124I-PET in patients with differentiated thyroid cancer. Eur J Nucl Med Mol I 2008;35:958-965.

11. Pettinato C, Monari F, Nanni C, Allegri V, Marcatili S, Civollani S, Cima S, Spezi E, Mazzarotto R, Fanti S. Usefulness of 124I PET/CT imaging to predict absorbed doses in patients affected by metastatic thyroid cancer and treated with 131I. Q J Nucl Med Mol Im 2012;56:509-514.

12. Helal BO, Merlet P, Toubert ME, Franc B, Schvartz C, Gauthier-Koelesnikov H, Prigent A, Syrota A. Clinical impact of (18)F-FDG PET in thyroid carcinoma patients with elevated thyroglobulin levels and negative (131)I scanning results after therapy. J Nucl Med 2001;42:1464-1469.
13. Piccardo A, Foppiani L, Morbelli S, Bianchi P, Barbera F, Biscaldi E, Altrinetti V, Villavecchia G, Cabria M. Could [18]F-fluorodeoxyglucose PET/CT change the therapeutic management of stage IV thyroid cancer with positive 131I whole body scan? Q J Nucl Med Mol Im 2011;55:57-65.
14. Giuffrida D, Prestifilippo A, Scarfia A, Martino D, Marchisotta S. New treatment in advanced thyroid cancer. J Oncol 2012:391629.
15. Leboulleux S, Schroeder PR, Busaidy NL, Auperin A, Corone C, Jacene HA, Ewertz ME, Bournaud C, Wahl RL, Sherman SI, Ladenson PW, Schlumberger M. Assessment of the incremental value of recombinant thyrotropin stimulation before 2-[18F]-Fluoro-2-deoxy-D-glucose positron emission tomography/computed tomography imaging to localize residual differentiated thyroid cancer. J Clin Endocr Metab 2009;94:1310-1316.
16. Middendorp M, Selkinski I, Happel C, Kranert WT, Grünwald F. Comparison of positron emission tomography with [18F]FDG and [68Ga]DOTATOC in recurrent differentiated thyroid cancer: preliminary data. Q J Nucl Med Mol Im 2010;54:76-83.
17. Heston TF, Wahl RL. Molecular imaging in thyroid cancer. Cancer Imaging 2010;10:1-7.

18. De Araujo-Filho VJ, Alves VA, de Castro IV, Lourenço SV, Cernea CR, Brandão LG, Ferraz AR. Vascular endothelial growth factor expression in invasive papillary thyroid carcinoma. Thyroid 2009;19:1233-1237.

19. Wong KK, Dvorak RA, Marzola MC, Grassetto G, Gross MD, Rubello D. Molecular imaging in the management of thyroid cancer. Q J Nucl Med Mol Im 2011;55:541-559.

20. Ciampi R, Vivaldi A, Romei C, Del Guerra A, Salvadori P, Cosci B, Pinchera A, Elisei R. Expression analysis of facilitative glucose transporters (GLUTs) in human thyroid carcinoma cell lines and primary tumors. Mol Cell Endocrinol 2008;291:57-62.

21. Mueller S, Kleinau G, Szkudlinski MW, Jaeschke H, Krause G, Paschke R. The superagonistic activity of bovine thyroid-stimulating hormone (TSH) and the human TR1401 TSH analog is determined by specific amino acids in the hinge region of the human TSH receptor. J Biol Chem 2009;284:16317-16324.

22. Szkudlinski MW, Teh NG, Grossmann M, Tropea JE, and Weintraub BD. Engineering human glycoprotein hormone superactive analogues. Nat Biotechnol 1996;14:1257-1263.

23. Leitolf H, Tong KP, Grossmann M, Weintraub BD, Szkudlinski MW. Bioengineering of human thyrotropin superactive analogs by site-directed "lysine-scanning" mutagenesis. Cooperative effects between peripheral loops. J Biol Chem 2000;275:27457-27465.

24. Gallagher SR. One-dimensional SDS gel electrophoresis of proteins. Current Protocols in Protein Science 2012;Chapter 10:Unit 10.1.1-44.

25. Wallaschofski H, Paschke R. Detection of thyroid stimulating (TSAB)- and thyrotropin stimulation blocking (TSBAB) antibodies with CHO cell lines expressing different TSH-receptor numbers. Clin Endocrinol (Oxf) 1999;50:365-372.

26. Ludgate M, Costagliola S, Danguy D, Perret J, Vassart G. Recombinant TSH-receptor for determination of TSH-receptor-antibodies. Exp Clin Endocrinol 1992;100:73-74.

27. Schönberger J, Bauer J, Spruss T, Weber G, Chahoud I, Eilles C, Grimm D. Establishment and characterization of the follicular thyroid carcinoma cell line ML-1. J Mol Med (Berl) 2000;78:102-110.

28. Wyllie FS, Haughton MF, Rowson JM, Wynford-Thomas D. Human thyroid cancer cells as a source of iso-genic, iso-phenotypic cell lines with or without functional p53. Br J Cancer 1999;79:1111-1120.

29. Bjorke H, Andersson K. Automated, high-resolution cellular retention and uptake studies in vitro. Appl Radiat Isot 2006;64:901-905.

30. Harper PA, Juliano RL. Isolation and characterization of Chinese hamster ovary cell variants defective in adhesion to fibronectin-coatedcollagen. J Cell Biol 1980;87:755-763.

31. Chianelli M, Signore A, Fritzberg AR, Mather SJ. The development of technetium-99m-labelled interleukin-2: a new radiopharmaceutical for the in

vivo detection of mononuclear cell infiltrates in immune-mediated diseases. Nucl Med Biol 1997;24:579-586.

32. Soluri A, Massari R, Trotta C, Montani L, Iurlaro G, Mangano M, Scopinaro F, Scafè R. New imaging probe with crystals integrated in the collimator's square holes. Nucl Instr Meth Phys Res A. 2005;554:331-339.
33. Malviya G, de Vries EF, Dierckx RA, Signore A. Synthesis and evaluation of 99mTc-labelled monoclonal antibody 1D09C3 for molecular imaging of major histocompatibility complex class II protein expression. Mol Imaging Biol 2011;13:930-939.
34. Campennì A, Violi MA, Ruggeri RM, Sindoni A, Moleti M, Vermiglio F, Baldari S 2010 Clinical usefulness of 99mTc-MIBI scintigraphy in the postsurgical evaluation of patients with differentiated thyroid cancer. Nucl Med Commun 2010;31:274-279.
35. Pazaitou-Panayiotou K, Tiensuu Janson E, Koletsa T, Kotoula V, Stridsberg M, Karkavelas G, Karayannopoulou G. Somatostatin receptor expression in non-medullary thyroid carcinomas. Hormones (Athens). 2012;11:290-296.
36. Carneiro-Pla D. Ultrasound elastography in the evaluation of thyroid nodules for thyroid cancer. Curr Opin Oncol 2013;25:1-5.
37. Yuan Y, Yue XH, Tao XF. The diagnostic value of dynamic contrast-enhanced MRI for thyroid tumors. Eur J Radiol 2012;81:3313-3318. Epub 2012 May 17.

38. Boufraqech M, Patel D, Xiong Y, Kebebew E 2013 Diagnosis of thyroid cancer: state of art. Exp Opin Med 2013;7:331-42.

39. Bartolazzi A, D'Alessandria C, Parisella MG, Signore A, Del Prete F, Lavra L, Braesch-Andersen S, Massari R, Trotta C, Soluri A, Sciacchitano S, Scopinaro F. Thyroid cancer imaging in vivo by targeting the anti-apoptotic molecule galectin-3. PLoS One. 3:e3768.

40. Sager S, Kabasakal L, Halac M, Maecke H, Uslu L, Önsel Ç, Kanmaz B. Comparison of 99mTc-HYNIC-TOC and HYNIC-TATE octreotide scintigraphy with FDG PET and 99mTc-MIBI inlocal recurrent or distant metastatic thyroid cancers. Clin Nucl Med 2013;38:321-325.

41. Rodrigues M, Li, S, Gabriel M, Heute D, Greifeneder M, Virgolini I. 99mTc-depreotide scintigraphy versus 18F-FDG-PET in the diagnosis of radioiodine-negative thyroid cancer. J Clin Endocr Metab 2006;91:3997-4000.

42. Zhao D, Jin X, Li F, Liang J, Lin Y. Integrin αvβ3 imaging of radioactive iodine-refractory thyroid cancer using 99mTc-3PRGD2. J Nucl Med 2012;53:1872-1877.

43. Corsetti F, Chianelli M, Cornelissen B, Van de Wiele C, D'Alessandria C, Slegers G, Mather SJ, Di Mario U, Filetti S, Scopinaro F, Signore A. Radioiodinated recombinant human TSH: a novel radiopharmaceutical for thyroid cancer metastases detection. Cancer Biother Radiopharm 2004;19:57-63.

44. Willey KP. An elusive role for glycosylation in the structure and function of reproductive hormones. Hum Reprod Update 1999;5:330-355.

45. Szkudlinski MW, Grossmann M, Leitolf H, and Weintraub BD. Human thyroid-stimulating hormone: structure-function analysis. Methods 2000;21:67-81.

46. Reinfelder J, Maschauer S, Foss CA, Nimmagadda S, Fremont V, Wolf V, Weintraub BD, Pomper MG, Szkudlinski MW, Kuwert T, Prante O. Effects of recombinant human thyroid-stimulating hormone superagonists on thyroidal uptake of 18F-fluorodeoxyglucose and radioiodide. Thyroid 2011;21:783-792.

47. Szkudlinski MW, Thotakura NR, Tropea JE, Grossmann M, Weintraub BD. Asparagine linked oligosaccharide structures determine clearance and organ distribution of pituitary and recombinant thyrotropin. Endocrinology 1995.136:3325-3330.

48. Mather SJ, Ellison D. Reduction-mediated technetium-99m labeling of monoclonal antibodies. J Nucl Med 1990;31:692-697.

49. Bodei L, Ferone D, Grana CM, Cremonesi M, Signore A, Dierckx RA, Paganelli G. Peptide receptor terapie in neuroendocrine tumors. J Endocrinol Invest 2009;32:360-369.

Chapter 3

In vivo evaluation of TNF-alpha in the lungs of patients affected by sarcoidosis

Filippo Galli[1], Tiziana Lanzolla[1], Vittorio Pietrangeli[2], Gaurav Malviya[1], Alberto Ricci[2], Pierdonato Bruno[2], Paola Ragni[1], Francesco Scopinaro[1], Salvatore Mariotta[2], Alberto Signore[1]

[1]Nuclear Medicine Unit, Department of Medical-Surgical Sciences and Translational Medicine, Faculty of Medicine and Psychology, "Sapienza" University of Rome, Italy.
[2]Pneumology Unit, Department of Clinical and Molecular Medicine, Faculty of Medicine and Psychology, "Sapienza" University of Rome, Italy.

Biomed Res Int. 2015;2015:401341

ABSTRACT

Introduction: Sarcoidosis is a multi-systemic granulomatous disorder characterized by multiple non-caseating granulomas involving intra-thoracic lymph nodes and lung parenchyma. Recently, the use of anti-tumor necrosis factor alpha (anti-TNFα) agents has been introduced for therapy of chronic and refractory sarcoidosis with controversial results. Infliximab (Remicade®) is a chimeric monoclonal antibody (mAb) that recognizes and binds TNFα, neutralizing its biological effects. In the present study, ^{99m}Tc labelled infliximab was used to study the expression TNFα in sarcoid lesions and to evaluate its role as a predictive marker of response to therapy with Remicade®.

Material and Methods: A total of 10 patients with newly diagnosed sarcoidosis were enrolled together with 10 control patients affected by rheumatoid arthritis. All patients were studied by planar imaging of the chest with ^{99m}Tc-infliximab at 6 and 24 h and total body [^{18}F]-FDG PET/CT. Regions of interest were drawn over the lungs and the right arm and target-to-background ratios were analysed for ^{99m}Tc-infliximab. SUVmean and SUVmax were calculated over lungs for FDG.

Results and Discussion: Image analysis showed low correlation between T/B ratios and BAL results in patients despite positivity at [^{18}F]-FDG-PET.

Conclusion: In conclusion, patients with newly diagnosed pulmonary sarcoidosis, with FDG-PET and BAL positivity, showed a negative ^{99m}Tc-infliximab scintigraphy.

INTRODUCTION

Sarcoidosis is a multi-systemic granulomatous disorder characterized by multiple non-caseating granulomas involving intra-thoracic lymph nodes and lung parenchyma. Inflammatory lesions can occur also in other organs like eyes and skin and, although less frequently, also in liver, spleen, extra-thoracic lymph nodes, salivary glands, heart, nervous system, bones and muscles. Even if its aetiology is still unknown, the role of cell-mediated immunity in the formation and in the maintenance of typical granulomas has been clarified [1, 2]. For this reason immunosuppressive therapy remains the gold standard for treatment and in particular with corticosteroid that is the first therapy line [3]. However, serious side effects of steroid therapy and the loss of long-term efficacy of this treatment have led researchers to use new drugs. Recently, the use of anti-tumor necrosis factor alpha (anti-TNFα) agents has been introduced for therapy of chronic and refractory sarcoidosis [4-6]. TNFα is an important cytokine released by alveolar activated macrophages, implicated in the development of granulomas. Infliximab (Remicade®) is a chimeric monoclonal antibody (mAb) that recognizes and binds TNFα, neutralizing its biological effects [7]. However, the effectiveness of such therapy is still uncertain and under investigation [8]. It is indeed not well known if TNFα is sufficiently present in sarcoid lesions to play a relevant biological role despite its presence in BAL has been shown to correlate with the severity of alveolitis [9]. Nevertheless, which patient and which lesion has high levels of

TNFα and may respond to anti-TNFα therapy, is difficult to ascertain. In this view, the assessment of TNFα in sarcoid lesions by a non-invasive technique could be important to strengthen the hypothesis behind the use of anti-TNFα drugs and to select patients possibly responders to anti-TNFα drugs. Currently there are no specific diagnostic tools to directly evaluate the presence of anti-TNF-α in sarcoid lesions but several methods have been reported for measuring disease activity. Chest X-ray and pulmonary function tests (spirometry), the measurement of serum angiotensin-converting-enzyme (ACE) levels and ^{67}Ga-citrate scintigraphy, bronchoalveolar lavage (BAL) with evaluation of $CD4^+$ and $CD8^+$ lymphocytes, have all been used, and still are, as surrogate markers of diseases activity [10, 11]. In particular, [^{18}F]-Fluoro-2-deoxy-D-glucose PET/CT ([^{18}F]-FDG PET/CT) has been shown to be of high clinical value for evaluation of disease activity and extent and for therapy follow-up [12-15]. In the present study, we have used ^{99m}Technetium (^{99m}Tc) labelled infliximab in patients with newly diagnosed sarcoidosis for non-invasive in vivo scintigraphic evaluation of the presence of TNFα in pulmonary and lymph nodal sarcoid lesions. Patients were also studied by [^{18}F]-FDG PET/CT and BAL with lymphocyte phenotyping for complete evaluation of disease activity.

PATIENTS AND METHODS

Patients and diagnosis

Study design included 20 patients with newly diagnosed sarcoidosis at stage II-III to be prospectively recruited for [^{18}F]-FDG-PET/CT and ^{99m}Tc-infliximab scintigraphy and 10 control subjects (patients without sarcoidosis, but affected by rheumatoid arthritis (RA) to evaluate disease activity in joints). After enrolling all controls (7 females and 3 males, mean age 54$\pm$10 years) and 10 sarcoidosis patients, (8 females and 2 males, mean age 55$\pm$8 years) we performed an interim analysis and decided to stop recruitment, based on results. Sarcoidosis patients were symptomatic and presented respiratory symptoms of the disease; no one had involvement of specific organ but lungs, thoracic and extra-thoracic lymph nodes. They were also subjected to a standard assessment that included history and physical examination, with particular attention to respiratory disorders, blood test with peripheral blood counts and lymphocytes count ratio, X-ray examination of the chest, including X-ray and high resolution CT, bronchoscopy with bronchoalveolar lavage and bronchial biopsy, analysis of BAL with lymphocytes immune-phenotyping (2 patients refused to perform the BAL). The diagnosis of sarcoidosis was performed using histological demonstration of the presence of the typical non-caseating granulomas; others diseases such as Wegener's granulomatosis, tuberculosis, aspergillosis and neoplastic diseases were excluded for each patient. None of enrolled patients had previously been treated with

corticosteroid therapy or immunosuppressive drugs. The study was approved by the local medical ethical committee and each patient expressed written informed consensus.

[^{18}F]-FDG PET/CT

Within 2 months from clinical diagnosis of sarcoidosis, a [^{18}F]-FDG-PET/CT was performed after fasting for at least 6 h before the intravenous injection of [^{18}F]-FDG and with a serum glucose level lower than 160 mg/dl. Diazepam (5 mg) was administered to reduce muscle activity and activation of the brown fat. The activity of [^{18}F]-FDG to be administered was calculated for each patient according to the following formula [(weight in Kg/10 x 37 MBq) +1]. The PET scan was performed with hybrid PET/CT Gemini, (Philips, NL). Imaging acquisition started 60 minutes after the radiopharmaceutical injection from the upper thigh to the head, with a preliminary low-dose unenhanced CT scan (16 slice, 100 mAs) followed by PET imaging (2.5 min per bed position, 3D mode, matrix). Images were reconstructed with CT data by common iterative algorithm (OSEM, ordered subset expectation maximization, 2 iterations, 28 subsets) to obtain attenuation corrected images and anatomical mapping on functional images. [^{18}F]-FDG-PET/CT images were visually analysed and disease activity was assessed separately in the mediastinum, hilum, lung parenchyma, extra-pulmonary lymph nodes, even with obvious evaluation of liver, spleen, bone marrow, bones and joint, in order to highlight a possible involvement of these organs. Each site was scored either positive or

negative (positive = ^{18}F-FDG uptake higher than background; negative = [^{18}F]-FDG uptake lower or equal to background). The semi-quantitative analysis was based on the analysis of standardized uptake value (SUV) evaluated as SUV_{max} and SUV_{mean}, obtained by drawing regions of interest (ROIs) on trans-axial sections of lung parenchyma at the level of 3rd, 5th and 7th thoracic vertebral body. The SUV values obtained were then compared with those obtained in the control population.

^{99m}Tc-infliximab scintigraphy

The mAb infliximab was radiolabelled as previously described [16]. Briefly, 200 μl of $^{99m}TcO_4^-$ (666 MBq) were added to 200 μl of reduced mAb (200 mg/ml) followed by 7 μl of methylene diphosponate (MDP). After 10 minutes of incubation at room temperature, quality controls were performed by instant thin layer chromatography (ITLC). Silica gel strips and 0.9% NaCl solution were used respectively as stationary and mobile phase for labelling efficiency determination. Albumin pre-coated silica gel strips and H_2O:EtOH:NH_3 (5:3:1) solution were used for colloids evaluation. Within 1 week from the PET/CT scan, all patients performed a scintigraphic study with radiolabelled anti-TNF-α after intravenous injection of 370 MBq of ^{99m}Tc-infliximab. Whole body images and planar static images of chest were acquired at 6 and 24 h post-injection with a large field of view, two head, gamma camera (Sky Light, Philips, NL), equipped with low-energy high-resolution collimators and 20% energy windows centred at 140 KeV. Whole body images (matrix 512x1024) were acquired at a speed of 10 cm/min at 6

h and 5 cm/min at 24 h taking in account the decay of the radionuclide. Anterior and posterior thorax images (matrix 256x256) were acquired for 300 seconds at 6 h and 600 seconds at 24 h).

The results of scintigraphic studies were qualitatively analysed to identify any labelled mAb uptake and were visually compared with the pathological findings on PET images. A semi-quantitative analysis was performed drawing ROIs over each lung parenchyma (ROI_{lung}) including hilum, but excluding heart and spine, and a ROI over the upper right arm (ROI_{arm}) as background, excluding joints. The counts were normalized by area and the target-to-background (T/B) ratio (ROI_{lung}/ROI_{arm}) was calculated at 6 h and 24 h for each lung in anterior and in posterior views. The average value of anterior and posterior values was considered for each patient. Results were compared with control subjects that underwent ^{99m}Tc-infliximab for RA and therefore considered "pulmonary negative".

Statistical analysis

For each patient the average values of SUV_{max} and SUV_{mean}, obtained in lung parenchyma, were calculated both in sarcoidosis patients and controls, obtaining for each group the mean value ± SD. Similarly, the mean values ± SD of T/B ratios in sarcoidosis patients and control group were calculated at each time point (6 and 24 h). In sarcoidosis population correlations were made between mean SUV values and mean T/B ratio, mean SUV values and lymphocytes immune-phenotyping on BAL, mean T/B ratio and lymphocytes immune-phenotyping on BAL, in order to

assess the diagnostic accuracy of each methodology to evaluate disease activity. Students' t test was applied to assess the significance of relationship between the T/B ratio of sarcoidosis group and T/B ratio of control subjects.

RESULTS

[^{18}F]-FDG PET/CT

The qualitative analysis performed on PET/CT studies in lungs showed complete agreement with the staging previously made by pulmonologists according to radiological and biochemical findings (Figure 1). Furthermore, in 3/10 patients PET showed other extra-pulmonary sites of disease, with involvement of axillary and abdominal-pelvic lymph nodes, not previously known, demonstrating its high sensitivity. The mean values ± SD of SUV_{max} obtained in patients with sarcoidosis were 4.43 ± 3.20 whereas in control subjects mean values ± SD of SUV_{max} were 1.18 ± 0.20 ($p < 0.001$). These data are an expression of inflammation involvement of lung parenchyma in patients with sarcoidosis. The values of SUV_{max} and SUV_{mean} correlated perfectly; therefore for subsequent analysis only SUV_{max} will be reported even if also SUV_{mean} has always been considered. Despite the higher values of SUV_{max} in patients with sarcoidosis respect to controls, it was not possible to find a cut-off value above which to correlate the extent of uptake in the lung parenchyma with the degree of alveolitis. It was not also possible to obtain a significant correlation between lymphocyte immune-phenotyping results of BAL

(with particular reference to $CD4^+/CD8^+$ ratio) and the SUV_{max} values of patients with sarcoidosis. No correlation was also observed between SUV_{max} or SUV_{mean} values and the $CD4^+/CD8^+$ ratio in blood.

^{99m}Tc-infliximab scintigraphy

The qualitative analysis of scintigraphy with ^{99m}Tc-infliximab showed no pathological focal accumulation of the labeled antibody (table 1). Both images at 6 h, characterized by high vascular activity, and images at 24 h did not show the same pathological uptakes highlighted in the preliminary PET study (Figure 1 and 2). The pulmonary distribution of the two radiopharmaceuticals was different, being predominantly diffused in the case of ^{99m}Tc-infliximab and rather focal with hileal involvement in the PET scans.

Comparing T/B ratios on ^{99m}Tc-infliximab scintigraphy at 6 and 24 h, with SUV_{max} values of pulmonary uptake of FDG, no significant correlation was observed between these parameters. In only three patients was present a detectable diffuse bilateral lung uptake of anti-TNF-α at 6 h and 24 h on scintigraphic images, which could indicate increased levels of TNF-α in lung parenchyma of these patients. When we compared the mean values of lung uptake of labelled anti-TNF-α mAb in sarcoidosis patients and control subjects we found significant differences at 6 h (4.28 ± 0.57 vs 3.2 ± 0.74; patients vs controls; $p = 0.002$) but not at 24 h (3.15 ± 0.45 vs 2.7 ± 0.65; patients vs controls; $p = 0.057$). A moderate correlation was found between $CD4^+/CD8^+$ ratio peripheral blood lymphocytes and the value of

T/B ratio at 6 h (Figure 3) but no correlation was found between average value of T/B ratio at 6 or 24 h and, respectively, $CD4^+/CD8^+$ ratio and cellularity of BAL (Figure 4).

DISCUSSION

In the last decade, systemic autoimmune disease therapy has been revolutionized by the availability of biological drugs, or monoclonal antibodies, directed against a specific target implicated in the pathogenesis of disease. In patients with active sarcoidosis, the release of TNFα by activated alveolar macrophages has been widely documented in a lot of previous studies [17-21]. Infliximab (Remicade ®) is a chimeric monoclonal antibody of the type IgG1κ, with a variable region derived from murine anti-human TNFα and a constant sequence of human-derived IgG1. It was one of the first biological drugs to be used for the treatment of patients with sarcoidosis refractory to conventional therapy [22-26]. In particular, the multicenter phase II study of Baughman et al. [27] showed that in patients with sarcoidosis, symptomatic, refractory to corticosteroid therapy, treated with infliximab, there is a significant improvement of the forced vital capacity (FVC) without significant side effects related to the use of the drug. However, Panzelinas et al. [28] showed in a retrospective study, that in the majority of patients treated with infliximab, there was a recurrence of the disease about 3 months after discontinuation of the drug. Since biological therapies, such as infliximab, are

extremely expensive, it would be desirable to be able to accurately select patients who really might benefit from this type of therapies. To date, however, there are no diagnostic markers for therapy decision making. In order to answer this question, we undertook a study to assess whether scintigraphy with ^{99m}Tc-infliximab, showing directly the presence of TNFα in the lesions, may represent a marker for predicting the efficacy of biological therapy with anti-TNFα and then select the patients suitable for this type of treatment [29, 30]. Infliximab was labelled with high labelling efficiency, high specific activity and stability. Preliminary studies in vitro, in animals and humans have shown its usefulness in the evaluation of patients with Crohn's disease and rheumatoid arthritis [31-33]. [^{18}F]-FDG-PET has proven to be a very sensitive method in the evaluation of disease activity. Many studies have shown its higher sensitivity compared to ^{67}Gallium-citrate scintigraphy in the evaluation of disease and follow-up of therapy [34-41]. However, [^{18}F]-FDG-PET lacks specificity and cannot be used for the selection of patients to be treated with anti-TNFα. Its main role remains the diagnostic confirmation of disease, evaluation of the extension of the sites of disease and the follow-up.

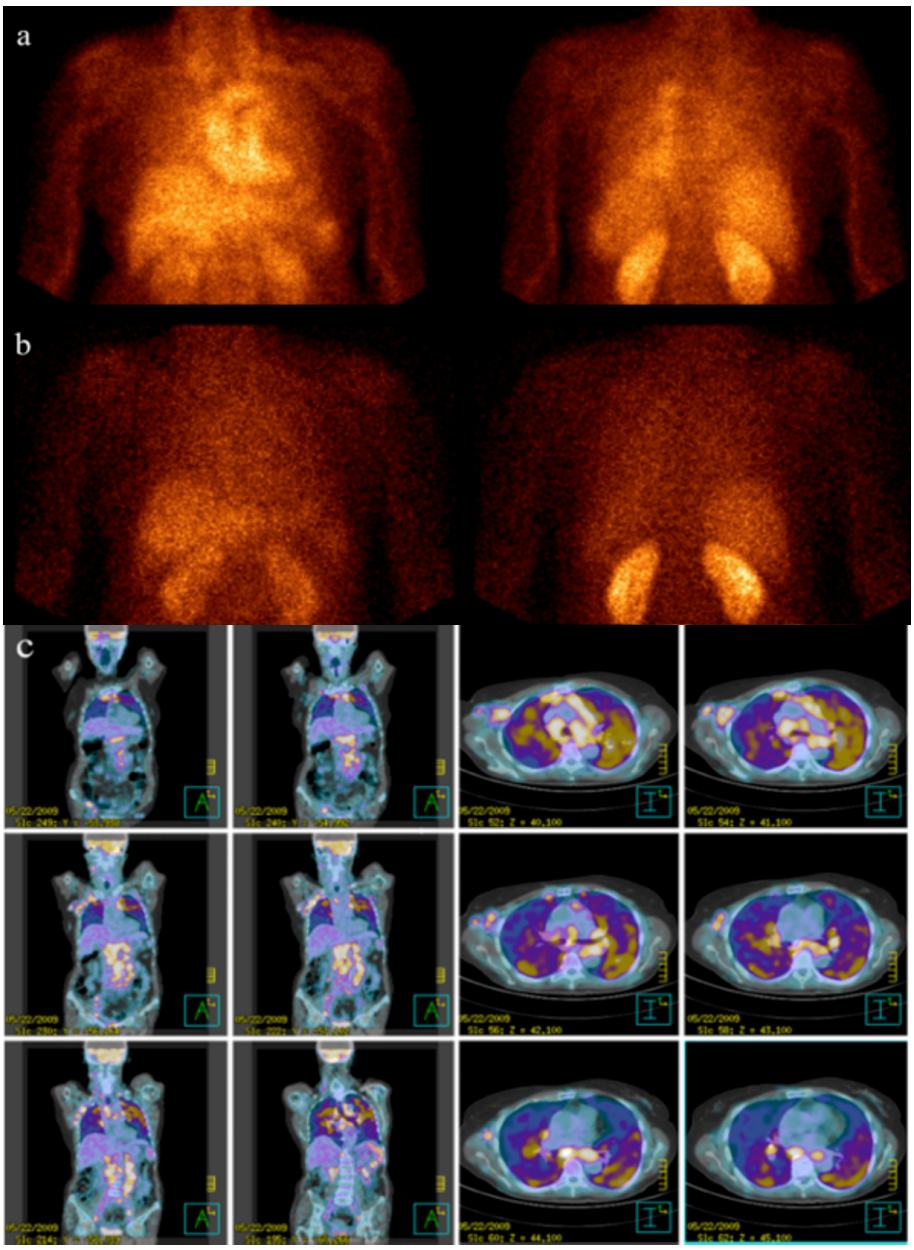

Fig. 1. ^{99m}Tc-Infliximab scintigraphy of a sarcoidosis patient (patient 3/F) acquired at 6 h (anterior and posterior views, a) and at 24 h (anterior and posterior views, b) showing a moderate and diffuse uptake in the lung parenchima. [^{18}F]-FDG-PET/CT images of the same patient showing a focal/hyleal uptake (coronal and transaxial sections, c).

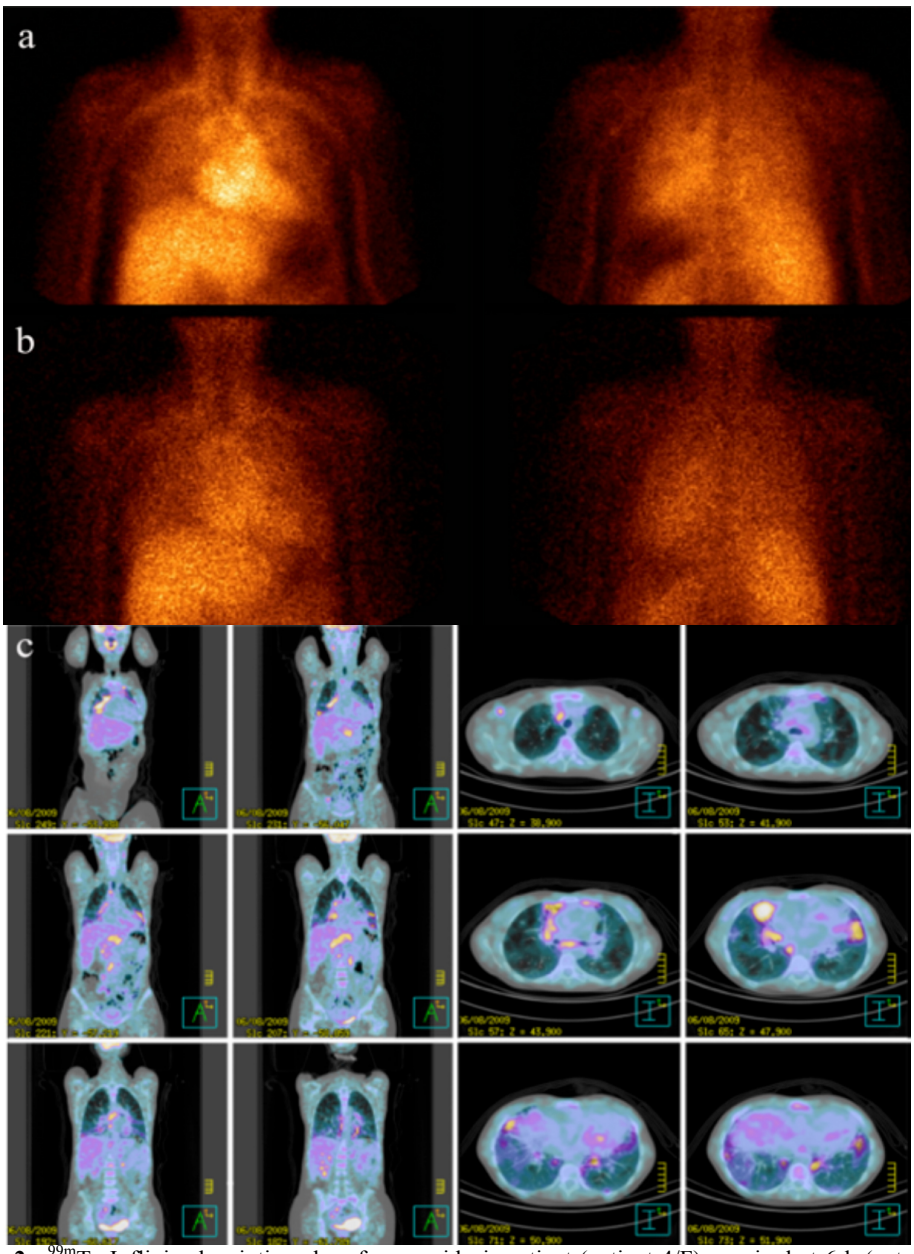

Fig. 2. ^{99m}Tc-Infliximab scintigraphy of a sarcoidosis patient (patient 4/F) acquired at 6 h (anterior and posterior views, a) and at 24 h (anterior and posterior views, b) showing a moderate and diffuse uptake in the lung parenchima. [^{18}F]-FDG-PET/CT images of the same patient showing a focal/hyleal uptake (coronal and transaxial sections, c).

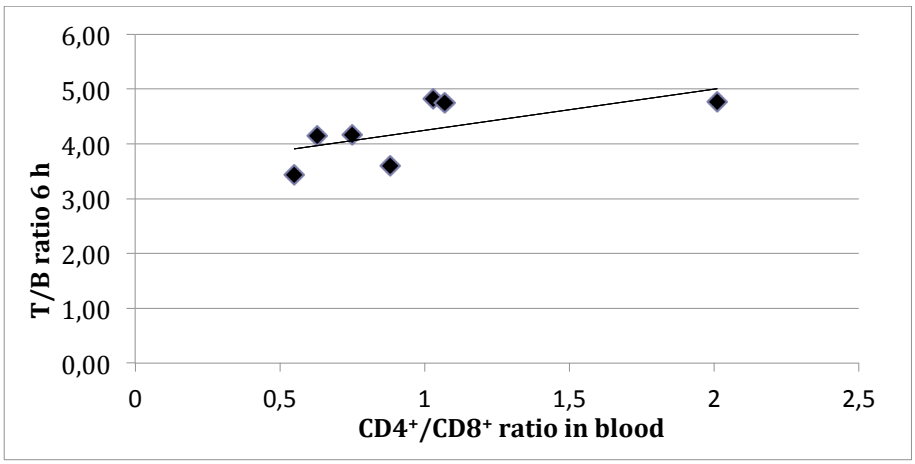

Fig. 3. Correlation between lung uptake of ^{99m}Tc-Infliximab at 6 h (T/B ratio) and $CD4^+/CD8^+$ ratio in peripheral blood lymphocytes. Correlation coefficient is r=0.2357 and p=0.05.

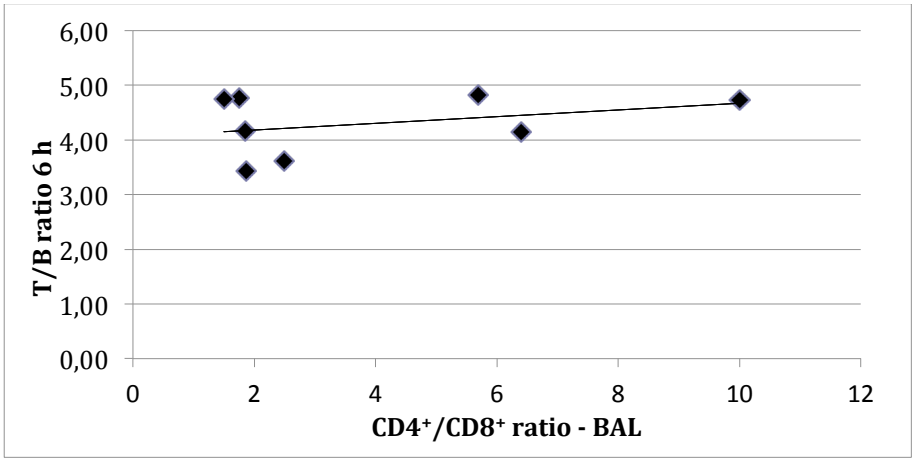

Fig. 4. Correlation between lung uptake of 99mTc-Infliximab at 6 h (T/B ratio) and $CD4^+/CD8^+$ ratio in lymphocytes from BAL. Correlation coefficient is r= 0.6487and p=n.s.

Table 1

Summary of SUV obtained by FDG-PET/CT and T/B values (average of right and left lung calculated in anterior and posterior images) in patients with sarcoidosis.

N°/SEX	STAGE	SUV_{max}	SUV_{mean}	T/B 6 h	T/B 24 h
1/F	I	1.91	0.54	4.16	2.84
2/F	II	3.47	0.99	4.34	2.75
3/F	II	4.38	2.19	3.52	3.49
4/F	II	2.64	0.79	4.82	3.97
5/M	I-II	3.05	1.02	3.61	3.14
6/F	II	5.28	1.25	4.77	3.24
7/M	I	2.23	0.73	4.14	2.72
8/F	II	12.87	4.55	4.73	3.41
9/F	II	3.01	0.88	3.43	2.49
10/F	II	5.48	0.90	4.73	3.42
Mean±SD		4.43±3.2	1.38±1.2	4.22±0.55	3.15±0.45

It is therefore right to compare the role of scintigraphy with ^{99m}Tc-infliximab in the evaluation of disease with the findings obtained with [^{18}F]-FDG-PET, but mainly for the selection of patients suitable for treatment with unlabelled anti-TNFα mAb. From our data, although on a limited series, it appears that with a qualitative examination, PET confirmed the staging performed by pulmonologists and allowed

us to identify locations of extra-thoracic disease, like axillaries and abdomino-pelvic lymph nodes. Inflammatory events in the lung parenchyma of sarcoidosis patients have been confirmed by higher SUV_{max} and SUV_{mean} respect to normal subjects. The lack of correlation between the $CD4^+/CD8^+$ lymphocytes ratio in BAL and the values of both SUV_{max} and SUV_{mean} in the lung, could be explained by the fact that the [^{18}F]-FDG is taken up by various cell types involved in the inflammatory sarcoid granuloma, confirming its poor specificity. Alternatively BAL is performed in a single lung segment whereas SUV was calculated over the whole lungs. Scintigraphy with labelled anti-TNFα mAb was qualitatively positive in 4 out of 10 patients (both stage III), showing at 6 and 24 h a widespread uptake of the radiopharmaceutical in both lungs. The values of T/B ratio calculated, both on the 6 and 24 h images, did not correlate with the values of SUV_{max} and SUV_{mean} calculated on ROI_{lung} of PET. There are many possible explanations for this different pattern of ^{18}F-FDG and ^{99m}Tc-Infliximab in sarcoidosis patients. One of them is that the two radiopharmaceuticals show different aspects of the same phenomenon: the intense [^{18}F]-FDG uptake by the cell populations responsible of alveolitis (macrophages, lymphocytes, etc.) and the presence of TNFα revealed by radiolabelled ^{99m}Tc-infliximab. Alternatively, there may be individual variability in the production of TNFα due to genetic reasons that depend on the stage of the disease.

The lack of a clear focal uptake in some patients could also be caused by the long half-life of the anti-TNFα mAb that resulted in high background activity from the

blood. This phenomenon is critical in highly perfused organs such as the lungs. In this case, the use of isotopes with longer half life, such as ^{89}Zr and ^{111}In, could help allowing to acquire imaging at later time points (e.g. 48 h or 72 h) thus improving T/B ratio due to clearance of radiopharmaceutical from the blood. Moreover, it should be kept in mind that contrarily to what happens in lesions where the targets of a radiopharmaceutical is a membrane bound receptors, TNFα is also a soluble molecule and a possible wash out or low concentration in the lesions could prevent the visualization of distinctive foci.

Indeed, on the basis of the review of literature, the most responsive patients to therapy with infliximab appear to be those with extra-pulmonary disease, with involvement of skin, nervous system, bone and ocular disease; it would be interesting to study these patients with ^{99m}Tc-infliximab scintigraphy in order to effectively assess the presence of TNFα in other extra-pulmunary tissues affected by sarcoidosis.

Our choice was to investigate patients with newly diagnosed sarcoidosis that did not undergo prior therapies, based on the need to study "naive" patients in which no previous immunosuppressive therapy was administered.

Despite to what we expected the T/B ratio calculated at 6 and 24 h did not correlate with the amount of lymphocytes in BAL, indicating that not all immune-mediated phenomena are characterized by high production of TNFα.

CONCLUSIONS

Labelled anti-TNFα mAb scintigraphy could be a good tool for the selection of patients to be treated with anti-TNFα drugs, however, in our study most of the examined patients showed a negative ^{99m}Tc-infliximab scintigraphy, underlining a low presence of TNFα even if [^{18}F]-FDG-PET/CT was highly positive.

REFERENCES

1. Bauhhman RP, Lower EE, du Bois RM. Sarcoidosis. Lancet 2003;361:1111-8.
2. Judson MA. Sarcoidosis: clinical presentation, diagnosis and approach to treatment. Am J Med Sci 2008;335:26-33.
3. Croft AP, Situnayake D, Khair O, Giovanni G, Carruthers D, Sivaguru A, Gordon C. Refractory multisystem sarcoidosis responding to infliximab therapy. Clin Rheumatol. 2012;31:1013-8.
4. Utz JP, Limper AH, Kalra S et al. Etanercept for the treatment of stage II and III progressive pulmonary sarcoidosis. Chest 2003;124:177-185.
5. Doty JD, Mazur JE, Judson MA. Chest 2005;127:1064-71.
6. Saleh S, Ghodsian S, Yakimova V et al. Effectiveness of infliximab in treating selected patients with sarcoidosis. Respir Med 2006;100:2053-9.
7. Sánchez-Cano D, Callejas-Rubio JL, Ruiz-Villaverde R, Ríos-Fernández R, Ortego-Centeno N. Off-Label Uses of Anti-TNF Therapy in Three Frequent Disorders: Behçet's Disease, Sarcoidosis, and Noninfectious Uveitis. Mediators Inflamm. 2013:286857.
8. Korsten P, Mirsaeidi M, Sweiss NJ. Nonsteroidal therapy of sarcoidosis. Curr Opin Pulm Med. 2013;19:516-23.

9. Domagała-Kulawik J, Skirecki T, Maskey-Warzechowska M, Grubek-Jaworska H, Chazan R. Bronchoalveolar lavage total cell count in interstitial lung diseases--does it matter? Inflammation. 2012;35:803-9.
10. Baughman RP, Ploysongsang Y, Roberts RD, Srivastava L. Effects of sarcoid and steroids on angiotensin-converting enzyme. Am Rev Respir Dis. 1983 Oct;128(4):631-3..
11. Winterbauer RH, Lammert J, Selland M et al. Bronchoalveolar lavage cell populations in the diagnosis of sarcoidosis. Chest 1993;104:352-61.
12. Nishiyama Y, Yamamoto Y, Fukunaga K et al. Comparative evaluation of 18F-FDG and 67Ga scintigraphy in patients with sarcoidosis. J Nucl Med 2006;47: 1571-6.
13. Braun JJ, Kessler R, Costantinesco A et al. 18F-FDG PET/CT in sarcoidosis management: review and report of 20 cases. Eur J Nucl Med Mol Imaging 2008;35: 1537-43.
14. Milman N, Mortensen J, Sloth C. Fluorodeoxyglucose PET scan in pulmonary sarcoidosis during treatment with inhaled and oral corticosteroids. Respiration 2003; 70:408-13.
15. Keijsers RG, Verzijbergen EJ, van den Bosch JM et al. 18F-FDG PET as a predictor of pulmonary function in sarcoidosis. Sarcoidosis Vasc Diffuse Lung Dis 2011;28(2):123-9.
16. Conti F, Malviya G, Ceccarelli F, Priori R, Iagnocco A, Valesini G, Signore A. Role of scintigraphy with ^{99m}Tc-infliximab in predicting the

response of intraarticular infliximab treatment in patients with refractory monoarthritis. Eur J Nucl Med Mol Imaging. 2012;39:1339-47.

17. Baughman RP, Iannuzzi M: Tumor necrosis factor in sarcoidosis and its potential for targeted therapy. BioDrugs 2003;17:425-31.
18. Steffen M, Pettersen J, Oldigs M et al: increased secretion of tumor necrosis facor alpha, interleukin-1-beta and interleukun-6 by alveolar macrophages from patients with sarcoidosis. J Allergy Clin Immunol 1993;91:939-49.
19. Ziegenhagen MW, Benner UK, Zissel G et al: Sarcoidosis: TNF-alpha release from alveolar macrophages and serum level of sIL-2R are prognostic markers. Am J Respir Crit Care Med 1997;156:1586-92.
20. Ziegenhagen MW, Rothe ME, Zissel G et al: Exaggerated TNF-alpha release of alveolar macrophages in corticosteroid-resistant sarcoidosis. Sarcoidosis Vasc Diffuse Lung Dis 2002;19:185-90.
21. Baughman RP, Strohofer SA, Buchsbaum J et al: Release of tumor necrosis factor by alveolar macrophages of patients with sarcoidosis. J Lab Clin Med 1990;115:36-42.
22. Doty JD, Mazur JE, Judson MA. Treatment of sarcoidosis with infliximab. Chest 2005; 127:1064-71.
23. Baughman R, Lower E. Infliximab in refractory sarcoidosis. Sarcoidosis Vasc Diffuse Lung Dis 2001;18:70-4.

24. Mallbris L, Ljunberg A, Hedblad MA, Larsson P, Stahle Backdahl M. Progressive cutaneous sarcoidosis responding to anti-tumor necrosis factor-alpha therapy. J Am Acad Dermatol 2003;48:290-3.
25. Roberts SD, Wilkes DS, Burgett RA, Knox KS. Refractory sarcoidosis responding to infliximab. Chest 2003;124:2028-31.
26. Saleh S, Ghodsian S, Yakimova V, Henderson J, Sharma OP. Effectiveness of infliximab in treating selected patients wiyh sarcoidosis. Respir Med 2006;100:2053-9.
27. Baughman R, Drent M, Kavuru M, Judson MA, Costabel U, Du Bois R, Albera C, Brutsche M. Infliximab therapy in patients with chronic sarcoidosis and pulmonary involvement. Am J Respir Crit Care Med 2006;174:795-802.
28. Panselinas E, Rodgers JK, Judson MA. Clinical outcomes in sarcoidosis after cessation of infliximab treatment. Respirology 2009;14:522-8.
29. Malviya G, Galli F, Sonni I, Pacilio M, Signore A. Targeting T and B lymphocytes with radiolabelled antibodies for diagnostic and therapeutic applications. Q J Nucl Med Mol Imaging. 2010;54:654-76.
30. Signore A, Lauri C, Galli F. Radiolabelled probes targeting infection and inflammation for personalized medicine. Curr Pharm Des. 2014;20:2338-45.
31. Conti F, Priori R, Cimenti MS, Coari G, Annovazzi A, Varesini G, Signore A. Successful treatment with intraarticular infliximab for resistano knee monoarthritis in a patient with spondylarthrophaty: a role for scintigraphy with 99mTc-infliximab. Arthritis Rheum 2005;52:1224-6.

32. Chianelli M, D'Alessandria C, Conti F, Priori R, Valesini G, Annovazzi A, Signore A. New radiopharmaceuticals for imaging rheumatoid arthritis. Q J Nucl Med Mol Imaging 2006;50:217-25.

33. D'Alessandria C, Malviya G, Viscido A, Aratari A, Maccioni F, Amato A, Scopinaro F, Cprilli R, Signore A. Use of a 99mTc labeled anti-TNFalpha monoclonal antibody in Crohn's disease: in vitro and in vivo studies. Q J Nucl Med Mol Imaging 2007;51:334-42.

34. Alavi A, Buchpiguel CA, Loessner A. Is there a role for FDG-PET imaging in the management of patients with sarcoidosis? J Nucl Med 1994;35:1650-2.

35. Zhuang H, Alavi A. ^{18}Fluorodeoxyglucose Positron Emission Tomographic Imaging in the detection and monitoring of infection and inflammation. Semin Nucl Med 2002; 32:47-59.

36. El-Haddad G, Zhuang H, Gupta N, Alavi A. Evolving role of Positron Emission Tomography in the management of patients with inflammatory and other benign disorders. Semin Nucl Med 2004;34:313-29.

37. Brudin LH, Valind SO, Rhodes CG, Pantin CF, Sweatman M, Jones T, Hughes JM. ^{18}Fluorine deoxyglucose uptake in sarcoidosis measured with positron emission tomography. Eur J Nucl Med 1994;21:297-305.

38. Milman N, Mortensen J, Sloth C. Fluorodeoxyglucose PET scan in pulmonary sarcoidosis during treatment with inhaled and oral corticosteroids. Respiration 2003;70: 408-13.

39. Nishiyama Y, Yamamoto Y, Fukunaga K, Takinami H, Twado Y, Satoh K, Ohkawa M. Comparative evaluation of ^{18}F-FDG PET and ^{67}Ga scintigraphy in patients with sarcoidosis. J Nucl Med 2006;47:1571-6.

40. Prager E, Wehrschuetz M, Bisail B, Woltsche M, Schwarz T, Lanz H, Sorantin E, Aigner RM. Comparison of 18F-FDG and 67Ga-citrato in sarcoidosis imaging. Nuklearmedizin 2008;47:18-23.

41. Teirstein AS, Machac J, Almeida O, Lu P, Padilla ML, Iannuzzi MC. Results of 188 whole-body fluorodeoxyglucose positron emission tomography scans in 137 patients with sarcoidosis. Chest 2007;132:1949-53.

Chapter 4

In vivo imaging of NK cell trafficking in tumors

F. Galli[1, 4], A. S. Rapisarda[1], H. Stabile[2], I. Manni[3], E. Bonanno[5], G. Piaggio[3], A. Gismondi[2], A. Santoni[2], A. Signore[1, 4]

[1]Nuclear Medicine Unit, Faculty of Medicine and Psychology, Department of Medical-Surgical Sciences and of Translational Medicine, "Sapienza" University, Rome, Italy.
[2]Department of Molecular Medicine, "Sapienza" University, Rome, Italy.
[3]Molecular Oncogenesis Laboratory, Experimental Oncology Department, Regina Elena National Cancer Institute, Rome, Italy
[4]Department of Nuclear Medicine and Molecular Imaging, University Medical Center Groningen, University of Groningen, The Netherlands.
[5]Department of Biomedicine and Prevention, "Tor Vergata" University, Rome, Italy.

J Nucl Med. 2015 Aug 13. pii: jnumed.114.152918

ABSTRACT

Introduction: Natural killer cells (NKs) are important effectors of the innate immune system with marked anti-tumor activity. Imaging NKs trafficking in vivo may be relevant to follow-up the efficacy of new therapeutic approaches aiming at increasing tumor-infiltrating NKs (TINKs). Specific aims of present study were (1) to efficiently target NKs using a ^{99m}Tc-anti-CD56 and (2) to image human NKs trafficking in SCID mice bearing a human cancer.

Material and Methods: The anti-CD56 mAb was radiolabelled with 99mTechnetium and in-vitro quality controls (QC) were performed to test labelling efficiency, stability and binding affinity to CD56. In-vivo biodistribution was performed by injecting 5.5MBq (104ng) of radiolabelled antibody in the tail vein of SCID mice, sacrificed at 1, 3, 6 and 24h p.i. Targeting experiments were performed in two groups of SCID mice inoculated subcutaneously with increasing number of human NKs in the right thigh (from 2.5x106 to 40x106) and human granulocytes (CD56-) or anaplastic thyroid cancer (ARO) cells in the contralateral thigh as control. TINKs trafficking imaging was achieved by injecting 5.5MBq of ^{99m}Tc-anti-CD56 mAb in SCID mice bearing ARO tumor xenografts in the right thigh, 24h after being reconstituted with 105 or 106 or 107 human NKs.

Results: Anti-CD56 mAb was radiolabelled achieving a radiochemical purity >97% with a specific activity of 3700MBq/mg and retained biochemical integrity and binding activity. In vivo studies revealed a physiological uptake in liver and

kidneys. Targeting experiments confirmed the specificity of labelled antibody to CD56+ cells. Human NK cells, injected in CD1 nude mice accumulated in the ARO tumors within 24h and were imaged as early as 3h after i.v. administration of ^{99m}Tc-anti-CD56.

Conclusions: ^{99m}Tc-anti-CD56 is a promising tool for in vivo imaging of TINK cell trafficking.

INTRODUCTION

Among surgery, radiation and chemotherapies, our immune system has a key role against tumors. Recent scientific advances have demonstrated its importance and potential in oncology. Indeed, both innate and adaptive immunity cells are involved in the immune surveillance process that prevents tumor development either by releasing cytokines or mediating long-lived, antigen-specific response. However, such mechanisms are often inhibited by tumor cells that can establish a suitable microenvironment to sustain their proliferation [1].

In the last 20 years, many new therapeutic strategies have been developed, aiming at increasing host response against tumors. These include cytokines, monoclonal antibodies (mAbs), vaccines, adoptive cell transfers and Toll-like receptor agonists [2-4]. In particular, Natural Killer cells (NKs) are a particular subset of lymphocyte with great cytotoxic potential. Approximately 90% of peripheral blood and spleen NKs are $CD56^{dim}CD16^{+}$ and possess high cytotoxic activity, whereas CD56brightCD16- cells have mainly an immune-regulatory role [5]. Under particular stimuli, NKs are able to kill certain targets, including tumor cells, even without any prior immunization. The interest around tumor infiltrating NKs (TINKs) increased after publication of several studies that correlated the presence of NKs with tumor prognosis [6]. High levels of TINKs are associated with good prognosis in patients affected by cancer [7-9]. Given their importance in the

response against tumors, many companies are developing drugs that are able to increase the number and efficacy of TINKs.

In this context, imaging NKs trafficking in-vivo may be relevant to follow-up the efficacy of such novel therapeutic approaches. Several attempts to image NKs have been done in the past years by different groups using direct labelling strategies that involve cell purification from peripheral blood, radiolabelling ^{111}In-oxine and re-administration in patients [10-11]. This approach has several limitations such as cell manipulation in culture and cell-function impairment after ex-vivo labelling. Several studies reported toxicity of ^{111}In-oxine on cells leading to improper migration into target organs [12, 13]. Thus, we investigated a novel approach for in-vivo cell labeling using a mAb that binds to CD56 antigen expressed on cell surface of the majority of human NKs [14]. The use of such radiopharmaceutical may allow imaging NKs directly in vivo, without the need of in vitro manipulation. Aims of present study were (1) to efficiently radiolabel this mAb with 99mTechnetium and (2) to image human NKs trafficking in SCID mice bearing a human cancer.

MATERIAL AND METHODS

Antibody

The C218 hybridoma cell line (producing the anti-CD56 mAb) was kindly provided by Dr. A. Moretta (Institute Gaslini, Italy) [15]. Hybridoma cells were

cultured in RPMI medium supplemented with 5% FCS in a “miniPERM” bioreactor (Sarsted, Germany). After 8 days of culture the medium was collected and clarified by centrifugation at 2000rpm for 10min. The mAb was purified from hybridoma supernatant using protein-G-based affinity chromatography (Thermo-Scientific, USA). The column was equilibrated with 10 volumes of binding buffer (0.1M phosphate, 0.15M NaCl) before loading the supernatant. Non-bound serum components were washed away with 10 volumes of binding buffer, then the mAb was eluted with 5 volumes of acidic elution buffer (Glycine-HCl 0.1M, pH 2.7) and small fractions of solution that passed from the column were collected and subjected to spectrofluorimetric analysis. Fractions with an optical density at 280 nm >0.1 were pooled and additionally purified through gel-filtration, using a dextran desalting column (Thermo-Scientific, USA).

Cell lines and NKs purification

The anaplastic thyroid cancer cell line (ARO) was cultured in DMEM high glucose (Gibco, Germany) supplemented with 10% FCS, penicillin/streptomycin (penicillin G 10000U and streptomycin 10mg) 10mL/l, amphotericin B (250 mg/ml) 10 mL/l, l-glutamine 1% (16). NKs were obtained from the blood of healthy donors. Healthy donors' peripheral blood mononuclear cells (PBMCs; 4×105 cells) were isolated by Lymphoprep gradient centrifugation and then co-cultured for 10 days with irradiated (30Gy) Epstein-Barr virus–transformed B-cell line RPMI 8866 (105 cells) at 37°C as previously described [17, 18]. After 10 days, cells were collected

and phenotypically characterized through immunofluorescence using anti-CD16 (3G8 BD Biosciences, USA), anti-CD56 (BD-Biosciences, USA) and anti-CD3 (BD-Biosciences, USA) mAb and analyzed by flow cytometry (BD-Biosciences, USA). On day 10 the cell population was routinely greater than 90% $CD56^{+}CD16^{+}CD3^{-}$, when purity was less than 90%, contaminant T-cells were eliminated by immunomagnetic negative selection with anti-CD3 mAb, in order to obtain a purity greater than 95%. Human granulocytes were isolated from healthy donors by Percoll gradient centrifugation as previously described [19].

Labelling of anti-CD56 mAb with ^{99m}Tc

Briefly, 1mg of lyophilized mAb was resuspended in 500µl of distilled water and this solution was purified by size exclusion chromatography using a G-25 Sephadex PD10 column (GE Healthcare, Sweden) and nitrogen-purged phosphate buffered saline (PBS) as eluent (20ml). Indirect labelling of anti-CD56 mAb was performed by conjugation of the mAb with the heterobifunctional linker S- HYNIC (succinimidyl-6-hydrazinonicotinate hydrochloride) (SoluLink, USA). The chelator (100mM in DMF) was added at different molar ratios (from 20:1 to 50:1) to a solution of antibody (20mM) in 100mM sodium phosphate/150mM NaCl buffer solution pH 7.6 - 8.0. The mixture was purified by G-25 Sephadex PD10 column chromatography using nitrogen-purged cold phosphate buffered saline (pH 7.4) as eluent. The number of HYNIC groups bound per molecule of antibody was determined by molar substitution ratio (MSR) assay. Briefly, 2µl of conjugated

anti-CD56 mAb were added to 18µl of a 0.5mM solution of 2-sulfobenzaldehyde in 0.1M 2-(N- morpholino)ethanesulfonic acid (MES) buffer, pH 5.0 and incubated at room temperature for 2 hours. After 2 hours the absorbance at 345nm of each reaction was measured with a spectrophotometer and the number of HYNIC groups per molecule was calculated as indicated in the SoluLink data sheet. To efficiently label the mAb-SHNH complex with ^{99m}Tc, to minimize the percentage of colloid formation and to optimize the influence of the amount of co-ligand on the labelling efficiency, titrations of tricine (Sigma-Aldrich Chemicals, UK - from 1 mg/ml to 200 mg/ml in PBS) and SnCl2 (Sigma-Aldrich Chemicals, UK - from 1 mg/ml to 10 mg/ml in 0.1 M HCl,) were performed with mAb-HYNIC complex (25µg) in 1M Sodium Acetate (pH 5.5), using different amounts of freshly eluted 99mTcO4- (100µl), while keeping a constant reaction volume.

In vitro quality controls of ^{99m}Tc-anti-CD56 mAb

Quality controls were performed using Instant Thin Layer Chromatography-Silica Gel (ITLC-SG) strips (VWR International, Italy) as described elsewhere [20]. The stability of the labelled antibody was measured in human serum and 0.9% NaCl solution at 37°C up to 24h. For this purpose, two aliquots of 100µl of ^{99m}Tc-anti-CD56 mAb were incubated with 900µl of fresh human blood serum and with 900µl of saline solution at 37°C. The percentages of free ^{99m}Tc and antibody-bound radioactivity were measured at 1h, 3h, 6h and 24h by ITLC-SG. In addition, a cysteine challenge assay was performed to check the in-vitro stability of the

radiolabelled antibody. ^{99m}Tc-anti-CD56 mAb was incubated at 37°C for 60 min at different cysteine:mAb molar ratios, which ranged from 500:1 at the highest cysteine concentration to zero in the absence of cysteine. At the end of the incubation time, each reaction mixture was evaluated by ITLC-SG as described above. This experiment was repeated in triplicates. Possible modifications induced by the labeling procedure on anti-CD56 mAb were tested by sodium dodecyl sulphate-polyacrylamide gel electrophoresis (SDS- PAGE) in non-reducing conditions, according to Laemmli's method [21]. Proteins were visualized by staining the gels with Coomassie Brilliant Blue (Pierce, USA). Radioactivity associated with each band was determined using a linear scanner (Bioscan Inc., USA). This experiment was performed after three different labellings.

Immunoreactive fraction assay

The immunoreactive fraction (IRF) assay was performed, using a constant concentration of radiolabelled mAb and serial dilutions of NKs, according with published method [20]. Cells were washed three times in PBS and resuspended in a cold 1% bovine serum albumin in PBS (BSA/PBS) solution. Radiolabelled mAb at a constant concentration (50ng/ml) in 1% BSA/PBS solution was added to different amounts of cells (final concentration ranging from $1x10^6$ to $0.08x10^6$ cells/ml) in triplicates with or without an excess of unlabeled antibody (100 fold molar excess). Cells were incubated for 2h at 4°C and then washed twice with 500µl of cold 1% BSA/PBS solution before counting cell-associated radioactivity

in a single well gamma-counter (Gammatom, Italy). Data were plotted as a double inverse plot of the applied radiolabelled antibody over the specific binding, as a function of the inverse cell concentration. In this plot, the origin of the abscissa represents infinite cell concentration, i.e. conditions of infinite antigen excess.

Uptake/retention assay (LigandTracer^{TM} assay)

Real time measurements of cellular uptake and retention were performed three times after different labelings, using a rotating radioimmuno-assay in a LigandTracerTM instrument (Ridgeview Instruments AB, Sweden) [22].

In a typical experiment, $CD56^{+}$ NKs ($5x10^{6}$) were resuspended in 1ml PBS and plated into fibronectin coated plastic circular Petri dishes and activated with 0.20M N-ethyl-N'-(dimethylaminopropyl)carbodiimide (EDC) and 0.05M N-hydroxysuccinimide (NHS). Each dish was then incubated with cells and placed in LigandTracer during continuous rotation for 1h, to allow release of weakly attached cells. After one gentle wash, the cell dishes were ready for measurement. Radiolabelled mAb (0.7nM) in PBS pH 7.4 supplemented with 7% cell culture medium devoid of FCS was then added.

When the radiolabelled antibody binds to the cells, a detector placed over the elevated part of the dish registers the cell-bound activity each time the cells pass through the detector. By following the activity over time, a real-time binding curve was obtained, using a LigandTracer Software 1.1 (Ridgeview Instruments AB,

Sweden). Data are exported and analysed with GraphPad software to determine the dissociation constant (K_d).

In vivo biodistribution and cell targeting

For animal experiments, the institutional and national guide for the care and use of laboratory animals was followed. For in vivo biodistribution studies 5.5MBq (100µl) of labelled anti-CD56 were injected in the tail vein of 12 SCID mice and static planar posterior images were acquired using a high resolution portable mini-gamma camera (HRγC) [23] at 1h, 3h, 6h and 24h, under light ether anaesthesia. At the end of each imaging point three mice were sacrificed and major organs were collected and counted in a single well gamma-counter. Time-activity curves in organs were created for both in vitro and ex vivo data. For cell targeting studies, two groups of 24 SCID mice were subcutaneously injected in the right thigh with increasing number of human NKs $CD56^+$ mixed with Matrigel® (BD-Biosciences, USA) ranging from $2.5x10^6$ to $40x10^6$. In the contralateral thigh of both groups, $CD56^-$ cells (ARO and human granulocytes respectively) were injected as negative control. After 1h, 5.5MBq of ^{99m}Tc-anti-CD56 were injected in the tail vein and planar posterior images were acquired at 1h, 3h, 6h and 24h.

Kinetic studies of NK infiltration in tumors

To investigate the kinetics of NKs infiltration in our xenograft model, an anaplastic thyroid cancer cell line (ARO) from a male donor (XY genotype) was injected

subcutaneously mixed with Matrigel® in the right thigh of 18 male SCID mice (XY genotype). After consistent tumor growth, 106 NKs from a female donor (XX genotype) were injected i.v. in the tail vein. After 3h, three mice were sacrificed and tumors were collected, formalin fixed and paraffin embedded. The same procedure was repeated at 6h, 12h, 24h, 48h and 72h. Histological analysis were performed at each time point, including haematoxylin-eosin staining of sections, immunohistochemistry and fluorescent in situ hybridization (FISH) for the Y chromosome allowing us to differentiate between exogenous human TINKs (XX genotype) from endogenous TINKs and ARO cells (XY genotype). Immunoperoxidase staining with an anti-CD57 mAb, revealed with DAB after secondary antibody incubation, was performed for the identification of $CD57^+$ TINKs. CD57 was chosen as NK marker to avoid any interference from injected anti-CD56.

Imaging of TINKs in SCID mice with ARO tumors

Imaging of exogenous human TINKs was performed in four groups of SCID mice (n=12) bearing an ARO tumor xenograft in the right thigh. Three groups received respectively 10^5, 10^6 and 10^7 human NKs, whereas the fourth group was used as negative control. After 24h (as determined from previous experiment), 5.5 MBq of ^{99m}Tc-anti-CD56 were injected in the tail vein of each mouse and planar posterior images were acquired at 1h, 3h, 6h and 24h p.i. by HRγC. After the last time point, mice were sacrificed for organ counting and histology.

RESULTS

Labelling and quality controls of anti-CD56 mAb

MSR analysis of HYNIC-conjugated mAb revealed the presence of 9.1, 18, and 23.5 molecules of chelator per molecule of antibody, when conjugated with 20:1, 30:1, and 50:1 HYNIC:mAb ratio, respectively. A ratio of 30:1 was selected as the formulation of choice since no modification of binding activity was observed (see next paragraph). Optimization of ^{99m}Tc labelling of HYNIC- mAb conjugate (25µg mAb, 30:1 HYNIC:mAb ratio, tricine 55.8mM, SnCl2 170µM, 92MBq, 10min incubation r.t.) gave a radiochemical purity >97% after purification by size exclusion chromatography. Specific activity was 3700MBq/mg. Radiolabelled anti-CD56 mAb was stable in both saline and human serum up to 24h (>90%). The cysteine challenge assay demonstrated a moderate stability up to 200-fold molar excess of cysteine (supplemental data). SDS-PAGE analysis showed no significant differences between the native and radiolabelled anti-CD56 mAb (see supplement material). Native, conjugated and radiolabelled mAb showed a band of approximately 150kDa (i.e. molecular weight of complete mAb). However, a small band of >250kDa was also present in both lanes and could be ascribed as dimers of the complete mAb, but the radioactivity was associated only with the band corresponding to the intact mAb.

In vitro binding experiments

The immunoreactive fraction assay data demonstrated a closely linear relationship of 'total applied/specific binding' as a function of the inverse cell concentration. Unspecific binding was negligible and 76.9% (SD=±3.5, SEM=1.73) of the radiolabelled mAb was immunoreactive (Figure 1). LigandTracer experiments showed that the radiolabelled mAb was able to bind to NKs over time, reaching a plateau between 1 and 2 h. After the replacement of the radioactive medium with PBS, the ^{99m}Tc-anti-CD56 was strongly retained on the cell surface with a very slow off-rate (Figure 2). A dissociation constant of $1.7x10^{-10}$ (SD=$\pm 0.02x10^{-10}$, SEM=$0.0153x10^{-10}$) was calculated by average of three different experiments. At the end of these experiments cells were all viable (as assessed by Trypan Blue exclusion) thus indicating no toxicity of the ^{99m}Tc-mAb to NKs over at least up to 33h.

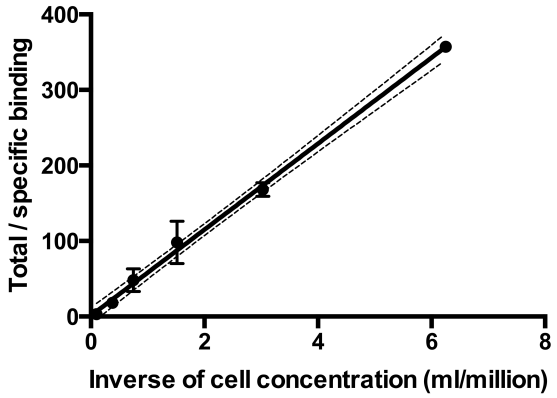

Figure 1. Double inverse plot of data obtained by immunoreactive fraction assay of radiolabelled ^{99m}Tc-anti-CD56 mAb. Each point represents the mean of three different experiments and error bars represent SD (y=56.88x+1.33, R2=0.997).

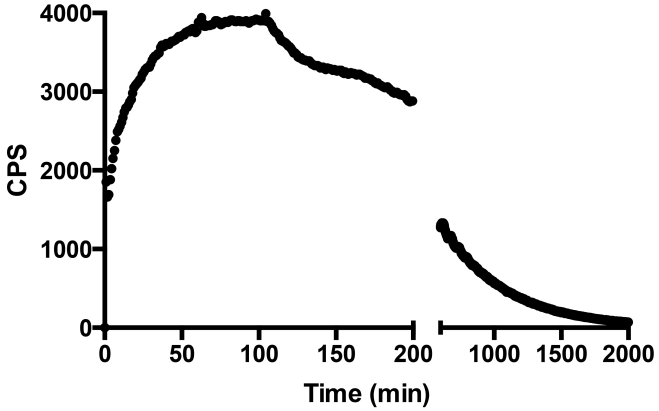

Figure 2. Binding trace graph (decay-corrected) for uptake of ^{99m}Tc-anti-CD56 mAb to human NKs in vitro reachingmaximum binding after 60 minutes. At this time point the radioactive medium was replaced with COLD PBS and retention studies were performed. Each point represents a single measurement on the same petri-dish over time.

In vivo biodistribution and cell targeting

In vivo biodistribution studies, summarized in Figure 3A, showed a high circulating activity up to 24h with predominant liver and, to a minor extent, kidney uptake. Blood and liver showed the highest %ID/g at 1h, whereas at 24h highest activity was detected in the spleen (Figure 3A). Cell targeting experiments demonstrated the possibility to image as little as $2.5x10^6$ NKs in a volume of 300µl, with a T/B ratio of 1.8 (SD=±0.1, SEM=0.0577) at 24h. Animals injected with more than 10^7 NKs showed a T/B ratio up to 4h at 24h (Figure 4).

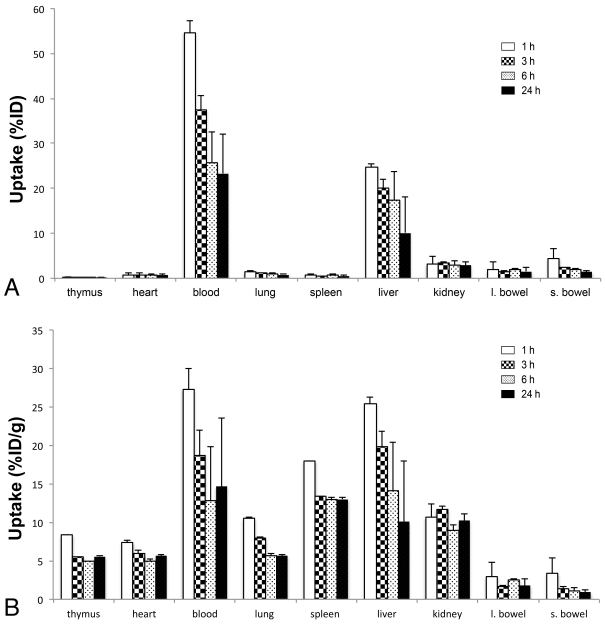

Figure 3. Biodistribution of radiolabelled anti-CD56 mAb at 1h (white bar), 3h (squared bar), 6h (dotted bar) and 24h (black bar) in normal mice. Data were expressed as %ID per organ (a) and %ID/g (b). Error bars denote standard deviation.

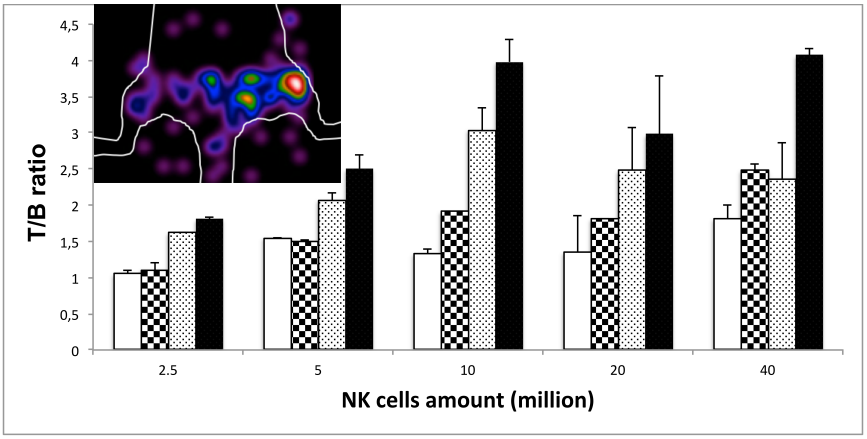

Figure 4. T/B ratios calculated in mice injected with increasing amounts of $CD56^+$ NKs in the right thigh (Target) and with same amounts of $CD56^-$ control cells in the left thigh (Background). Mice were imaged at 1h (white bar), 3h (squared bar), 6h (dotted bar) and 24h (black bar). The insert shows the image of the back of a mouse bearing a 10^6 NKs bolus after the injection of 5.5 MBq of radiolabelled mAb acquired 24h p.i..

Kinetic studies of NK cell infiltration in tumors

Studies of NKs kinetic in vivo demonstrated that they were able to infiltrate tumors after 3h p.i. with slight increment with time and no contamination of host NKs as showed by FISH analysis (Figure 5 and supplemental data). Most severe infiltration was observed between 12h and 24h whereas after 24h the tumor started to show necrotic areas induced by NKs killing of tumor cells. We therefore selected 24h as best time point for future experiments.

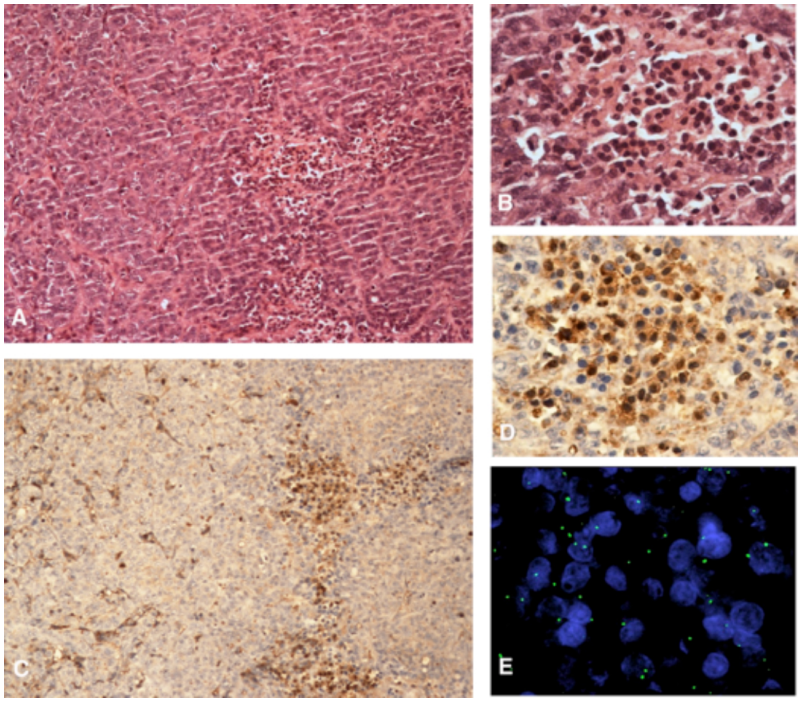

Figure 5. Haematoxylin eosin low power field showing a tumor infiltrated by numerous lymphocytes (A) demonstrated at higher magnification in B. Lymphocytic infiltrate was formed by natural killer cells as demonstrated by CD57 immuno-staining (brown cells in C and D). They were from the donor a female subject (and therefore not from the mouse host) as demonstrated by the absence of Y chromosome detected by FISH analysis only in cancer cells from male donor (light green dots in E).

Imaging of TINKs in SCID mice with implanted ARO tumors

The radiopharmaceutical allowed a clear visualization of tumor xenografts with almost no signal from negative controls. The highest uptake was detected at 24h p.i. with a target-to-background (T/B) ratio of 6.02 that correlated with the number of $CD56^{+}/CD57^{+}$ TINKs as confirmed by immunohistochemistry studies (Figure 6). Moreover, the number of NKs positively correlated with the size of the tumors (r2=0.89; p=0.001) and the radioactivity detected by ex-vivo organ counting (r2=0.90; p=0.001), (Figure 7). No correlation was found between the number of injected NK cells and the number of TINKs found in the tumor. Overall larger tumors were more infiltrated and showed more necrosis.

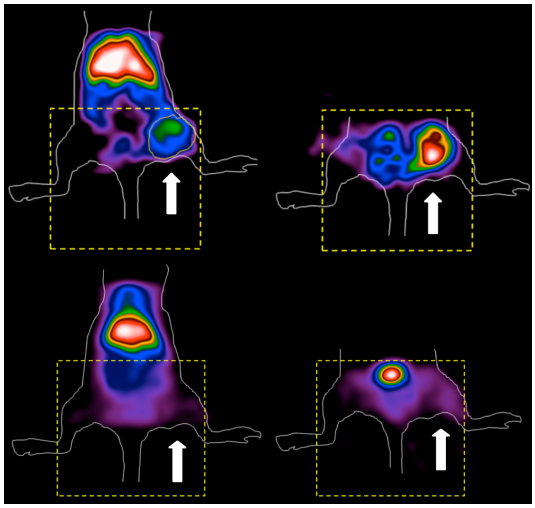

Figure 6. Top: Total body (left) and particular (right) scans of a mouse bearing an ARO xenograft (arrow) in the right thigh. The animal received i.v. 10^6 human NKs and after 24h 5MBq of radiolabelled anti-CD56. Images were performed after 24h from injection of the radiopharmaceutical. Bottom: As negative controls, mice bearing an ARO xenograft received i.v. only the radiolabelled antibody. Images were acquired at 24h p.i.. Each mouse is representative of a group of 3 mice.

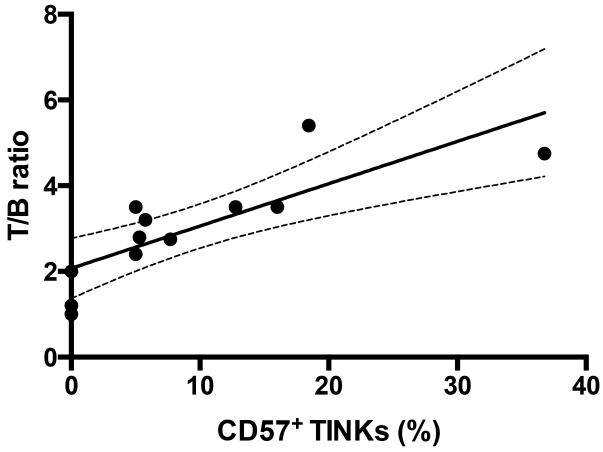

Figure 7. Correlation between TINKs in ARO tumors and calculated T/B ratio at 6h (p=0.005). Target (T) was calculated over the tumor and background (B) was calculated in a similar sized region over the contralateral thigh. The percentage of $CD57^+$ NKs in tumors correlates with the acquired radioactivity indicating that the radiolabelled anti- CD56 is able to specifically bind in vivo to $CD56^+/CD57^+$ NKs as revealed by both trafficking and immunohistochemistry studies. The line is the linear regression fit of all points (y=0.098x + 2.0877; R2=0.65433).

DISCUSSION

In the present study, we radiolabelled an anti-CD56 mAb as a novel radiopharmaceutical to image TINKs. This approach could be important in the development of novel drugs for immunotherapy of cancer, aimed at increasing NKs infiltration into tumors, to follow up the efficacy of these drugs. Indeed, it could allow researchers to monitor cell trafficking directly in-vivo. Despite the long half- life of mAbs, we have chosen ^{99m}Tc as isotope, since this anti-CD56 showed very high affinity binding in-vitro and in-vivo gave good visualization of TINKs within 3h and 24h after its i.v. administration, with fast disappearance from blood. The mAb was radiolabelled with a well- established technique based on the

use of SHNH as a bifunctional chelator obtaining a high labelling efficiency and stability. In vivo, in SCID mice lacking human NKs, the proposed radiopharmaceutical showed typical characteristics of other radiolabelled mAbs but with shorter circulating half-life and high uptake in the liver and at a lower extent in the kidneys. After reconstitution of mice with human NKs, the biodistribution of the labelled antibody changed, showing lower circulating half-life and higher liver and spleen activity due to specific binding to NKs homing in these tissues. These data are in agreement with those reported by Ray et al [24] that hypothesised that either NKs could be resident in the liver or the organ itself is responsible for the metabolization of both radiopharmaceutical and cells. In vivo targeting of Matrigel® immobilized NKs reached the maximum T/B ratio between 6h and 24h, suggesting this time frame as the best choice for imaging. In our in vivo studies we demonstrated a rapid infiltration of tumors by NKs starting as early as 3h after i.v. administration of cells without any contamination from endogenous NKs, as revealed by immunohistochemistry and FISH staining. We can therefore speculate that murine NKs (present in SCID mice) do not efficiently recognize and infiltrate human xenograft tumors. The number of TINKs positively correlated with tumor size and the percentage of necrosis over time, highlighting a direct killing effect of TINKs on the lesion and the full functionality of these cells. Imaging experiments in mice bearing ARO xenografts demonstrated a clear uptake of the radiopharmaceutical with a T/B of 6.02 at 24h. Moreover, tumor size, together with the number of TINKs, positively correlated also with the

radioactivity detected by ex-vivo counting and by in- vivo HRγC imaging. This clearly indicates that it is possible to image TINKs in vivo with ^{99m}Tc- anti-CD56. Our study also opens the possibility to improve the described imaging technique by using a positron-emitting isotope. Indeed, other attempts of imaging NKs have been reported in literature including MRI [25], fluorescence and bioluminescence imaging [26], SPECT [27] and PET [28, 29]. Till now no technique emerged as superior among the others, but nuclear medicine approaches proved to be most promising for human studies. To this aim, human NKs have been labelled ex-vivo with 111In-oxine and re-administered in patients with metastatic melanoma [30]. Interesting, but preliminary results were also reported in patients with renal or colon carcinoma [31, 32]. Nevertheless, authors reported that ^{111}In-oxine may have detrimental effects on NKs and is rapidly released from labelled cells, thus increasing background activity. Our approach overcomes these limitations and proved to be suitable for NKs imaging in vivo with no toxicity to cells. A limitation of our work is certainly the mouse model that may not reflect the situation in humans. Indeed our SCID mice were reconstituted with a supra-physiological amount of human NKs and they rapidly infiltrated the human xenograft. In humans, the number of NKs infiltrating a tumor, or its metastasis, may be much lower than in our experiments, particularly in basal conditions. Many drugs, already commercially available, may however significantly increase the number of TINK thus allowing their in vivo detection.

CONCLUSIONS

This pilot study demonstrates that it is possible to efficiently image NKs in vivo and their trafficking in human tumors implanted in immune deficient mice. Further studies are needed to confirm the application of this technique to monitor the efficacy of different therapeutic strategies aiming at increasing NKs recruitment in tumors.

ACKNOWLEDGMENTS

This work was supported by grants from the Italian Association for Cancer Research (AIRC and AIRC 5xmille) and by "Sapienza" University research projects. We also wish to acknowledge the no-profit association Nuclear Medicine Discovery for support.

REFERENCES

1. Catchpole B, Gould SM, Kellett-Gregory LM, Dobson JM. Immunosuppressive cytokines in the regional lymph node of a dog suffering from oral malignant melanoma. J Small Anim Pract. 2002;43:464–467.
2. Becknell B, Caligiuri MA. Interleukin-2, interleukin-15, and their roles in human natural killer cells. Adv Immunol. 2005;86:209–239.
3. Ma HL, Whitters MJ, Konz RF et al. IL-21 activates both innate and adaptive immunity to generate potent antitumor responses that require perforin but are independent of IFN-gamma. J Immunol. 2003;171:608–615.
4. Baxevanis CN, Perez SA, Papamichail M. Cancer immunotherapy. Crit Rev Clin Lab Sci. 2009;46:167–189.
5. Cheng M, Chen Y, Xiao W, Sun R, Tian Z. NK cell-based immunotherapy for malignant diseases. Cell Mol Immunol. 2013;10:230-52.
6. Imai K, Matsuyama S, Miyake S, Suga K, Nakachi K. Natural cytotoxic activity of peripheral-blood lymphocytes and cancer incidence: an 11-year follow-up study of a general population. Lancet. 2000;356:1795–1799.
7. Coca S, Perez-Piqueras J, Martinez D et al. The prognostic significance of intratumoral natural killer cells in patients with colorectal carcinoma. Cancer 1997;79: 2320–2328.

8. Jin J, Fu B, Mei X, Yue T, Sun R, Tian Z, Wei H. CD11b(-)CD27(-) NK cells are associated with the progression of lung carcinoma. PLoS One 2013;8:e61024.
9. Kalinski P, Giermasz A, Nakamura Y et al. Helper role of NK cells during the induction of anticancer responses by dendritic cells. Mol Immunol 2005;42:535-9.
10. Meller B, Frohn C, Brand JM et al. Monitoring of a new approach of immunotherapy with allogenic ^{111}In-labelled NK cells in patients with renal cell carcinoma. Eur J Nucl Med Mol Imaging 2004;31;403-407.
11. Galli F, Histed S, Aras O. NK cell imaging by in vitro and in vivo labelling approaches. Q J Nucl Med Mol Imaging 2014;58:276-83.
12. Signore A, Sensi M, Pozzilli C, Negri M, Lenzi GL, Pozzilli P. Effect of unlabeled indium oxine and indium tropolone on the function of isolated human lymphocytes. J Nucl Med 1985;26:612-5.
13. Signore A, Beales P, Sensi M, Zuccarini O, Pozzilli P. Labelling of lymphocytes with indium 111oxine: effect on cell surface phenotype and antibody-dependent cellular cytotoxicity. Immunol Lett 1983;6:151-4.
14. Pozzilli P, Signore A, Pozzilli C. Detrimental effect of indium-111 on human-lymphocytes. J Nucl Med. 1984;25:830.
15. Zarcone D, Viale O, Cerruti G et al. Antibodies to adhesion molecules inhibit the lytic function of MHC-unrestricted cytotoxic cells by preventing their activation. Cell Immunol 1992;143:389-404.

16. Corsetti F, Chianelli M, Cornelissen B et al. Radioiodinated recombinant human TSH: a novel radiopharmaceutical for thyroid cancer metastases detection. Cancer Biother Radiopharm 2004;19:57-63.
17. Perussia B, Ramoni C, Anegon I, Cuturi MC, Faust J, Trinchieri G. Preferential proliferation of natural killer cells among peripheral blood mononuclear cells cocultured with B lymphoblastoid cell lines. Nat Immun Cell Growth Regul 1987;6:171-188.
18. Stabile H, Carlino C, Mazza C et al. Impaired NK-cell migration in WAS/XLT patients: role of Cdc42/WASp pathway in the control of chemokine-induced beta2 integrin high-affinity state. Blood 2010;115:2818-26. Epub 2010 Feb 3.
19. Hjorth R, Jonsson AK, Vretblad P. A rapid method for purification of human granulocytes using percoll. A comparison with dextran sedimentation. J Immunol Methods 1981;43:95-101.
20. Malviya G, Anzola KL, Podestà E et al. (99m)Tc-labeled rituximab for imaging B-lymphocyte infiltration in inflammatory autoimmune disease patients. Mol Imaging Biol 2012;14:637-46.
21. Gallagher SR. One-dimensional SDS gel electrophoresis of proteins. 2012 Current Protocols in Protein Science Chapter 10:Unit 10.1.1-44.
22. Bjorke H, Andersson K. Automated, high-resolution cellular retention and uptake studies in vitro. Appl Radiat Isot 2006;64:901-905.

23. Soluri A, Massari R, Trotta C et al. New imaging probe with crystals integrated in the collimator's square holes. Nucl Instr Meth Phys Res, A 2005;554:331-339.

24. Rai A, Chakravarty AK. Homing of radiolabelled recombinant interleukin-2 activated_natural killer cells and their efficacy in adoptive immunotherapy against murine fibrosarcoma. J Biosci 2007;32:1299-305.

25. Sheu AY, Zhang Z, Omary RA, Larson AC. MRI-monitored transcatheter intra-arterial delivery of SPIO-labeled natural killer cells to hepatocellular carcinoma: preclinical studies in a rodent model. Invest Radiol 2013;48;492-499.

26. Edinger M, Cao YA, Verneris MR, Bachmann MH, Contag CH, Negrin RS. Revealing lymphoma growth and the efficacy of immune cell therapies using in vivo bioluminescence imaging. Blood 2003;101;640–648.

27. Jha P, Golovko D, Bains S et al. Monitoring of NK-Cell Immunotherapy using non-invasive Imaging Modalities. Cancer Res 2010;70;6109-6113.

28. Melder RJ, Brownell AL, Shoup TM, Brownell GL, Jain RK. Imaging of activated natural killer cells in mice by positron emission tomography: preferential uptake in tumors. Cancer Res 1993;53;5867-5871.

29. Melder RJ, Brownell AL, Shoup TM, Brownell GL, Jain RK. Imaging of activated natural killer cells in mice by positron emission tomography: preferential uptake in tumors. Cancer Res. 1993;53;5867-5871.

30. Schäfer E, Dummer R, Eilles C et al. Imaging pattern of radiolabelled

lymphokine-activated killer cells in patients with metastatic malignant melanoma. Eur J Nucl Med. 1991;18:106-10.

31. Matera L, Galetto A, Bello M et al. In vivo migration of labeled autologous natural killer cells to liver metastases in patients with colon carcinoma. J Transl Med. 2006;4; 49.
32. Meller B, Frohn C, Brand JM et al. Monitoring of a new approach of immunotherapy with allogenic ^{111}In-labelled NK cells in patients with renal cell carcinoma. Eur J Nucl Med Mol Imaging. 2004;31;403-407.

Chapter 5

Imaging of angiogenesis with ^{99m}Tc-HYNIC-VEGF$_{165}$

Filippo Galli[1,2], Marco Artico[3], Samanta Taurone[3], Isabella Manni[4], Enrica Bianchi[3], Giulia Piaggio[4], Bruce D. Weintraub[5], Mariusz Skudlinski[5], Rudi A.J.O. Dierckx[2], Alberto Signore[1,2]

[1]Nuclear Medicine Unit, Department of Medical-Surgical Sciences and of Translational Medicine, Faculty of Medicine and Psychology, "Sapienza" University of Rome, Rome, Italy.
[2]Department of Nuclear Medicine and Molecular Imaging, University Medical Centre Groningen, University of Groningen, Groningen, The Netherlands.
[3]Department of Sensory Organs, Sapienza University of Rome, Rome, Italy.
[4]Molecular Oncogenesis Laboratory, Experimental Oncology Department, Regina Elena National Cancer Institute, Rome, Italy
[5]Trophogen Inc., Rockville, MD, USA

Submitted to Molecular Imaging and Biology

ABSTRACT

Introduction: Angiogenesis is the main process responsible for tumor growth and metastatization. The principal effector of such mechanism is the vascular endothelial growth factor (VEGF) secreted by cancer cells and other components of tumor microenvironment, under specific stimuli. Radiolabelled VEGF analogues may provide a useful tool to noninvasively imaging tumor lesions and evaluate the efficacy of anti-angiogenic drugs, aimed at blocking the VEGFR pathway. Aim of the present study was to radiolabel the human $VEGF_{165}$ analogue with ^{99m}Technetium (^{99m}Tc) and evaluate the expression of VEGFR in both cancer and endothelial cells in the tumor microenvironment.

Material and Methods: The human VEGF-A165 analogue was successfully labelled with ^{99m}Tc using an indirect method via succinimidyl-6-hydrazinonicotinate hydrochloride conjugation. Several in vitro quality controls (QC) including SDS-PAGE, cysteine challenge and cell binding assay on HUVEC cells were performed to assess its retained structure and biological activity. In vivo studies included biodistribution studies and tumor targeting experiments in athymic nude CD-1 mice xenografted with different cell lines (ARO, K1 and HT29). Immunohistochemistry was performed on excised tumors to confirm VEGF receptor (VEGFR) expression in the lesion and endothelial cells.

Results: Human VEGF-A_{165} analogue was labelled with high labelling efficiency (>95%) and high specific activity. The radiolabelled molecule retained its biological activity and structural integrity as confirmed by in vitro QC. In tumor

targeting experiments, a focal uptake of radiolabelled $VEGF_{165}$ was observed in every xenografted tumor with different tumor-to-background ratios. Immunohistochemical analysis of excised tumors revealed an inverse correlation between VEGF and uptake of the radioactive hormone. On the other hand a positive correlation between radioactive $VEGF_{165}$ and VEGFR1 was also observed.

Conclusions: Human VEGF-A_{165} was successfully radiolabelled with 99mTc and may provide a suitable radiopharmaceutical to image angiogenesis and evaluate the efficacy of anti-angiogenic drugs. However, VEGFR imaging suffers from quenching effects of endogenous VEGF produced by cancer and other cells of the microenvironment.

INTRODUCTION

Angiogenesis is the vital physiological process involving the growth and remodelling of new blood vessels from pre-existing one and is implicated in a number of diseases including cancer. Indeed, neoangiogenesis is essential for tumor growth as well as crucial for local and distant metastatization through both blood and lymphatic vessels [1, 2]. The most potent angiogenic cytokine is the vascular endothelial growth factor A (VEGF-A), a member of the subfamily of heparin-binding glycoproteins with potent angiogenic, lymphangiogenic, vascular, and lymphatic permeability-enhancing activities [3]. It has been shown to be up-regulated in tumor and highly proliferating endothelial cells. Such overexpression has been associated with progression, metastatization and poor outcome in particularly aggressive cancers [4]. Therefore, together with its receptor (VEGFR), also expressed in both endothelial and neoplastic cells, it plays a key role in many types of cancer being distinctive angiogenic markers [5, 6]. This has led to the development of targeted therapies in various preclinical models of neoplasms. These strategies are based on drugs able to bind either VEGF or VEGFR blocking the VEGFR pathway and, consequently, the growth induced by its ligand. Nowadays, some of these drugs have been approved for human use and proved to be effective in many solid tumors [7]. The most widely used in clinical practice is the anti-VEGF monoclonal antibody (mAb) bevacizumab that binds the free VEGF. Others, like the tyrosine kinase inhibitors (TKIs) sorafenib and

sunitinib, are able to target the VEGFR2 blocking the signalling cascade [8]. It has been reported that the majority of patients benefits from targeted therapies, but a small fraction fails to show even initial benefits. The reasons may range from the involvement of parallel angiogenic pathways to the absence of the targets [9]. Therefore, it would be important to predict which patients would benefit from a specific targeted therapy and several studies indicated the possibility to image angiogenic markers with the use of radiopharmaceuticals targeting VEGF or VEGFR. In particular, since VEGFR is expressed also in some cancer cells, this technique will be useful in both early detection and cancer treatment monitoring [10-12]. Studies with radiolabelled anti-angiogenic agents have been reported in the literature and many of them were characterized by drawbacks that slowed or blocked the shift from preclinical to clinical trials. Such drawbacks ranged from poor binding affinity to exaggerated liver uptake [13]. In the present study we radiolabelled a $VEGF_{165}$ analogue with 99m-technetium (^{99m}Tc) to image angiogenesis and characterize VEGFR expression in tumor microenvironment of cell lines from different cancers.

MATERIALS AND METHODS

Labelling of VEGF-A_{165} with ^{99m}Tc

The human hVEGF-A_{165} analogue with a molecular weight of 19 KDa was provided by Trophogen Inc. and radiolabelled with 99mTc through an indirect

method after conjugation with the bifunctional chelator 6-hydrazinonicotinamide (HyNic). Briefly, $VEGF_{165}$ (0.5 mg) was incubated with a 8-fold molar excess of succinimidyl-6-hydrazinonicotinate hydrochloride (SHNH, SoluLink, USA) for 2 h at room temperature in the dark. At the end of the incubation free SHNH was removed by size exclusion chromatography using a G-25 Sephadex PD10 column (GE Healthcare, UK) and nitrogen-purged phosphate buffer saline (pH 7.4) as eluent. The number of HYNIC groups bound per molecule of $VEGF_{165}$ was determined by a molar substitution ratio (MSR) assay. Briefly, conjugated $VEGF_{165}$ (2 µl) was added to a 0.5 mM solution (18 µl) of 2-sulfobenzaldehyde in 0.1 M 2-(N-morpholino) ethanesulfonic acid (MES) buffer (pH 5.0) and incubated at room temperature for 2 hours. Phosphate buffer saline (PBS) alone was used as blank and duplicates were prepared. After 2 hours the absorbance at 345 nm of each reaction was measured with a spectrophotometer and the number of HYNIC groups per molecule was calculated as indicated in the SoluLink data sheet. Radiolabelling was performed incubating 30 µg of $VEGF_{165}$ (in 100 µl PBS) with 300 MBq of freshly eluted $^{99m}TcO_4^-$ (100 µl), 100 µl of tricine (Sigma-Aldrich Chemicals, UK) (from 0.9 mg/ml to 200 mg/ml PBS) and 5 µl SnCl2 (Sigma-Aldrich Chemicals, UK) (from 2 mg/ml to 20 mg/ml 0.1 M HCl). Labelling efficiency (LE) and colloids percentage were measured up to 30 minutes of incubation. After labelling, an additional purification by size exclusion chromatography was performed using a Zeba Spin Column (Thermo Scientific, USA) to remove any free $^{99m}TcO_4^-$, tricine and $SnCl_2$.

In vitro quality controls

Quality controls were performed using instant thin layer chromatography-silica gel (ITLC-SG) strip (Pall Life Sciences, USA). Results were analysed by a radio-scanner (Bioscan Inc., USA) to calculate the LE of ^{99m}Tc-HYNIC-VEGF$_{165}$. The mobile phase for LE determination was a 0.9% NaCl solution, whereas for colloid determination was a NH_3:H_2O:EtOH (1:5:3) solution. Quality controls were performed before and after the purification with a Zeba Spin column. Additionally, reverse phase HPLC was carried out using a C8 Kinetex 4.6 x 250 mm column and a gradient of H_2O (A) and acetonitrile (B) with 0.1 % TFA. The following gradient was used: 0-5 min 0-5% B, 5-20 min 5-95% B, 20-25 min 95% B and 25-30 min 95-5%B. Stability assays were performed adding 100 µl of ^{99m}Tc-HYNIC-VEGF$_{165}$ to a vial containing 900 µl of fresh human blood serum and to another containing 900 µl of 0.9% NaCl solution. Both vials were incubated up to 24 hours at 37°C. The radiochemical purity was measured at 1, 3, 6 and 24 hours by ITLC analysis. In addition, a cysteine challenge assay was performed incubating the labelled $_{VEGF165}$ at 37°C for 60 min with different cysteine concentration, ranging from 1000:1 (cysteine:VEGF$_{165}$) to 0.1:1 molar ratio. For each time point, radiochemical purity was evaluated by ITLC as described above. All known chemical forms of ^{99m}Tc-cysteine have Rf values between 0.5 and 1, when normal saline was used as mobile phase. Integrity of the labelled VEGF$_{165}$ molecule was also checked by sodium dodecyl sulphate–polyacrylamide gel electrophoresis under nonreducing conditions, according to the method of Laemmli [14]. Proteins were visualized by

staining the gels with Coomassie Brilliant Blue (Thermo Scientific, USA). Radioactivity associated with each band was determined scanning the gel with a radio-scanner.

Cell lines

$VEGFR^+$ cell line, human umbilical veins endothelial cells (HUVEC) were cultured in F-12K medium supplemented with 10% FCS, 100 IU/ml penicillin, 100 µg/ml streptomycin, 2 mM L-glutamine and EGM®-2 Bulletkit (Lonza, USA) (15). The anaplastic thyroid cancer cell line (ARO), the colorectal cancer cell line (HT29) and the poorly differentiated thyroid cancer cell line (K1) were grown in DMEM high glucose (Gibco, USA) supplemented with 10% FCS, 100 IU/ml penicillin, 100 µg/ml streptomycin and 2 mM L-glutamine [16-18]. VEGF production was reported for each cell line, but HUVEC cells.

In vitro binding studies

Measurements of cell uptake and retention of labelled VEGF-A_{165}, was performed in vitro using a semi automatic system: LigandTracerTM (Ridgeview Instruments AB, Sweden) [19]. Briefly, 10^6 HUVEC cells were seeded in a tilted Petri dish and incubated in a humified incubator at 37°C and 5% CO2 for 24 hours. The dish was then placed in the LigandTracer and allowed to rotate continuously for 15 minutes to allow release of weakly attached cells. After one gentle wash, 2 ml of 30 nM radiolabelled $VEGF_{165}$ was added to the cell culture medium and the dish started to

rotate for 3 hours. The device was then stopped, the liquid removed and replaced with culture medium without labelled $VEGF_{165}$ for calculating release of radioactivity from cells. A binding/release curve was obtained by non-linear regression analysis with GraphPad Prism (GraphPad Software Inc, USA) to calculate the Kd value.

In vivo biodistribution and imaging studies

For animal experiments, the institutional and national guide for the care and use of laboratory animals was followed. Imaging studies were performed with a previously described high-resolution portable mini-gamma camera (HRC), IP-Guardian (Li-Tech S.r.l., Italy) [20]. For in vivo biodistribution studies, 5.5 MBq (100 µl) of labeled $VEGF_{165}$ were injected in the tail vein of 12 nude CD-1 mice and static planar posterior images were acquired using the HRC at 1, 3, 6 and 24 hours, under light ether anaesthesia. At the end of each imaging point three mice were and major organs were collected and counted in a single well gamma-counter. In vivo cell-targeting experiments were performed in 36 nude CD-1 mice that were divided in three groups. Each group was injected subcutaneously in the right thigh with respectively 10^6 ARO, HT29 and K1 cells mixed with BD Matrigel (BD Biosciences, USA) (1:1) After tumor growth (approximately 0.6 cm^3, in 20 days), 5.5 MBq of labelled $VEGF_{165}$ were administered i.v. in the tail vein and static planar posterior HRC images were acquired at 1, 3, 6 and 24 hours, under light ether anaesthesia. At each time point 3 mice were euthanized for ex-vivo counting.

Major organs and tumors were collected, weighted and counted for radioactivity with a single well gamma-counter (Gammatom, Italy).

Blocking studies

Blocking studies were performed in four mice injected with 1 million HT29 cells mixed with Matrigel® in the right thigh. After tumor growth (about 1 cm3), 5 MBq of 99mTc-VEGF165 were injected in the tail vein and images were acquired with a portable mini-gamma camera at 1 h and 3 h post-injection.

After 3 days, ^{99m}Tc-HYNIC-VEGF$_{165}$ was pre-incubated for 1 h with 3.5 fold molar excess of recombinant human VEGFR2-Fc chimera (BioLegend Inc., USA) that acts as a soluble decoy receptor (TRAP) that has been proved to prevent the binding of VEGF to endothelial cells. After the incubation, a dose of 5 MBq was injected in the tail vein of 3 of the 4 mice previously imaged and images were acquired with a portable mini-gamma camera at 1 h and 3 h post-injection.

After 3 more days, a 100 fold molar excess of unlabelled VEGF$_{165}$ (COLD) was injected in the tail vein of the same 3 mice and after 10 minutes 5 MBq of ^{99m}Tc-HYNIC-VEGF$_{165}$ were injected. Images were acquired with a portable mini-gamma camera at 1 h and 3 h post-injection. Region of interest were drawn on the tumor and on the contralateral leg in each image and target-to-background (T/B) ratios were calculated.

Immunohistochemical analysis

For light microscope immunohistochemical analysis, small fragments of each excised tumor (ARO, HT29 and K1) were processed according to ABC/HRP technique (avidin complexed with biotinylated peroxidase). These samples were washed in PBS, fixed in 10% formalin and embedded in paraffin according to a standard procedure. Serial 3-µm thick sections were cut using a rotative microtome, mounted on gelatin-coated slides and processed for immunohistochemistry. These sections were de-paraffinized in xylene and dehydrated. They were immersed in citrate buffer (pH 6) and subjected to microwave irradiation twice for 5 minutes. Subsequently, all sections were treated for 30 minutes with 0,3% hydrogen peroxide in methanol to quench endogenous peroxidase activity. To block non-specific binding, the slides were incubated with M.O.M. Mouse Ig Blocking Reagent (Vector Laboratories Burlingame, CA, USA) for 1 h at room temperature. The slides were incubated overnight at 4°C with the following antibodies: i) mouse anti-VEGF monoclonal antibody (Santa Cruz Biotechnology, CA, USA); ii) mouse anti-VEGF Receptor 1 [Flt-1/EWC] monoclonal antibody (Abcam, ab9540, UK); iii) mouse anti-VEGF Receptor 2 [KDR/EIC] monoclonal antibody (Abcam, ab9530, UK). Optimal antisera dilutions and incubation times were assessed in a series of preliminary experiments. After exposure to the primary antibodies, slides were rinsed twice in phosphate buffer and incubated for 1h at room temperature with the appropriate secondary biotinylated goat anti-mouse IgG (Vector Laboratories Burlingame, CA,

USA, BA9200 and BA1000) and with peroxidase- conjugated avidin (Vectastain Elite ABC Kit Standard* PK 6-100) for 35 minutes. After a further wash with phosphate buffer, slides were treated with 0,05% 3,3-diaminobenzidine (DAB) and 0,1% H2O2 (DAB substrate kit for peroxidase, Vector Laboratories SK-4100). Finally, sections were counterstained with Mayer's haematoxylin and observed using a light microscope. Negative control experiments were carried out: i) by omitting the primary antibody; ii) by substituting the primary antibody with an equivalent amount of non-specific immunoglobulins; iii) by pre-incubating the primary antibody with the specific blocking peptide (antigen/antibody = 5 according to supplier's instructions). The staining assessment was made by two experienced observers in light microscopy. Immunoreactivity of VEGF, VEGF-R1, and VEGF-R2 was assessed in all samples. The intensity of the immune reaction was assessed microdensitometrically using an IAS 2000 image analyser (Delta Sistemi, Rome, Italy) connected via a TV camera to the microscope. The system was calibrated taking as zero the background obtained in sections exposed to non-immune serum. Ten 100 μm2 areas were delineated in each section using a measuring diaphragm. The quantitative data regarding the intensity of immune staining were analysed statistically using analysis of variance (ANOVA) followed by Duncan's multiple range test as a post hoc test.

RESULTS

Labelling with ^{99m}Tc and quality controls

Highest labelling efficiency was obtained when the analogue was conjugated with a ratio HYNIC:$VEGF_{165}$ of 8:1. Determination of molar substitution ratio of HYNIC-conjugated $VEGF_{165}$ demonstrated that an average of 4.3 molecules of SHNH were bound per molecule of analogue. Higher ratios were not selected to avoid over-conjugation of the hormone and possible structural modification. Optimization of the labelling procedure of the HYNIC-$VEGF_{165}$ conjugate (30 µg) with ^{99m}Tc showed that, after 10 minutes of incubation, the use of 100 µl of tricine (0.5 mM) and 5 µl of SnCl2 (50 nM) allowed to obtain the highest LE (65 %) and the lowest amount of colloids (<5%). After Zeba spin purification we were able to obtain a radiochemical purity of > 95 %. Specific activity of resulting ^{99m}Tc-HYNIC-$VEGF_{165}$ was 190 MBq/nmol. Radiolabelled $VEGF_{165}$ was stable up to 24 h in both in human serum and in a 0.9% NaCl solution at 37 °C, as well as in solutions containing increasing cysteine concentrations. A slight decrease in the radiochemical purity was observed only at high cysteine concentrations (>500:1). Gel electrophoresis of radiolabelled, conjugated and unconjugated analogue showed no significant differences and the absence of significant degradation or aggregation resulting from conjugation and/or labelling.

In vitro binding studies

Kinetic biding assay with LigandTracer showed an increasing uptake of labelled $VEGF_{165}$ from HUVEC cells that reached a plateau after 50 minutes (Fig. 1). Retention studies revealed a slow dissociation rate from membrane bound receptors in the following 2 hours, with a Kd of 192 pM.

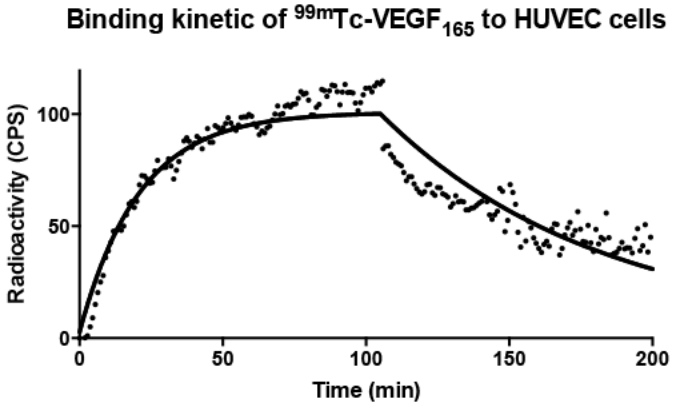

Koff	Kon	Hotnm	Bmax	Kd
= 0.0279	1.450e+008	= 0.0500	566.2	= 1.924e-010

Fig. 1. Kinetic binding assay of radiolabelled $VEGF_{165}$. At maximal binding, the medium was replaced with cold PBS for retention studies.

In vivo high-resolution imaging

Biodistribution studies of ^{99m}Tc-HYNIC-$VEGF_{165}$ in mice showed a high and persistent uptake by the liver and a moderate uptake by the kidneys with almost no signal from other organs and blood pool. Single organ counting revealed a high %ID/g also in the lungs and spleen (Fig. 2). In vivo targeting experiments showed a focal uptake in the right thigh of each group bearing tumor xenografts with a T/B ratio of 4.5 at 1 h p.i in mice bearing a HT29

xenograft. Animals bearing ARO and K1 cells showed a T/B of 3.5 and 2.3 respectively that decreased over time (Fig. 3).

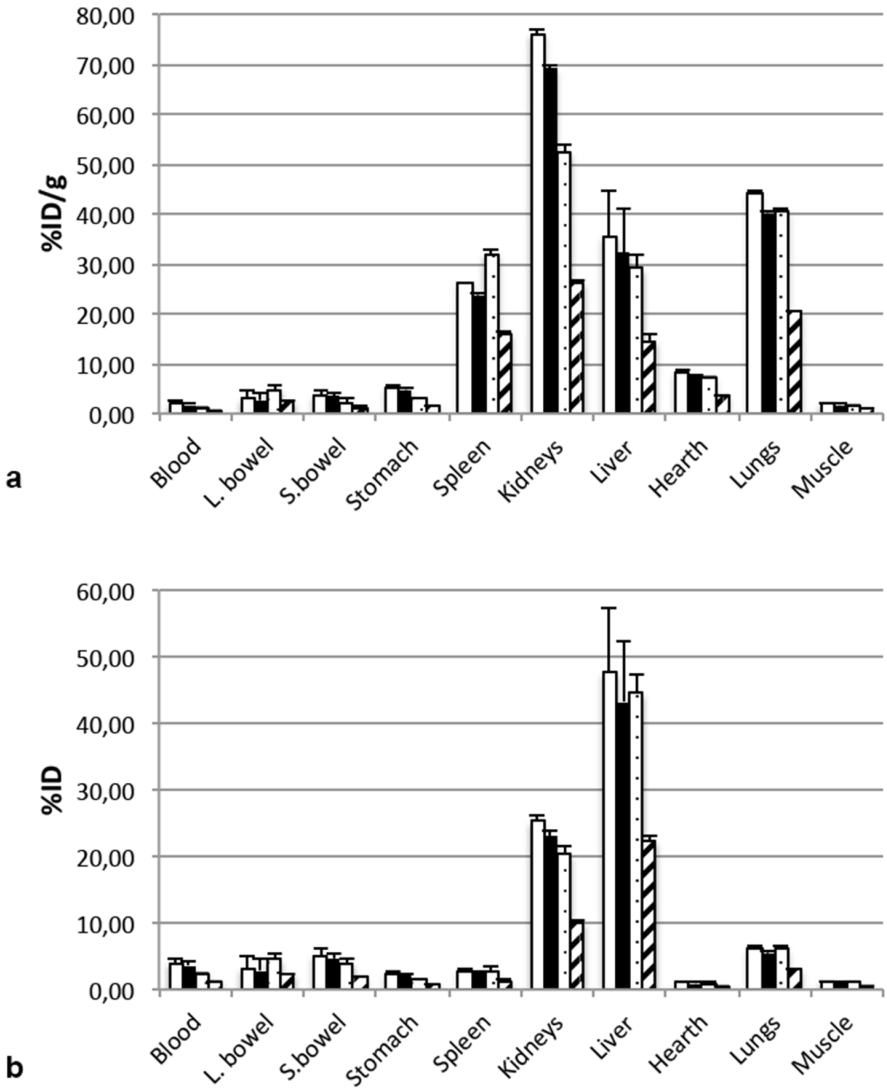

Fig. 2. Single organ counts at 1 h (white bar), 3 h (black bar), 6 h (dotted bar), and 24 h (lined bar). Data are shown as % ID over time. Each point is the average of three mice. Error bars represent standard deviation.

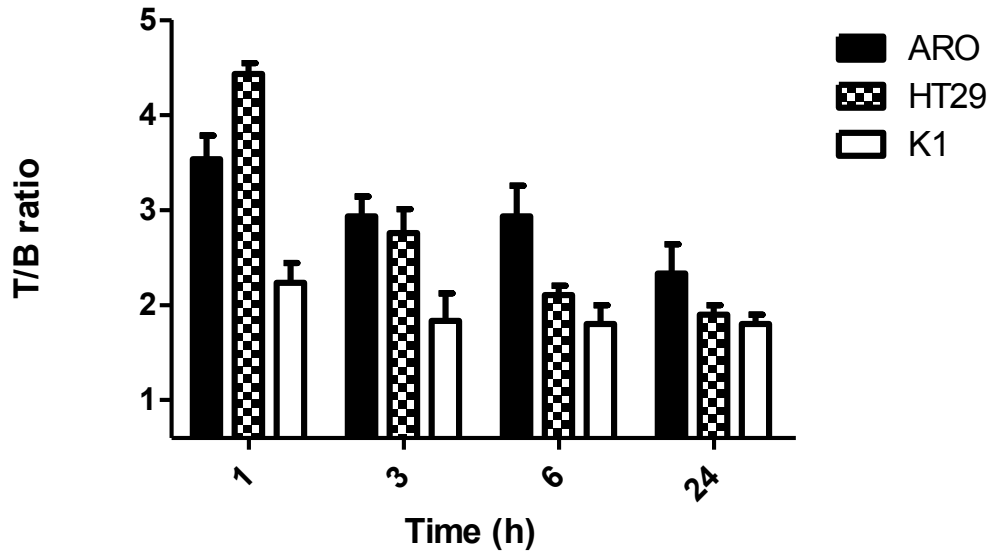

Fig. 3. T/B ratios calculated at 1h, 3h and 6h in mice bearing a ARO (black bar), HT29 (squared bar) or K1 (white) xenograft.

Blocking studies

Blocking studies with ^{99m}Tc-HYNIC-VEGF$_{165}$ confirmed the results of previous targeting experiments. After pre-incubation of the radiopharmaceutical with recombinant VEGFR2-Fc, a main liver and spleen uptake, with reduced signal from kidneys, was detected, resembling the typical biodistribution of a non-specific radiolabelled antibody (Fig. 4a). The overall uptake in tissues was lower and the uptake in the tumor was consistently reduced. Similar findings were obtained after the pre-injection of a 100 fold molar excess of unlabelled VEGF$_{165}$ with the exception of the signal from kidneys, which looks similar to the signal obtained with labelled VEGF only. Calculated T/B ratios for the "HOT" group

reflected the data obtained with the previous experiments with a maximum uptake reached at 1 h that slowly decreases with time (Fig. 4b). The T/B ratio in the TRAP group was reduced by 70% due to the co-incubation with VEGFR2-Fc at 1 h and the T/B ratio in the "COLD" group was reduced by 60% at 1 h.

A

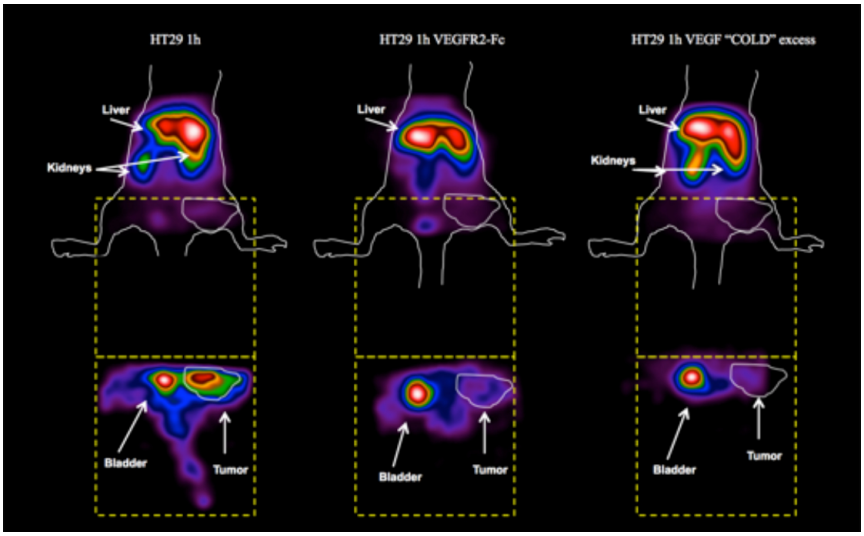

B

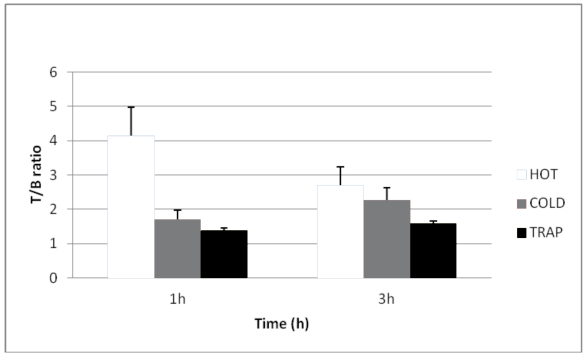

Fig 4. a) Body images (top) and particulars of the back (bottom) of the same mouse injected with 150 µCi of 99mTc-VEGF (left), 150 µCi of 99mTc-VEGF following pre-incubation with a 3.5 fold molar excess of VEGFR2-Fc (middle) and 150 µCi of 99mTc-VEGF following pre-injection of a 100 fold molar excess of unlabelled VEGF (right). b) T/B ratios at 1 h and 3 h calculated on the images obtained from the HOT (99mTc-VEGF), COLD (99mTc-VEGF+unlabelled VEGF) and TRAP (99mTc-VEGF+VEGFR2-Fc) groups. Values are the mean of 3 mice per each group. Error bars represent standard deviation.

Minor blocking was evident at 3 h in both TRAP and “COLD” group mainly due to the decreased activity in tumors of the control group.

Immunohistochemical analysis

IHC analysis on excised tumor showed the presence of VEGF, VEGFR1 and VEGFR2 on both the lesion and the surrounding vessels at different extents (Fig. 5). After semi-quantitative analysis of expression levels, a higher amount of free VEGF was present in lesions derived from K1 cell lines (33.2%), followed by HT29 (15.7%) and ARO cells (10.6%). VEGFR1 and 2 were present heterogeneously between tumor cells and blood vessels, revealing that even cancer may express VEGF receptors on the plasma membrane. IHC data were compared with the uptake of radioactive VEGF165 and an inverse correlation was observed between endogenous VEGF and T/B ratio ($p=0.01$, Fig. 6b). On the other hand, a positive correlation was observed between radioactive VEGF165 uptake and VEGFR1 ($p=0.03$, Fig. 6a).

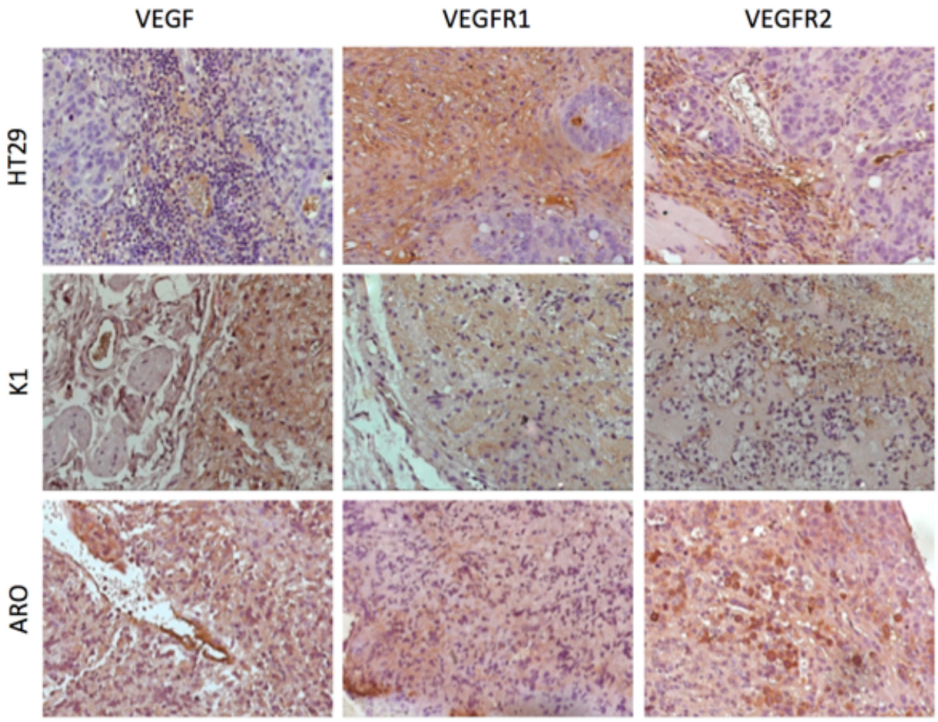

Fig 5. IHC analysis of VEGF and VEGFRs expression on HT29, K1 and ARO excised tumors.

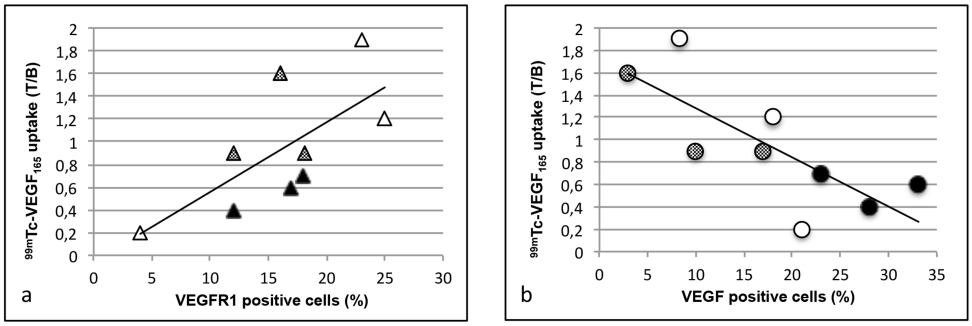

Fig 6. Correlation between ^{99m}Tc-VEGF$_{165}$ uptake and VEGFR1 positive cells (%) (a) and between ^{99m}Tc-VEGF$_{165}$ uptake and VEGF positive cells (%) (b) in ARO (grey), HT29 (white) and K1 (black) cell lines.

DISCUSSION

Imaging of tumor microenvironment is a promising approach to non-invasive diagnoses of cancer metastases and to monitor the efficacy of new drugs. Given its role in metastatization and tumor growth, angiogenesis offers both diagnostic and therapeutic targets like VEGF and its receptors. As an example, in undifferentiated thyroid cancer, TKIs blocking the VEGF/VEGFR pathway, represent an alternative and promising therapeutic approach [21]. Unfortunately, severe side effects have been reported in some patients after long time treatment. Therefore, a non-invasive diagnostic tool to predict the response to therapy and evaluate drug efficacy is vitally needed. In the past many attempts have been done to develop radiopharmaceuticals to image angiogenesis with promising results. Among them, ^{111}In, ^{89}Zr or ^{64}Cu radiolabelled bevacizumab was able to efficiently image xenograft from ovarian cancer, but the high radiation burden to the patient and the low availability of ^{89}Zr and ^{64}Cu were some of the drawbacks of its use. Other groups tried to use recombinant human VEGF to overcome the long half-life of mAbs and used radioiodine or ^{99m}Tc as the isotopes of choice [13]. In the present study, we followed the same approach to strengthen the hypothesis that the use of recombinant human VEGF to target angiogenesis is a promising methodology to develop non-invasive diagnostic tools and monitor novel targeted drugs development. The use of a recombinant hormone would avoid any problems from

HAMA antibodies and the very low amount, in terms of micro-doses, required for a scintigraphic study should not raise any concern about a potential biologic effect of such radiopharmaceuticals and in particular on the pro-angiogenic effect that VEGF analogues may have on existing blood vessels. In vitro binding assays on VEGFR expressing cell line HUVEC, showed that radiolabelled $VEGF_{165}$ was able to bind its receptor on the plasma membrane within 1 h with a very low K_d and these findings support the assumption that very low amounts will be required for in vivo imaging. Indeed, by injecting nanomol amounts of ^{99m}Tc-$VEGF_{165}$ we were able to visualize lesions from 3 different cell lines. We also were able to prove that the binding was specific for the VEGFR performing blocking studies pre-injecting animals with a 100-fold molar excess of unlabelled $VEGF_{165}$ or VEGFR-Fc that saturated all the available receptors thus reducing the binding of the labelled hormone of 60% and 70% respectively. Backer et al raised the problem that VEGF-based probes uptake in the tumor area was reported to be highly heterogeneous, probably because of the combination of several mechanisms like non-uniform perfusion of tumor vasculature, differential receptor occupancy by host VEGF or differential accessibility of VEGF receptors on luminal and subluminal surfaces of the endothelium [22]. Therefore, the clinical value of such imaging agents would have been depended on their ability to characterize the prevalence of VEGF receptors. To address this point, we performed immunohistochemical analysis of each tumor imaged with ^{99m}Tc-$VEGF_{165}$ that confirmed variability in VEGFR1 and VEGFR2 receptor expression and ligand

occupancy on both host endothelium and cancer cells. Despite these important results, a high liver uptake was detected, confirming previous findings from other groups [23, 24]. This study highlights an important aspect that has not been considered before: the role of both endogenous VEGF production and VEGFR expression on imaging strategies. While for other ligand receptor system, the endogenous production of the ligand may not be highly relevant for imaging the receptor ligand (i.e. IL-2 and IL-2 receptor) [25], here we show that the high production of endogenous VEGF by tumor cells hampers the possibility to image its receptors. This has been demonstrated by evaluating the presence of both VEGF and VEGFR in tumor sections by immunoperoxidase staining and by imaging with radiolabelled $VEGF_{165}$. Indeed we found an inverse correlation between ^{99m}Tc-$VEGF_{165}$ uptake and $VEGF_{189}$ expression by immunoperoxidase and a positive correlation between ^{99m}Tc-$VEGF_{165}$ uptake and VEGFR1 expression by immunoperoxidase, indicating high presence of VEGF and VEGFR, being the latter occupied by soluble endogenous VEGF and not detectable by radiolabelled $VEGF^{165}$. In the light of our results we can better interpret previously published studies with radiolabelled VEGF (both $VEGF_{121}$ and $VEGF_{165}$) [24, 25] that showed very poor tumor uptake, in contrast with studies with radiolabelled anti-VEGF mAb that showed high tumor uptake [26]. All together, these data confirm our findings that the presence of high VEGF levels in tumors, particularly those advanced with highly hypoxic tumor microenvironment and aggressive phenotypes, may saturate VEGF receptors, thus limiting the possibility to image

receptors. Overexpression of soluble VEGFR in some tumors and significant sequestration of VEGF on cell surface heparin-sulfate proteoglycans may also contribute to highly variable imaging results in different tumors. One possible limitation of our study is the limited number of animals used. However, in mice bearing K1 tumors, or ARO or HT29, we found highly consistent data supporting the very low variability within the same cell line. Nevertheless, different tumors showed different levels of VEGF/VEGFR. Another possible limitation could be that the semi-quantitative evaluation of $VEGF_{189}$ that we performed by immunohistochemistry, may not represent the real production of $VEGF_{121}$ and $VEGF_{165}$. However, these forms are splicing variants of the same molecule and usually expressed in similar quantities [27]. Overall we believe that the above considerations may have a limited impact on the final conclusion that VEGFR imaging in tumors by using radiolabelled VEGF is extremely variable, influenced by the presence of endogenous VEGF and unrelated to VEGFR receptor expression. It can be extrapolated that an accurate in vivo evaluation of tumor angiogenesis should include both VEGF and VEGFR imaging, unless it will be demonstrated the predominant clinical relevance of one over the other. Finally, the development of a superagonist VEGF analogue could allow the use a molecule with a greatly increased affinity for its receptor, overcoming the quenching effect due to endogenous VEGF.

CONCLUSIONS

Imaging of angiogenesis by targeting VEGFR with radiolabelled VEGF analogues may be a complementary approach to evaluate angiogenic status of tumors. This approach may allow the evaluation of anti-angiogenic drugs at both preclinical and clinical stages in combination with VEGF imaging. Our results indicate that VEGFR expression is variable in both tumors and its imaging is hampered by endogenous VEGF production. Therefore, additional studies are required to fully understand the VEGF/VEGFR relationships in different cancers and establish a more accurate and angiogenic phenotype-determined imaging protocols.

ACKNOWLEDGMENTS

This study was funded by grants from the Italian Association for Cancer Research (AIRC IG-2013 14151) and by “Sapienza” University research projects. We also wish to acknowledge the no-profit association Nuclear Medicine Discovery for support.

REFERENCES

1. Folkman J. Angiogenesis in cancer, vascular, rheumatoid and other disease. Nat Med 1995;1:27-31.
2. Carmeliet P, Jain RK. Angiogenesis in cancer and other diseases. Nature (Lond) 2000;407:249-257.
3. Neufeld G, Cohen T, Gengrinovitch S, Poltorak Z. Vascular endothelial growth factor (VEGF) and its receptors. FASEB J 1999;13:9-22.
4. De Araujo-Filho VJ, Alves VA, de Castro IV et al. Vascular endothelial growth factor expression in invasive papillary thyroid carcinoma. Thyroid 2009;19:1233-1237.
5. Weidner N, Carrol PR, Flax J, Blumenfeld W, Folkman J. Tumor angiogenesis correlates with metastasis in invasive prostate carcinoma. Am J Pathol 1993;143:401-409.
6. Joseph IB, Nelson JB, Denmeade SR, Isaacs JT. Androgens regulate vascular endothelial growth factor content in normal and malignant prostatic tissue. Clin Cancer Res 1997;3:2507-2511.
7. Hurwitz H, Fehrenbacher L, Cartwright T et al. Bevacizumab (a monoclonal antibody to vascular endothelial growth factor) prolongs survival in first-line colorectal cancer (CRC): results of a phase III trial of bevacizumab in combination with bolus IFL (irinotecan, 5-fluorouracil, leucovorin) as first-line therapy in subjects with metastatic CRC, in Proceedings of the Annual

Meeting of the American Society of Clinical Oncology; 2003 May 31; Chicago, IL. Vol 22, pp 3646, American Society of Clinical Oncology, Chestnut Hill, MA.

8. Gruber JJ, Colevas AD. Differentiated Thyroid Cancer: Focus on Emerging Treatments for Radioactive Iodine-Refractory Patients. Oncologist. 2015 Feb;20:113-26.
9. Gotink KJ, Verheul HMW. Anti-angiogenic tyrosine kinase inhibitors: what is their mechanism of action? Angiogenesis. 2010;13: 1–14.
10. Toi M, Inada K, Suzuki H, Tominaga T. Tumor angiogenesis in breast cancer: its importance as a prognostic indicator and the association with vascular endothelial growth factor expression. Breast Cancer Res Treat 1995;36:193-204.
11. Folkman J. Angiogenesis: an organizing principle for drug discovery? Nat Rev Drg Discov. 2007;6:273-286.
12. Cai W, Rao J, Gambhir SS. How molecular imaging is speeding up anti-angiogenic drug development and testing. Nat Clin Pract Oncol. 2007;4:556-557.
13. Cai W, Chen X. Multimodality molecular imaging of tumor angiogenesis. J Nucl Med. 2008;49:113S–128S.
14. Laemmli UK. Cleavage of structural proteins during the assembly of the head of bacteriophage T4. Nature 1970;227:680-685.
15. Zenner HL, Collinson LM, Michaux G, Cutler DF. High-pressure freezing

provides insights into Weibel-Palade body biogenesis. J Cell Sci 2007;120(Pt 12):2117-25.

16. Ke CC, Liu RS, Yang AH et al. CD133-expressing thyroid cancer cells are undifferentiated, radioresistant and survive radioiodide therapy. Eur K Nucl Med Mol Imaging. 2013;40:61-71.
17. Paudyal B, Paudyal P, Shah D, Tominaga H, Tsushima Y, Endo K. Detection of vascular endothelial growth factor in colon cancer xenografts using bevacizumab based near infrared fluorophore conjugate. J Biomed Sci 2014;21:35.
18. Galli F, Manni I, Piaggio G, et al. (99m)Tc-labeled-rhTSH analogue (TR1401) for imaging poorly differentiated metastatic thyroid cancer. Thyroid 2014;24:1297-308.
19. Bjorke H, Andersson K. Automated, high-resolution cellular retention and uptake studies in vitro. Appl Radiat Isot 2006;64:901-905.
20. Soluri A, Massari R, Trotta C et al. New imaging probe with crystals integrated in the collimator's square holes. Nucl Instrum Methods Phys Res A 2005;554:331-339.
21. Schneider TC, Abdulrahman RM, Corssmit EP, Morreau H, Smit JW, Kapiteijn E. Long-term analysis of the efficacy and tolerability of sorafenib in advanced radio-iodine refractory differentiated thyroid carcinoma: final results of a phase II trial.Eur J Endocrinol. 2012;167:643-50.
22. Backer MV, Levashova Z, Patel V et al. Molecular imaging of VEGF

receptors in angiogenic vasculature with single chain VEGF-based probes. Nat Med 2007;13:504-9.

23. Blankenberg FG, Backer MV, Levashova Z, Patel V, Backer JM. In vivo tumor angiogenesis imaging with site-specific labeled (99m)Tc-HYNIC-VEGF. Eur J Nucl Med Mol Imaging 2006;33:841-8.
24. Kang CM, Koo HJ, Choe YS, Choi JY. 68Ga-NODAGA-VEGF121 for in vivo imaging of VEGF receptor expression. Nucl Med Biol 2014;41:51-7.
25. Signore A, Chianelli M, Annovazzi A et al. 123I-interleukin-2 scintigraphy for in vivo assessment of intestinal mononuclear cell infiltration in Crohn's disease. J Nucl Med 2000;41:242-9.
26. Gaykema SB, Browers AH, Lub-de Hooge MN et al. 89Zr-bevacizumab PET imaging in primary breast cancer. J Nucl Med 2013;54:1014-8.
27. Cai C, Bottcher MC, Werner JA, Mandic R. Differential expression of VEGF121, VEGF165 and VEGF189 in angiomas and squamous cell carcinoma cell lines of the head and neck. Anticancer Res 2010;30:805-10.

Chapter 6

Summary/Samenvatting

Cancer is one of the major causes of morbidity and mortality worldwide. New anti-cancer therapies consist in targeted drugs against markers overexpressed by tumor cells. However, intra- and inter-tumor heterogeneity may lead to failure of such therapies that may be given to the patients with severe side-effects. New insights in tumor microenvironment led researchers not to focus only on the cancer cell itself, but also on the deep interaction between the tumor and the microenvironment that sorrounds it. Tumor microenvironment comprises the sum of cellular and non cellular components that is able to sustain tumor growth and promote metastatization. Markers and cells expressed in tumor microenvironment are now being studied as targets for both therapeutic and diagnostic strategies. Indeed, new drugs like TKIs inhibit microenviromental pathways that lead to neoangiogenesis, reducing the nutrient supply to cancer cells. Therefore, when direct targeting of cancer cells fails, because absence of the target or a high degree of heterogeneity, it would be possible to exploit such alternative pathways, treating cancer indirectly. In this scenario, there is the need of a non-invasive tool to characterize each lesion before planning the most appropriate therapy. This will allow to save money, time and reduce the side-effects as much as possible. Nuclear medicine offers a wide set of potential radiopharmaceuticals to image markers expressed by both cancer cells and microenvironment allowing also a pre-clinical and clinical evaluation at both pre-clinical and clinical stages. In this thesis we present four different strategies to image tumor specific antigens and microenvironment focusing on cancer, immune system and angiogenesis.

The first approach, described in chapter 2, consists in targeting the TSHR expressed by thyroid cancer non-iodine uptaking metastases. Thyroid cancer is a common neuroendocrine tumor with a good prognosis in most cases. Treatment consists in total thyroidectomy followed by ablation of the remnant tissue with radioiodine. However, in 10-20% of patients affected by metastases, cells may lose the NIS symporter and, therefore, the capacity to concentrate radioiodine. This leads to the need of alternative diagnostic and therapeutic approaches. Therefore we propose the use of a radiolabelled superagonist rhTSH analogues with increased biopotency and affinity for the TSHR respect to wild type TSH. Such analogues were radiolabelled with ^{99m}Tc using HYNIC as a bifunctional chelator. In vitro experiments showed a high in vitro stability with retained structure and biological activity, with a Kd 5 times lower than wild type TSH. In vivo it was possible to image small tumor xenograft of $TSHR^+$ cells, with neglibile uptake from control cells. It was also possible to image an intrathyroidal thyroid cancer in a dog with a spontaneous tumor. If results will be confirmed in humans it will be possible to provide a radiopharmaceutical to pre-operatively stage and follow-up patients affected by non-iodine uptaking metastases.

Since chronic inflammation has an important role in triggering the establishment of tumor microenvironment, many new drugs aim at modulating the inflammatory response. For this purpose, radiolabelled mAbs have been used with success to image cytokines or lymphocytes. Therefore, in chapter 3, we described the use ^{99m}Tc labelled infliximab in patients with newly diagnosed sarcoidosis for non-

invasive in vivo scintigraphic evaluation of the presence of TNFα in pulmonary and lymph nodal sarcoid granulomas. Patients were also studied by [18F]-FDG-PET/CT and BAL with lymphocyte phenotyping for complete evaluation of disease activity. Infliximab was labelled with high labelling efficiency, high specific activity and stability. Preliminary studies in vitro, in animals and humans have already shown its usefulness in the evaluation of TNFα in patients with Crohn's disease and rheumatoid arthritis. Therefore, we tried to apply the same strategy to benign tumors like granulomas. From our data, although on a limited series, it appears that with a qualitative examination, PET confirmed the staging performed by pulmonologists and allowed us to identify locations of extra-thoracic disease, like axillaries and abdomino-pelvic lymph nodes. Inflammatory events in the lung parenchyma of sarcoidosis patients have been confirmed by higher SUV_{max} and SUV_{mea}n respect to normal subjects. There was a lack of correlation between the $CD4^+/CD8^+$ lymphocytes ratio in BAL and the values of both SUVmax and SUVmean in the lung. This could be explained by the fact that the [^{18}F]-FDG is taken up by various cell types involved in the inflammatory sarcoid granuloma, confirming its poor specificity. Scintigraphy with labelled anti-TNFα mAb was qualitatively positive in 4 out of 10 patients (both stage III), showing at 6 and 24 h a widespread uptake of the radiopharmaceutical in both lungs. The values of T/B ratio calculated, both on the 6 and 24 h images, did not correlate with the values of SUV_{max} and SUV_{mean} calculated on ROI_{lung} of PET.

Similarly, in chapter 4 we described a novel approach for in-vivo cell labeling using a mAb that binds to CD56 antigen expressed on cell surface of the majority of human NK cells that are the main effectors of the immune-surveillance against tumors. The use of such radiopharmaceutical may allow to image NK cells directly in vivo, without the need of in vitro manipulation. It was possible to efficiently radiolabel the anti-CD56 mAb with ^{99m}Tc with high labelling efficiency and in vitro stability. The structure and the biological properties of the mAb were not altered by the radiolabelling methods. In vivo, in SCID mice lacking human NK cells, the proposed radiopharmaceutical showed typical characteristics of others radiolabelled mAb but with shorter circulating half-life and high uptake in the liver and at a lower extent in the kidneys. After reconstitution of mice with human NK cells, the biodistribution of the labelled antibody changed, showing lower circulating half-life and higher liver and spleen activity due to specific binding to NK cells homing in these tissues. Targeting experiments confirmed the possibility to follow NK infiltration into tumors with a high target-to-background ratio. The number of TINKs positively correlated with tumor size and the percentage of necrosis over time, highlighting a direct killing effect of TINKs on the lesion and the full functionality of these cells. This approach could be important in the development of novel drugs for immunotherapy of cancer, aimed at increasing NK infiltration into tumors, to follow up the efficacy of these drugs in vivo. Indeed, it could allow researchers to monitor cell trafficking directly in vivo.

Finally, in Chapter 5 we described the radiolabelling of the $VEGF_{165}$ analogue with ^{99m}Tc to image tumor angiogenesis in different cell lines. In vitro binding assays on VEGFR expressing cell line HUVEC, showed that radiolabelled $VEGF_{165}$ was able to bind its receptor on the plasma membrane within 1 h with a very low Kd and these findings support the assumption that very low amounts will be required for in vivo imaging. Indeed, by injecting nanomolar amounts of ^{99m}Tc-$VEGF_{165}$ we were able to visualize very small lesion from 3 different cell lines. We also were able to prove that the binding was specific for the VEGFR performing displacement studies pre-injecting animals with a 100-fold molar excess of unlabelled $VEGF_{165}$ or VEGFR-Fc that saturated all the available receptors thus reducing the binding of the labelled hormone of 60% and 70% respectively. The study highlights an important aspect that many times is not taken in account: the implication that both endogenous VEGF production and VEGF receptors may have on imaging strategies.

De gebeurtenissen die progressie van de tumor en metastatization rijden starten binnen de kankercel zelf, dat mutaties en accumuleert de-differentiëren tot het bereiken van een zeer onstabiele podium. Maar deze gebeurtenissen alleen onvoldoende zijn om duurzame metastase ontwikkeling en groei te handhaven. Ondersteuning door de gastheer is vereist om angiogenese te remmen en immuunrespons dat kankercellen zou doden. De som van deze gebeurtenissen het gevolg van de interactie tussen de tumor en de cellulaire of niet-cellulaire componenten die de kankercellen omgeven. Dit concept bereikte steeds belangrijker in de afgelopen jaren als gevolg van de mogelijkheid om een breed scala van therapeutische strategieën die delen en routes betrokken bij de totstandkoming van tumor micro richten. Er is echter gemeld dat kanker laesies, zelfs binnen dezelfde patiënt kunnen verschillende markers tot expressie dus nodig twee verschillende therapeutische benaderingen. Daarom is er de behoefte aan een niet-invasief middel voor elke laesie te karakteriseren voor het plannen van de meest geschikte therapie. Hierdoor zal geld, tijd besparen en de neveneffecten te verminderen zoveel mogelijk. In dit scenario, biedt de nucleaire geneeskunde een brede reeks van veelbelovende radiofarmaceuticals aan om verschillende componenten van de micro-omgeving te richten. De ontwikkeling en het testen van sommige radiofarmaceuticals zijn beschreven in deze scriptie

De eerste benadering, beschreven in hoofdstuk 2, bestaat de gerichtheid op de TSHR door schildklierkanker niet-jood terughalen metastasen uitgedrukt. Schildklierkanker is een gemeenschappelijk neuroendocriene tumor met in de

meeste gevallen een positieve prognose. De behandeling bestaat uit de totale verwijdering van de schildklier gevolgd door ablatie van het overblijvende weefsel met radioactief jodium. Maar 10-20% van de patiënten verliezen door metastasen-cellen de symporter NIS en derhalve ook het vermogen om rioiodine te concentreren. Dit leidt tot de noodzaak van alternatieve diagnostische en therapeutische benaderingen. Daarom stellen we het gebruik van een radioactief gemerkte superagonist rhTSH analogen met verhoogde biopotency en affiniteit voor de TSHR opzichte van wild type TSH. Dergelijke analogen werden radioactief gemerkt met ^{99m}Tc via HYNIC als bifunctionele chelator. In vitro experimenten werd een hoge in vitro stabiliteit met behoud van de structuur en de biologische activiteit aangetoond, met een Kd 5 keer lager dan wild type TSH. In vivo was het mogelijk om de kleine tumor xenograft van TSHR + cellen, met niet noemenswaardige opname van controle cellen, te zien. Het was ook mogelijk om intrathyroidal schildklierkanker bij een hond met een spontane tumor te verbeelden. Als deze resultaten bij de mens worden bevestigd zal het mogelijk zijn om een radiofarmaceuticum in een pre-operatief

stadium te verschaffen en dit toe te passen op patiënten die getroffen zijn door niet jodium opnemende uitzaaiingen.

In hoofdstuk 3 beschrijven we het gebruik ^{99m}Tc gelabelde infliximab bij patiënten met nieuw gediagnosticeerde sarcoïdose voor niet-invasieve scintigrafische evaluatie van de aanwezigheid van TNFa in pulmonaire en lymfe knooppunten sarcoïde laesies. Patiënten werden ook bestudeerd door [^{18}F]FDG-PET/CT en BAL

met lymfocyten fenotyperen voor volledige evaluatie van de activiteit van de ziekte. Infliximab werd gelabeld met hoge merkingsrendement, hoge specifieke activiteit en stabiliteit. Voorlopige studies in vitro, bij dieren en mensen hebben zijn nut bij het evalueren van de ziekte van Crohn en reumatoïde artritis getoond. Uit onze gegevens, maar op een beperkte reeks, blijkt dat een kwalitatief onderzoek PET de staging , die werd uitgevoerd door longspecialisten, bevestigde en dit gaf de gelegenheid om de plaaten van extra-thoracale ziekte te identificeren zoals oksels en abdominoperineale lymfeklieren. Ontstekingen in het longweefsel van sarcoïdose patiënten zijn bevestigd door hogere SUVmax en SUVmean ten opzichte van normale patiënten. Er is een gebrek aan correlatie tussen $CD4^+/CD8^+$ lymfocyten verhouding BAL en de waarden van zowel SUV_{max} en SUV_{mean} in de longen. Dit kan worden verklaard door het feit dat de [^{18}F]-FDG wordt opgenomen door verschillende celtypen betrokken bij de inflammatoire sarcoïde granuloom, dit bevestigt de slechte details.Scintigrafie met gelabelde anti-TNFα mAb was kwalitatief gezien positief in 4 van de 10 patiënten (zowel stadium III), waarin bij 6 en 24 ha men een grootschalige introductie van de radiofarmaceutische in beide longen kon waarnemen. De waarden van T/B-verhouding berekend zowel in de 6 en 24 uur beelden, kwam niet overeen met de waarden van SUVmax en SUVmean berekend met ROIlung PET.

In hoofdstuk 4 beschrijven we een nieuwe benadering voor cel kwalificatie in vivo die met een monoklonaal antilichaam (mAb) zich bindt aan CD56 antigen expressie op het cel ppervlak van de meeste menselijke NK-cellen. Het gebruik

van dergelijke radiofarmaceutici staan toe dat de NK-cellen direct in vivo te zien zijn, zonder de noodzaak van manipulatie in vitro. Het was mogelijk om efficiënt radioactief merken van de anti-CD56 mAb met ^{99m}Tc met hoog merkingsrendement te beschouwen in vitro stabiliteit. De structuur en de biologische eigenschappen van het mAb werden niet veranderd door radioactieve procedure. In vivo in SCID muizen zonder humane NK cellen, vertoonde de voorgestelde radiofarmaceutische typische kenmerken van andere radioactieve kenmerken met mAb maar met kortere circulerende halveringstijd en hoge opname in de lever en in mindere mate in de nieren. Na reconstitutie van muizen met humane NK-cellen, veranderde de biologische verdeling van het gemerkte antilichaam, met lagere circulerende halveringstijd en hogere lever- en milt activiteit als gevolg van specifieke binding aan NK cellen die zich in deze weefsels bevindt. Gerichte experimenten bevestigden de mogelijkheid de NK infiltratie in de tumoren te volgen, tumoren met een hoge target-to-background ratio. Het aantal TINKS liggen positief met de grootte van de tumor en het percentage van de necrose tijd, dit benadrukt een directe dodende werking van TINKS op de laesie en de volledige functionaliteit van deze cellen. Deze aanpak kan belangrijk zijn in de ontwikkeling van nieuwe geneesmiddelen voor kanker immunotherapie, ter verhoging van NK infiltratie in tumoren, daarna komt de follow- up en de doeltreffendheid van de nazorg van deze middelen in vivo. Inderdaad,de het zou de onderzoekers de mogelijkheid geven om het celverkeer rechtstreeks te monitoreren in vivo.

In hoofdstuk 4 beschrijven we de radioactieve labeling van de $VEGF_{165}$ gelijk met ^{99m}Tc om tumor angiogenese in verschillende cellijnen te aanschouwen. In vitro bindingsassays op VEGFR expressie cellijn HUVEC toonden aan dat radioactieve gemerkte $VEGF_{165}$ receptor op het plasmamembraan binnen 1 uur kon binden met een zeer lage Kd en deze bevindingen ondersteunen de hypothese dat zeer kleine hoeveelheden nodig zijn voor in vivo beeldvorming . Immers, door het injecteren van nanomolaire hoeveelheden 99mTc-VEGF165 konden we een zeer kleine laesie van 3 verschillende cellijnen zien.Wij waren ook in staat om te bewijzen dat VEGFR uitgevoerde verplaatsing studies om vooraf dieren injecteren met een 100-voudige molaire overmaat ongelabeld $VEGF_{165}$ of VEGFR-Fc alle beschikbare receptoren verzadigd waren en de zodoende binding van het gemerkte hormoon van 60% en 70% was. De studie lichtte een belangrijk aspect op dat nooit in aanmerking is genomen en impliceert dat zowel de endogene productie van VEGF en VEGF productie en VEGF-receptoren kunnen bevatten op de beeldvorming strategieën.

Chapter 7

Conclusions and future perspectives

Given the high degree of dedifferentiation and heterogeneity that may be encountered in cancer, in recent years the therapeutic and diagnostic approaches in clinical practice are slowly changing to a molecular level. This is because of the need to fully characterize each disease and to plan the best available therapy for each situation. From this point nuclear medicine techniques may greatly contribute to develop novel radioparmaceuticals virtually against any kind of available marker. Therefore, researchers are focusing on radiolabelling many peptides, hormones or mAbs to find the most suitable for their purpose. For example, in the field of thyroid cancer the need of a diagnostic and therapeutic tool to both image and treat non-iodine uptaking metastases is an open challenge since years. Many radiopharmaceuticals have been and are being studied over the years but, till now, none of them proved a great superiority and ^{131}I ^{18}F-FDG are still the most used for DTC and PDTC diagnosis and follow up. Indeed, given the high degree of dedifferentiation and heterogeneity of thyroid cancer, it is not easy to find specific ubiquitary markers present in DTC, PDTC and ATC. In the present thesis we proposed a completely novel approach to image non-iodine uptaking metastases focusing not only on the cancer cell itself, but also on the components that contribute to the formation of the microenvironment.

Superagonist rhTSH analogues, TNFα, anti-CD56 mAb and $VEGF_{165}$ were selected against four different targets present on tumor cells or the microenvironment. These molecules were radiolabelled with the same validated procedure, using ^{99m}Tc as the isotope of choice. The bifunctional chelator HYNIC

was used to indirectly radiolabel each compound using tricine as a coligand and $SnCl_2$ as reducing agent. This methodology was minimally invasive and the molecular structure was retained as confirmed by in vitro quality controls. QC included ITLC and HPLC analysis with different stationary and mobile phases, SDS-PAGE electrophoresis and HYNIC quantification experiments. In vitro binding assays on cells expressing the targets of the four radiopharmaceuticals were performed to prove that also their biological activity was retained with high affinity and specificity. Such experiments were important to plan animal studies were we could visualize tumor xenograft from DTC, PDTC and ATC derived cell lines.

Our approach may change the management of patients affected by cancer.

On the basis of the degree of differentiation and tumor type we can select the most appriopriate radiopharmaceutical to image metastases or exploiting microenviromental targets. Additionally, such tools, could allow to select patients for the most appropriate targeted therapy, that may range from immunotherapy to antiangiogenetic therapies using anti-VEGF mAb or TKI blocking the VEGFR signalling. This will save money and time allowing to select patients and predict the outcome of the therapy.

The possibility to image pro-inflammatory factors in vivo, with the ultimate goal of image cancer-related inflammation, was also explored in granulomas, which are benign tumors composed by inflammatory cells. Since the presence of TNF was not significantly reported in analysed lesions, it could be possible to conclude that

the studied patients, would not have benefit from anti-TNF targeted therapy. This is a practical example of in vivo characterization of lesions and therapy decision-making.

In the future we would like to follow this very same approach and extend it to many cancer types, to develop new tools and strategies against as many marker as possible, in order to increase our arsenal against cancer.

Finally, in the future it will be possible to radiolabel such radiopharmaceuticals with positron emitting isotopes to take advantage of PET resolution and quantification. On the other hand, tumor specific radiopharmaceutials like TR1401 could be radiolabelled with beta-emitting isotopes. This will allow diagnosing and treating lesions with the same pharmaceutical as proved by the introduction of theranostics like DOTA-TOC and DOTA-NOC.

Chapter 8

Curriculum Vitae

Filippo Galli

22-March-1985
Via colle dell'oro, 8 05100 Terni (TR) Italy
Mobile: +393402932086
E-mail: filippo.galli@hotmail.com

Education

Present: Ph.D. student in nuclear medicine, at the University Medical Centre Groningen (UMCG), Groningen, The Netherlands. In affiliation with the Nuclear Medicine Unit, Faculty of Medicine and Psychology, Department of Medical-Surgical Sciences and Translational Medicine, "Sapienza" University.

January-December 2012: 2nd level university master degree in "Science and Technologies of Radiopharmaceuticals", 110 cum Laude, Faculty Pharmacy, University of Rome "Sapienza".

October 2010: Master degree in "Medical, cellular and molecular biotechnologies", 110 cum Laude. Faculty of Medicine and Pharmacy, University of Rome "Sapienza".

October 2007: Bachelor in "Biotechnology" (first level in tertiary education), 107/110. Faculty of Natural Sciences, University of Rome "Tor Vergata".

Research experience

Present: Ph.D. student in nuclear medicine at the U.O.C. of Nuclear Medicine, "Sapienza" University of Rome, Italy. Involvement in basic and pre-clinical research on radiolabelling of monoclonal antibodies and peptides for molecular imaging of inflammatory diseases and cancer.

January 2008 – October 2010: Specialization student in the Nuclear Medicine laboratory – Prof. A. Signore – University of Rome "Sapienza", S. Andrea Hospital: Thesis and experience in labeling peptides with gamma and positron emitting isotopes for imaging tumors and host response to tumors.

2006 – 2007: Stage and thesis in the laboratory of Microbiology – Prof. P. Ghelardini – University of Rome "Tor Vergata": Visualization of mismatch repair in bacteria

Awards, Fellowships & Research Projects

August 2014 - Best young presenting researcher at the 22th Meeting of the International Research group in Immuno-Scintigraphy and Therapy (IRIST), Cancun, Mexico.

July 2014 – P.I. in the University Research Project: Radiolabelling and in vitro studies with a novel anti-CD56 monoclonal antibody for NK cell targeting

July 2013 – P.I. in the University Research Project: Radiolabelled VEGF Analogues For Diagnostic Purposes In Ovarian And Thyroid Cancer.

November 2012 - Best young presenting researcher at the 21th Meeting of the International Research group in Immuno-Scintigraphy and Therapy (IRIST), Bertinoro, Italy.

November 2010 – Fellowship in the AIRC project 10359: Radiolabelled TSH superagonist analogue for diagnostic purposes in thyroid cancer.

April 2010 – Best young presenting researcher at the 20th Meeting of the International Research group in Immuno-Scintigraphy and Therapy (IRIST), Groningen, The Netherlands.

February 2009 - COST-BM0607 bursary of the European Community (February-April 2009) for 2 months at the Department of radiopharmacy of Prof. Helmut Maecke and the department of infectious diseases of dr. Andrej Trampuz at the Universitatsspital Basel (Switzerland).

Publications

Galli F, Rapisarda AS, Stabile H, Manni I, Bonanno E, Piaggio G, Gismondi A, Santoni A, Signore A. In vivo imaging of NK cell trafficking in tumors. J Nucl Med. 2015 Aug 13. pii: jnumed.114.152918. [Epub ahead of print]

Ceccarelli F, Perricone C, Galli F, Valesini G, Conti F. Use of 99mTc-labelled Anti-TNF Monoclonal Antibodies to Assess Patients Affected by Inflammatory Arthropathies. Int J Radiol Med Imag 2015, 1: 102.

Signore A, Glaudemans AW, Galli F, Rouzet F. Imaging infection and inflammation. Biomed Res Int. 2015;2015:615150.

Galli F, Lanzolla T, Pietrangeli V, Malviya G, Ricci A, Bruno P, Ragni P, Scopinaro F, Mariotta S, Signore A. In vivo evaluation of TNF-alpha in the lungs of patients affected by sarcoidosis. Biomed Res Int. 2015;2015:401341.

Baldoni D, Waibel R, Bläuenstein P, Galli F, Iodice V, Signore A, Schibli R, Trampuz A. Evaluation of a Novel Tc-99m Labelled Vitamin B12 Derivative for Targeting Escherichia coli and Staphylococcus aureus In Vitro and in an Experimental Foreign-Body Infection Model. Mol Imaging Biol. 2015 Apr 10.

Galli F, Iodice V, Lauri C, Signore A. New approaches to image thyroid cancer cells and microenvironment. Q J Nucl Med Mol Imaging. 2015;59(2):184-96.

Lauri C, Di Traglia S, Galli F, Pizzichini P, Signore A. Current status of PET imaging of differentiated thyroid cancer with second generation radiopharmaceuticals. Q J Nucl Med Mol Imaging. 2015;59(1):105-15.

Signore A, Capriotti G, Chianelli M, Bonanno E, Galli F, Catalano C, Quintero AM, De Toma G, Manfrini S, Pozzilli P; Action LADA Group. Detection of insulitis by pancreatic scintigraphy with 99mTc-labeled IL-2 and MRI in patients with LADA (Action LADA 10). Diabetes Care. 2015;38(4):652-8.

Malviya G, Galli F, Sonni I, Signore A.Imaging T-lymphocytes in inflammatory diseases: a nuclear medicine approach. Q J Nucl Med Mol Imaging. 2014;58(3):237-57.
Galli F, Histed S, Aras O. NK cell imaging by in vitro and in vivo labelling approaches. Q J Nucl Med Mol Imaging. 2014;58(3):276-83.

Galli F, Manni I, Piaggio G, Balogh L, Weintraub BD, Szkudlinski MW, Fremont V, Dierckx RA, Signore A. 99mTc-labelled-rhTSH analogue (TR1401) for imaging poorly differentiated metastatic thyroid cancer. Thyroid. 2014 24(8):1297-308.

Glaudemans AW, Bonanno E, Galli F, Zeebregts CJ, de Vries EF, Koole M, Luurtsema G, Boersma HH, Taurino M, Slart RH, Signore A. In vivo and in vitro evidence that 99mTc-HYNIC-interleukin-2 is able to detect T lymphocytes in vulnerable atherosclerotic plaques of the carotid artery. Eur J Nucl Med Mol Imaging. 2014; 41(9):1710-9.

Erba PA, Glaudemans AW, Veltman NC, Sollini M, Pacilio M, Galli F, Dierckx RA, Signore A. Image acquisition and interpretation criteria for (99m)Tc-HMPAO-labelled white blood cell scintigraphy: results of a multicentre study. Eur J Nucl Med Mol Imaging. 2014 Apr;41(4):615-23.

Signore A, Lauri C, Galli F. Radiolabelled probes targeting infection and inflammation for personalized medicine. Curr Pharm Des. 2014;20(14):2338-45.

Glaudemans AW, de Vries EF, Galli F, Dierckx RA, Slart RH, Signore A. The use of (18)F-FDG-PET/CT for diagnosis and treatment monitoring of inflammatory and infectious diseases.
Clin Dev Immunol. 2013;2013:623036.

Glaudemans A.W.J.M, Galli F, Pacilio M, Signore A. Leukocyte and bacteria imaging in prosthetic joint infection. Eur Cells Mater 2013; 25:61-77

Karczmarczyk U, Garnuszek P, Maurin M, Di Gialleonardo V, Galli F, Signore A, Mikołajczak R. Investigation of 99mTc-labelling of recombinant human interleukin-2 (rhIL-2) via hydrazinonicotinamide (HYNIC). Nucl Med Biol Nucl Med Biol. 2010;37:795-803.

Malviya G, Galli F, Sonni I, Pacilio M, Signore A. Targeting T and B lymphocytes with radiolabelled antibodies for diagnostic and therapeutic applications. Q J Nucl Med Mol Imaging. 2010;54:654-76.

Chianelli M, Boerman O C, Malviya G, Galli F, Oyen W J G, Signore A. Receptor binding ligands to image infection. Curr Pharm Des. 2008;14:3316-3325

Book Chapters

Signore A, de Vries EFJ, Galli F and Malviya G. Chapter 22: Applications of molecular small-animal imaging in inflammation and infection. Molecular Imaging of Small Animals: Instrumentation and Applications, 9781493908943 pp. 637 - 683.

Chapter 9

Acknowledgments

To me, these is the most difficult chapter to write! I have never been good in these kind of things.

I would like to thank so many people…but I feel I should to start with my promotors, Prof. Alberto Signore and Rudi Dierckxs that gave me this great opportunity to conduct a very interesting PhD project.

In particular, prof. Signore, you did teach me more than you may think, in life (even in the kitchen) and from a professional point of view. You had a contagious enthusiasm and lot of patience in my first steps in this field. You gave me many opportunities to catch and I hope I will have the possibility to have more of them, continuing to work and collaborate with you for a long period. Thank you again for you guidance and positivity.

I would also like to thank dr. Giulia Piaggio, being always very kind, in each possible situation, and helping me so much, together with Isa during these period.

Also thanks to the Nuclear Medicine Unit of S. Andrea hospital and its director. I have been your guest for so many years! I really enjoyed this period of my career. Va detto che è un reparto dove non ci si annoia mai sia professionalmente che non, mi sono trovato molto bene con tutti!

Gaurav, I really miss the time we spent together, thank you so much. धन्यवाद् Is that correct? You have been a very funny teacher, colleague and friend. The very first things I learned about nuclear medicine and India came from your teachings.

Dear collaborators, many thanks to all of you. In particular to you, Bruce and Mariusz, that supported me from the beginning with wisdom, enthusiasm and very long e-mails! If I am writing this thesis it is also thanks to your help.

To my paranymph, thank you for sharing with me this important moment of my life. Grazie in particolare a Giulia, Danilo (anche se non viene) e Claudia, siete sempre stati al mio fianco come amici e colleghi durante tutto il periodo universitario.

To Sarita and Gerda..thank you for your kind help!

Infine, visto che ancora non trovo le parole giuste…

Un inquantificabile GRAZIE a tutta la mia grande famiglia, che mi ha sostenuto, in ogni modo possibile durante questi anni. Cercando di evitare giri di parole, vorrei dirvi:

Grazie Francesca di essermi vicina, sostenermi, amarmi, innervosirti e condividere con me una vita, che essa stessa merita di essere ringraziata. Mi hai sopportato in questi giorni di stesura e sei sempre al mio fianco in ogni situazione con una forza d'animo, dolcezza ed onestà di cui tutti si accorgono, e tanti ti invidiano. Ti amo.

Grazie mamma e papa, senza di voi, davvero questa tesi non sarebbe mai stata scritta. Non potrò mai ringraziarvi abbastanza per tutto l'amore e il support incondizionato che mi avete sempre donato. Siete due persone fantastiche e dovete esserne orgogliose. Vi voglio bene.

Grazie ai miei secondi genitori, (in ordine alfabetico!), Zia Donatella, Zio Duilio e Zia Luigina. Mi avete sempre trattato e voluto bene come un figlio. E io vi voglio bene allo stesso modo. Ci siete sempre stati in ogni modo come dei veri genitori e abbiamo passato insieme momenti belli e momenti brutti. Ma ne abbiamo passati tanti…e spero tanti altri ne passeremo.

Grazie al resto della mia famiglia e ad Adriano e Tiziana. Anche se da poco, ci siete sempre stati vicini con premura. Grazie di cuore.

Grazie a Riccardo, Marchito, Luca&Marco e Alessandro, anche se ultimamente passiamo meno tempo insieme, il mio affetto per voi è sempre lo stesso.

Infine, grazie nonno e di nuovo grazie zia, di tutto. Sarebbe stata una gioia avervi presenti. Ma in fondo ci sarete lo stesso, in quest'avventura come nelle prossime…